Coherent terahertz emission from $Bi_2Sr_2CaCu_2O_{8+\delta}$ intrinsic Josephson junction stacks

Dissertation
der Mathematisch-Naturwissenschaftlichen Fakultät
der Eberhard Karls Universität Tübingen
zur Erlangung des Grades eines
Doktors der Naturwissenschaften
(Dr.rer.nat.)

vorgelegt von
Boris André Gross
aus Leonberg

Tübingen
2013

Tag der mündlichen Qualifikation:	05.02.2013
Dekan:	Prof. Dr. Wolfgang Rosenstiel
1. Berichterstatter	Prof. Dr. Reinhold Kleiner
2. Berichterstatter	Prof. Dr. Dieter Kölle

Abstract

In recent years, terahertz technology has become a rapidly growing sector, driven by the demands of a vast range of (potential) applications. The terahertz spectral range roughly spans from 300 GHz to 30 THz. In the low terahertz range, there is a lack of good and compact devices, that emit electromagnetic waves. Particularly, coherent, narrow-band and continuous-wave sources are lacking, and researchers are following many different approaches to fill this gap. The thesis at hand contributes to the exploration of one of those sources: Operating intrinsic Josephson junctions as emitters in the terahertz spectral range.
Josephson junctions (JJs) work as direct current (dc) voltage to frequency converters, if operated in the resistive state. 1 mV voltage drop generates a frequency of about 484 GHz. Intrinsic Josephson junctions (IJJs) in the high temperature superconductor $Bi_2Sr_2CaCu_2O_{8+\delta}$ (BSCCO) are adequate candidates for emitting devices; the layered structure of the material intrinsically provides stacks consisting of 1.5 nm thick, nearly perfectly equal JJs. The fabrication of a series of hundreds of JJs in a stack of micrometer thickness is easily feasible, which is essential for high power frequency generation. Further, the energy gap of BSCCO is in principle large enough to allow for frequencies up to more than 10 THz. The key challenge is the synchronization of all IJJs in order to produce coherent radiation. In 2007, a research team from Argonne National Laboratories succeeded in detecting coherent terahertz radiation from more than 500 synchronized IJJs in a mesa structure. The frequencies ranged from 350 to 850 GHz with output powers up to 0.5 μW. They proposed the formation of electromagnetic standing waves in the cavity of the mesa as synchronization mechanism. Coming from the fully resistive state (nonzero voltage across all junctions), the radiation occurred in the bias regime, where groups of junctions switch back to the zero voltage state and heating is not severe, as observed for higher dc input power.
For the present thesis, similar structures have been fabricated by H.B. Wang from the National Institute for Material Science in Japan. As preliminary studies suggested, the terahertz emission should also take place for higher input powers, where two electrothermal domains have formed in the mesa, a hot spot and a colder, still superconducting part. This presumption could be confirmed within the present work. Imaging with low-temperature scanning laser microscopy (LTSLM) allowed us to visualize the hot spots in combination with standing wave patterns in the terahertz emission regime. Using various sample geometries, we were able to demonstrate the interaction between the wave patterns and the hot spot, as well as the deliberate manipulation of these processes.

In order to determine the linewidth of the radiation, measurements with a superconducting integrated receiver were performed in collaboration with the Kotel'nikov Institute of Radio Engineering and Electronics in Moscow. These measurements revealed a linewidth of about 50 MHz in the presence of a hot spot, which is one order of magnitude smaller as compared to radiation occurring for low bias currents, where no hot spot is present.
Investigating the heat balance in one of our mesas from a theoretical perspective, we showed that the formation of electrothermal domains (in particular hot spots) is founded in the strong temperature dependence of the electrical conductivity in c-axis direction of BSCCO. Solving the heat-diffusion equation in three dimensions for the actual sample geometry allowed us to establish realistic temperature profiles of our samples.
Most samples that feature coherent terahertz emission were fabricated in a mesa geometry. We showed that samples fabricated with the so-called double-sided fabrication technique emit terahertz radiation in a similar manner.

Kurzfassung

Der Bereich der Terahertztechnologie hat sich in den letzten Jahren sehr schnell entwickelt, angetrieben von den Anforderungen einer Vielzahl (potentieller) Anwendungen. Das Terahertzspektrum umfasst ungefähr den Frequenzbereich von 300 GHz bis 30 THz. Im Bereich niedriger Terahertzfrequenzen mangelt es an guten und kompakten Bauelementen, die elektromagnetische Wellen emittieren. Besonders fehlen kohärente, schmalbandige und kontinuierlich betreibbare Emissionsquellen. Die Forschung verfolgt viele verschiedene Ansätze, um diese Lücke zu schließen. Die vorliegende Dissertation trägt zur Erforschung einer dieser Quellen bei: Die Verwendung von intrinsischen Josephsonkontakten als Emitter im Terahertzspektralbereich.
Im resistiven Zustand betrieben lassen sich Josephsonkontakte als Konverter von Gleichspannungen in Wechselspannungen verwenden. Dabei erzeugt eine Gleichspannung von 1 mV eine Wechselspannung bei etwa 484 GHz. Intrinsische Josephsonkontakte in dem Hochtemperatursupraleiter $Bi_2Sr_2CaCu_2O_{8+\delta}$ (BSCCO) sind geeignete Kandidaten für die Verwendung als Terahertzemitter; die Schichtstruktur des Materials stellt bereits intrinsisch Stapel aus 1.5 nm dicken, nahezu identischen Josephsonkontakten zur Verfügung. Die Herstellung von hunderten, in Serie geschalteten Josephsonkontakten in einem mikrometerdicken Stapel ist ein Leichtes, was essentiell für die Erzeugung großer Ausgangsleistungen ist. Darüber hinaus erlaubt die supraleitende Energielücke von BSCCO im Prinzip Frequenzen bis über 10 THz. Die größte, zu überwindende Schwierigkeit ist die Synchronisierung von allen intrinsischen Josephsonkontakten, sodass kohärente Strahlung erzeugt wird. 2007 gelang es einer Forschergruppe aus den Argonne National Laboratories, kohärente Terahertzstrahlung von mehr als 500 synchronisierten, intrinsischen Josephsonkontakten in einer Mesastruktur zu detektieren. Der zugängliche Frequenzbereich reichte von 350 bis 850 GHz, bei Ausgangsleistungen von bis zu 0.5 μW. Es wurde vermutet, dass sich in der Kavität des Mesas stehende elektromagnetische Wellen bildeten und als Synchronisationsmechanismus dienten. Ausgehend vom vollständig resistiven Zustand (alle Kontakte weisen einen Spannungsabfall auf) trat die Terahertzstrahlung in dem Strombereich auf, in dem einzelne Gruppen von Kontakten in den spannungslosen Zustand zurückschalten. Heizeffekte sind in diesem niederen Strombereich relativ schwach, wurden aber für höhere Eingangsleistung beobachtet.
Für die vorliegende Arbeit wurden ähnliche Strukturen von H.B. Wang am National Institute for Material Science in Japan hergestellt. Vorausgehende Untersuchungen legten nahe, dass die Emission von Terahertzstrahlung auch für höhere Eingangsleistungen auftreten sollte. In diesem Bereich entstehen zwei elektrothermische Domänen in den Mesastrukturen, eine heißere (sog. Hotspot) und eine kältere,

noch supraleitende Domäne. Diese Vermutung konnte im Rahmen der vorliegenden Dissertation bestätigt werden. Dabei konnten die elektrothermischen Domänen in Kombination mit Strukturen von elektromagnetischen, stehenden Wellen im Emissionsbereich mittels Tieftemperaturrasterlasermikroskopie abgebildet werden. Unter Verwendung unterschiedlicher Probengeometrien konnte die Interaktion des Hotspots und der Wellenstrukturen, sowie deren gezielte Manipulation demonstriert werden.
Um die Linienbreite der Strahlung zu bestimmen, wurden Messungen mit einem supraleitenden, integrierten Receiver am Kotel'nikov Institute of Radio Engineering and Electronics in Moskau durchgeführt. Diese Messungen zeigten eine Linienbreite von etwa 50 MHz in Anwesenheit des Hotspots in der Probe. Dies ist etwa eine Größenordnung weniger als in dem Bereich, in dem keine Domänenbildung vorliegt.
Durch die theoretische Untersuchung der Wärmebalance in einer Mesa konnten wir zeigen, dass die Bildung von elektrothermischen Domänen sich in der starken Temperaturabhängigkeit der elektrischen Leitfähigkeit in c-Achsenrichtung von BSCCO begründet. Das Lösen der dreidimensionalen Wärmediffusionsgleichung für tatsächliche Probengeometrien ermöglichte es uns, realistische Temperaturprofile für die Mesas zu erstellen.
Die meisten BSCCO Strukturen, die Emission von kohärenter Terahertzstrahlung aufweisen, wurden in Form von Mesas hergestellt. Wir konnten zeigen, dass Proben, die unter Verwendung der sogenannten doppelseitigen Fabrikationsmethode hergestellt wurden, in gleicher Weise Terahertzstrahlung emittieren.

List of publications and contributions

Publications

The publications of this cumulative thesis are listed below. They are attached at the very end of the thesis and summarized in chapter 2.

Publication 1 H.B. Wang, S. Guénon, **B. Gross**, J. Yuan, Z.G. Jiang, Y.Y. Zhong, M. Grünzweig, A. Iishi, P.H. Wu, T. Hatano, D. Koelle, and R. Kleiner
Coherent Terahertz Emission of Intrinsic Josephson Junction Stacks in the Hot Spot Regime
Phys. Rev. Lett. **105**, 057002 (2010)

Publication 2 S. Guénon, M. Grünzweig, **B. Gross**, J. Yuan, Z. G. Jiang, Y. Y. Zhong, M. Y. Li, A. Iishi, P. H. Wu, T. Hatano, R. G. Mints, E. Goldobin, D. Koelle, H. B. Wang, and R. Kleiner
Interaction of hot spots and terahertz waves in $Bi_2Sr_2CaCu_2O_8$ intrinsic Josephson junction stacks of various geometry
Phys. Rev. B **82**, 214506 (2010)

Publication 3 J. Yuan, M. Y. Li, J. Li, **B. Gross**, A. Iishi, K. Yamaura, T. Hatano, K. Hirata, E. Takayama-Muromachi, P. H. Wu, D. Koelle, R. Kleiner, H. B. Wang
Terahertz emission from $Bi_2Sr_2CaCu_2O_{8+\delta}$ intrinsic Josephson junction stacks with all-superconducting electrodes
Supercond. Sci. Technol. **25**, 075015 (2012)

Publication 4 M. Y. Li, J. Yuan, N. Kinev, J. Li, **B. Gross**, S. Guénon, A. Ishii, K. Hirata, T. Hatano, D. Koelle, R. Kleiner, V. P. Koshelets, H. B. Wang, P. H. Wu
Linewidth dependence of coherent terahertz emission from $Bi_2Sr_2CaCu_2O_8$ intrinsic Josephson junction stacks in the hot-spot regime
Phys. Rev. B **86**, 060505(R) (2012)

Publication 5 **B. Gross**, S. Guénon, J. Yuan, M.Y. Li, J. Li, A. Ishii, R.G. Mints, T. Hatano, P.H. Wu, D. Koelle, H.B. Wang, and R. Kleiner
Hot-spot formation in stacks of intrinsic Josephson junctions in $Bi_2Sr_2CaCu_2O_8$
Phys. Rev. B **86**, 094524 (2012)

Contributions

The following sections outline which contributions have been made to the publications by other researchers and me. All listed publications resulted from the cooperation between our institute at Tübingen University and the NIMS in Tsukuba, Japan, with H.B. Wang being our direct project partner. The samples used for the publications have been fabricated by H.B. Wang and his team in Tsukuba.

Publication 1

A terahertz detection setup was built for this publication. It has been planned by S. Guénon, constructed by M. Grünzweig, J. Yuan, S. Guénon and H.B. Wang, and further improved and adjusted by S. Guénon and me. Many terahertz detection (J. Yuan, Z.G. Jiang, Y.Y. Zhong and me) and LTSLM (H.B. Wang, S. Guénon and me) measurements have been performed, most of them not directly entering the manuscript. Data analysis and the preparation of the manuscript has been done by H.B. Wang, S. Guénon, R. Kleiner and me.

Publication 2

The terahertz detection measurements appearing in this manuscript have been performed by the NIMS team, while the LTSLM data has been acquired by M. Grünzweig, S. Guénon, H.B. Wang and me. Also data analysis and manuscript preparation has been done by M. Grünzweig, S. Guénon, H.B. Wang, R. Kleiner and me.

Publication 3

The sample presented in publication 3 was measured by the NIMS team with respect to terahertz emission, investigations with LTSLM were performed by me. Data has been analyzed and the manuscript has been composed by J. Yuan, H.B. Wang, R. Kleiner and me.

Publication 4

For this publication, a cooperation with the Kotel'nikov Institute of Radio Engineering and Electronics in Moscow was started. Measurements were performed by H.B. Wang, M.Y. Li, N. Kinev and V.P. Koshelets. Data analysis was done by M.Y. Li, H.B. Wang, R. Kleiner and me. In particular, I performed temperature simulations and related evaluation of data. The manuscript has been written by H.B. Wang, R. Kleiner and me.

Publication 5

The stimulus to this publication was given by S. Guénon by spotting manuscripts from E. Spenke written in the 1930s [1, 2], adopting the physics and applying it to BSCCO IJJ stacks. All measurements, except for the temperature dependence of the resistance, all calculations, simulations and data analysis were performed by me. Valuable expertize on hot spots was given by R.G. Mints. The manuscript itself arose from frequent exchanges of the drafts between R. Kleiner and me.

Contents

Chapter 1

Introduction

In the past decades interest in the terahertz spectral range, roughly spanning from 300 GHz to 30 THz, has grown immensely. Many new terahertz technologies have been developed, recognizing a vast range of potential applications [3–5]. Plenty of physical phenomena have their typical energies and frequencies lying in the terahertz range, such as e.g. vibrations and rotations in molecules or superconducting energy gaps. Thus, the terahertz spectral range is pivotal for probing fundamental physical interactions and for applications [4]. This covers sectors such as information and communication technology [6], biology, medical and material sciences, security, quality control of food, non-destructive evaluation and global environmental monitoring [5, 7–10].

Modern devices give access to a broad range of the electromagnetic spectrum. From radio to microwave frequencies electronics can be operated, being limited in speed mainly by the carrier mobility in semi-conducting structures [10–13]. In the optical range, lasers are the most employed devices, however, infrared photonics operate only down to about 20 THz [12]. Between these two limitations lies the so-called terahertz gap, which typically refers to the lower terahertz range, cf. Fig. 1.1. An important ongoing issue is the development of adequate terahertz radiation sources in this gap. Besides broadband pulsed emitters, which are e.g. used for terahertz time-domain spectroscopy [4], also coherent, narrow-band and continuous-wave (CW) sources are needed. Important quantities are tunability, output power, minimum linewidth and compactness. The diversity in devices is rich [5, 10], and

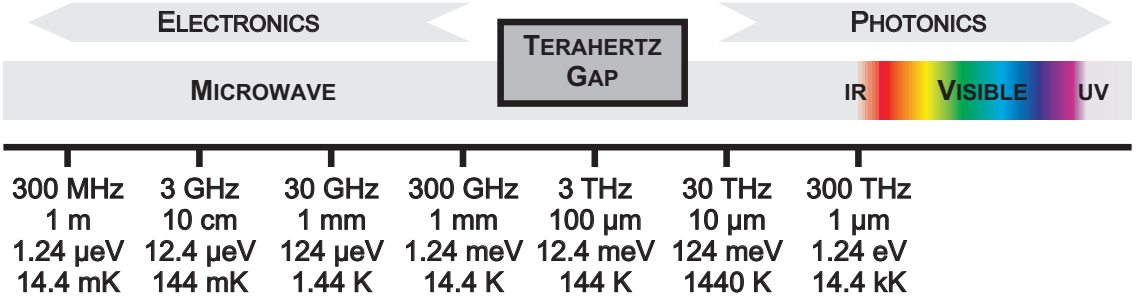

Figure 1.1: The terahertz gap. After [14].

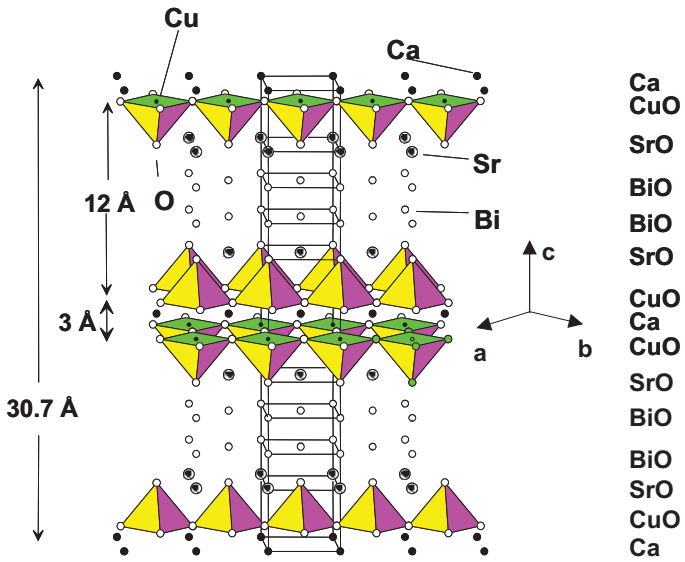

Figure 1.2: $Bi_2Sr_2CaCu_2O_{8+\delta}$ crystal structure. From [18].

all of them operate in a limited range of output parameters. Hence, improvement of existing techniques and searching for new ways of generating terahertz waves is an active field of research.

One approach to generate CW terahertz waves is based on Josephson junctions (JJs). Operated in the resistive state, the supercurrents oscillate across the barrier of the device with a frequency $f = V/\Phi_0$, with V being the voltage across the junction and the magnetic flux quantum $\Phi_0 = h/2e \approx 1$ mV/484 GHz. Here, h is the Planck constant and e the elementary charge. This makes a JJ a perfect voltage-to-frequency converter, easily covering the whole terahertz range by applying a few millivolts. However, JJs are limited in frequency by the superconducting energy gap, restricting conventional JJs roughly to $f \lesssim 700$ GHz. A single JJ typically has an output power in the sub-nanowatt range, a second major drawback for the usage as a terahertz source [15]. In 1986, the cuprate superconductors were discovered [16], which have much larger superconducting energy gaps, increasing the potentially accessible frequencies to several THz. A few years later, the intrinsic Josephson effect in $Bi_2Sr_2CaCu_2O_{8+\delta}$ (BSCCO) was discovered by Kleiner et al. [17]. Like all cuprate superconductors, BSCCO has a layered structure. Superconducting copper oxide planes alternate with insulating bismuth oxide an strontium oxide planes, naturally forming stacks of JJs, where one junction has a thickness of 1.5 nm, cf. Fig. 1.2. It is therefore easily feasible to fabricate hundreds of intrinsic Josephson junctions (IJJs) in series, using standard fabrication techniques, and a lot of research has been performed on such structures [19]. However, in order to produce coherent radiation with high output power, many junctions need to oscillate in phase and synchronizing the junctions is a key issue. In the past, researches investigated rather small devices, with lateral dimensions of several tens of micrometers and maybe less than 50 junctions [20, 21]. Synchronizing and understanding few junctions rather than large numbers was expected to be the easiest approach, but success was modest.

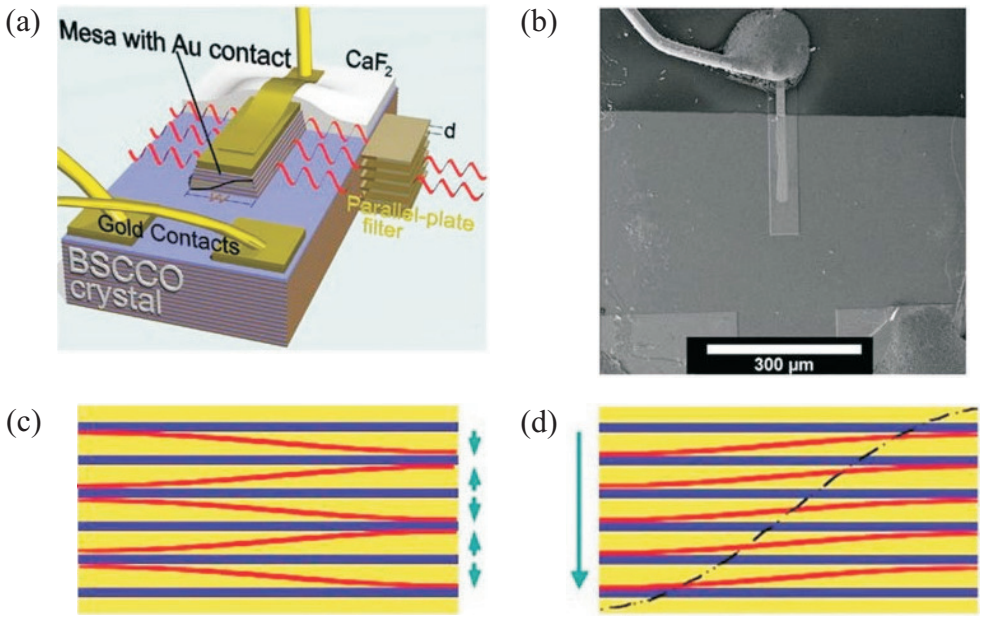

Figure 1.3: (a) Schematic of the BSCCO mesas. The applied c-axis current excites the fundamental cavity mode (solid half-wave) on the width w of the mesa, and high-frequency electromagnetic radiation is emitted from the side faces (red waves), whose polarization and frequency are analyzed with parallel-plate filters. (b) Scanning electron microscopy image of the mesa. Schematics of the anti-phase (c) and of the in-phase (d) mode. The blue and yellow layers are the CuO_2 layers and Bi-Sr-O layers. The red waves represent the alternating electric field. In the anti-phase mode the electric field on the long side face largely cancels, resulting in negligible emission. For the in-phase mode, the electric fields from each junction add to create an intense standing wave (black dashed line) and strong emission. Caption and figures from [22]. Reprinted with permission from AAAS.

In 2007, Ozyuzer et al. reported success in operating more than 500 IJJs that oscillated in phase, producing CW and coherent radiation with an output power up to approximately 0.5 μW at frequencies ranging from 350 to 850 GHz [22]. The essential difference to previous attempts was the use of rather large devices; the fabricated structures in form of mesas had widths varying from 40 μm to 100 μm, a length of 300 μm, and a height of about 1 μm, corresponding to roughly 700 IJJs on BSCCO single crystals, cf. Fig. 1.3 (a) and (b). They detected terahertz radiation when decreasing the bias current, coming from the fully resistive state (i.e. all IJJs in the stack are resistive), just before some of the IJJs switched back to the superconducting state, cf. Fig. 1.4 (a) for the corresponding current-voltage characteristic (IVC) and the detected bolometric radiation signal. For all of their measurements the Josephson relation $f = NV/\Phi_0$ was fulfilled. Here, N is the junction number. This strongly suggested the Josephson current as origin of the radiation. Fourier transform infrared spectroscopy (FTIR) measurements showed sharp emission lines with an instrument-resolution limited linewidth of about 9 GHz (full-width-at-half-maximum), cf. Fig. 1.4 (b). The inset in Fig. 1.4 (b) shows, that the observed radiation frequency scaled with the inverse width of the mesas. This

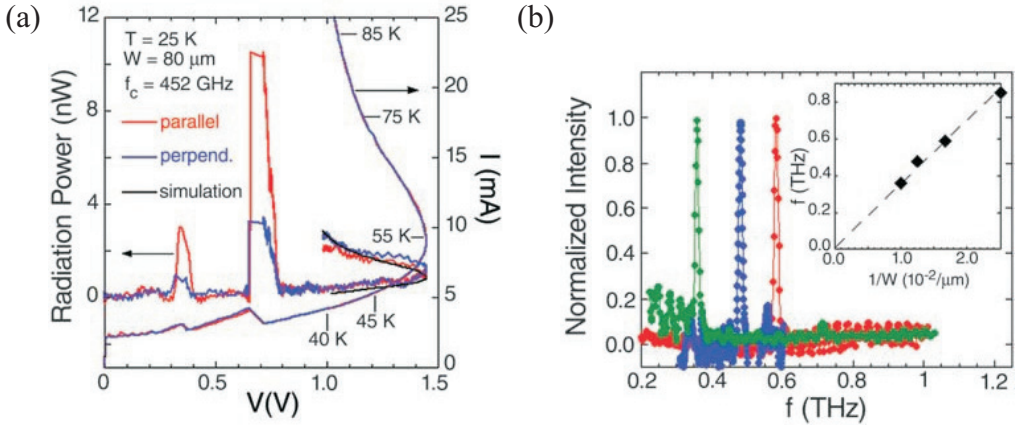

Figure 1.4: (a) Current-voltage characteristics and radiation power of the 80-μm mesa. The voltage dependence of the current (right y-axis) and of the radiation power (left y-axis) at 25 K for parallel and perpendicular settings of the filter with 0.452 THz cut-off frequency are shown for decreasing bias in zero applied magnetic field. Polarized Josephson emission occurs near 0.71 and 0.37 V, and unpolarized thermal radiation occurs at higher bias. The black solid line is a simulation of the thermal radiation. (b) Far-infrared spectra of the Josephson radiation. Sharp emission lines are clearly resolved. The observed line width of 9 GHz (full-width-at-half-maximum) is instrument-resolution limited. The scaling of the emission frequency with the inverse mesa width, shown in the inset, demonstrates that a cavity resonance on the width is excited. Caption and figures from [22]. Reprinted with permission from AAAS.

observation lead to the conjecture, that the IJJs are synchronized by a standing electromagnetic wave, that is formed by multiple reflections in the cavity formed by the side surfaces of the mesa, cf. Fig. 1.3 (c) and (d). For coherent emission of the IJJ stacks a radiation power $P \propto N^2$ is expected [23, 24]. This could be directly shown by Ozyuzer et al. for the detected radiation. Besides terahertz emission, strong heating of the samples was identified in the IVCs and the bolometer signals, a well known phenomenon in BSCCO structures [25–32].
These results triggered intense research on terahertz emission from large BSCCO mesas. The following paragraphs are meant to give the reader an overview of the recent development from both an experimental and theoretical point of view.

To the best knowledge of the author, all of the large BSCCO IJJ stacks that emit in the terahertz regime have been made from BSCCO single crystals, grown by floating zone technique. The "standard" structure is a mesa [22, 33–43], mostly in rectangular shape and covered with a metal (usually Au) layer of varying thickness. Usually, photo lithography, standard depositing methods and ion milling have been used as fabrication techniques. Similar mesas have been fabricated using focused ion beam (FIB) milling [41, 44, 45]. In this case a groove separates the mesa from the base crystal, in contrast to the standard mesas, that stand on top of the base crystal. It is possible to remove a mesa from the base crystal, and attach it to a (sapphire) substrate covered with gold [41, 45], leading to an Au-BSCCO-Au structure. Stacks with all-superconducting electrodes also show terahertz emission. The corresponding

fabrication method is described in **publication 3**, and summarized in chapter 2.3. For all structures mentioned above, fabrication parameters such as oxygen-doping level of the BSCCO crystals [36], top-electrode thickness [42] or steepness of the edges [36, 46] need to be well chosen in order to produce samples that show significant terahertz radiation.

Terahertz emission occurring in the retrapping regime of the IVC, i.e. for low bias currents, as observed by Ozyuzer et al. [22], is typically a non-reversible process. The emission occurs on the return branch in the IVC, when the bias current is reduced. When some of the IJJs have switched back to the superconducting state, increasing the current will not make them switch to the resistive state again. Before terahertz emission occurs, some IJJs may have switched back to the superconducting state and therefore not necessarily all junctions are synchronized and contribute to the terahertz radiation. The dc input power is not too large in this emission regime, and therefore a roughly homogeneous temperature distribution in the stack is expected, elevated by a few Kelvin with respect to the bath temperature T_b. Terahertz radiation appears for T_b in a range of approximately 10 to 60 K. The following summarizes the recent findings on terahertz emission *occurring for low bias currents*. The accessible frequency range of roughly 300 to 950 GHz has not been extended significantly since the first measurements [22]. However, a tunability by voltage of several percent has been found [34, 40], which was attributed to the trapezoidal shape of the mesas, a side-effect of the sample fabrication. The idea is, that the trapezoidal shape leads to a cavity with not only one, but a small range of resonance frequencies. By varying the voltage different frequencies are accessible. No systematic study of the output power dependence on the steepness of the sidewalls has been performed, hence, it remains unclear, if this is the origin of the tunability due to the voltage. Also variation of the bath temperature leads to a frequency tunability in the several percent range, which is ascribed to the temperature dependence of the mode velocities of the cavity resonances [40].

Higher harmonics of the fundamental radiation frequency f_1, following $f_n = n \cdot f_1$ with n being an integer, have been observed up to the 4th order for rectangular mesas [33]. This is expected for resonances in the cavity model. In contrast, disk-shaped mesas have cavity resonances that do not fulfill this condition. In experiment, a match between the fundamental cavity frequency and the detected main peak has been observed [44]. However, the higher harmonics were still found at integer multiples of f_1, suggesting that the cavity resonance should not be the primary source of radiation. This is illustrated in Fig. 1.5 (a), which depicts the spectra for three disk-shaped mesas, showing f_1 and higher harmonics.

The (azimuthal and altitudinal) angular dependence of the radiation for rectangular [35, 37] and disk-shaped [44] mesas has been measured, cf. Fig. 1.5 (b) for the altitudinal radiation intensity distribution of a disk-shaped mesa. The distributions were tried to be modeled via standard antenna theory by introducing a dual source generation of the terahertz radiation [37, 44]: The ac-Josephson current consists of a uniform part and an inhomogeneous part that excites a cavity resonance mode in the mesa, which locks the radiation frequency [47–49]. In this way, the measured patterns can be reproduced satisfactorily, cf. Fig. 1.5 (b). However, the experimen-

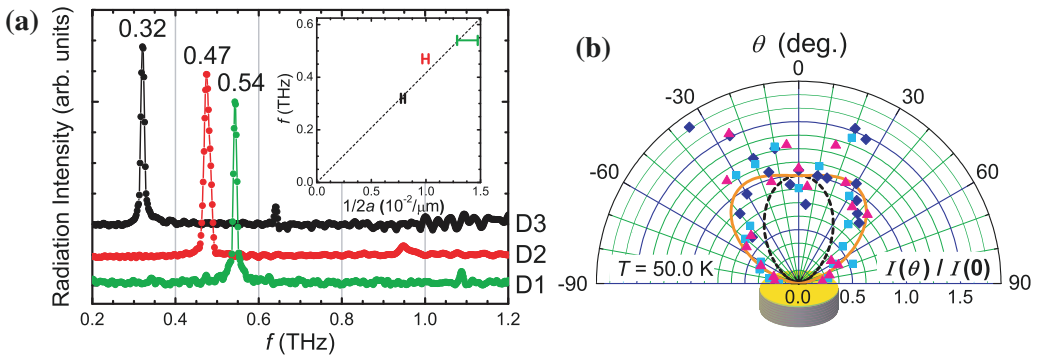

Figure 1.5: (a) FTIR radiation spectra for three disk-shaped mesas. The inset shows the observed fundamental frequencies vs $1/(2a)$, with the disk radius a. The dashed line represents the expected fundamental frequency in the cavity model. (b) Polar plot of the distribution of the altitudinal radiation intensity from disk-shaped mesa D3 for three different runs (different symbols). The solid orange line is a dual-source model fit, with the cavity component shown by the black, dashed curve. Figures and modified caption from [44]. © 2010 by the American Physical Society.

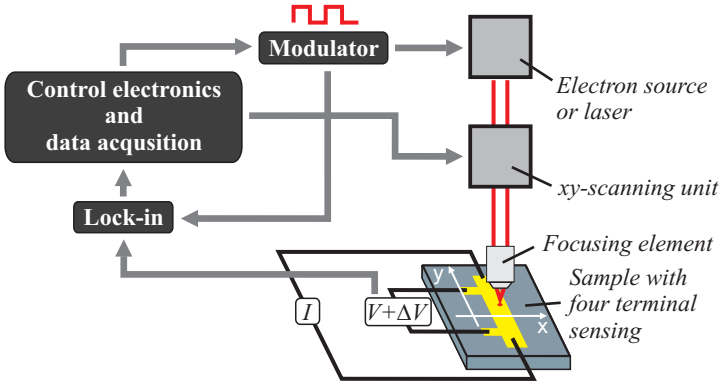

Figure 1.6: Scheme of the working principle of low-temperature scanning microscopy. Modified from [52].

tal data are not of good quality due to the difficult alignment needed during the measurements. In a dual source model, the observation of integer higher harmonics in disk-shaped mesas as mentioned before would be explained. It is questionable though, if the processes in the stacks are adequately reflected, since the phase dynamics in the stack are reduced to the simple dual source term.
The total output power has been estimated with values around 5 μW [33, 35], and for one case 30 μW [50] has been reported. The linewidth of the radiation generated by mesa structures is between 500 MHz and several GHz [43]. For an Au-BSCCO-Au structure also about 500 MHz was found as lowest value [41].

Measurements with low-temperature scanning laser microscopy (LTSLM) [51] in Tübingen University on rectangular mesas supported the idea of standing electromagnetic waves in the cavity of the mesa as synchronization mechanism, or at least as a relevant mechanism for terahertz emission. With low-temperature scanning

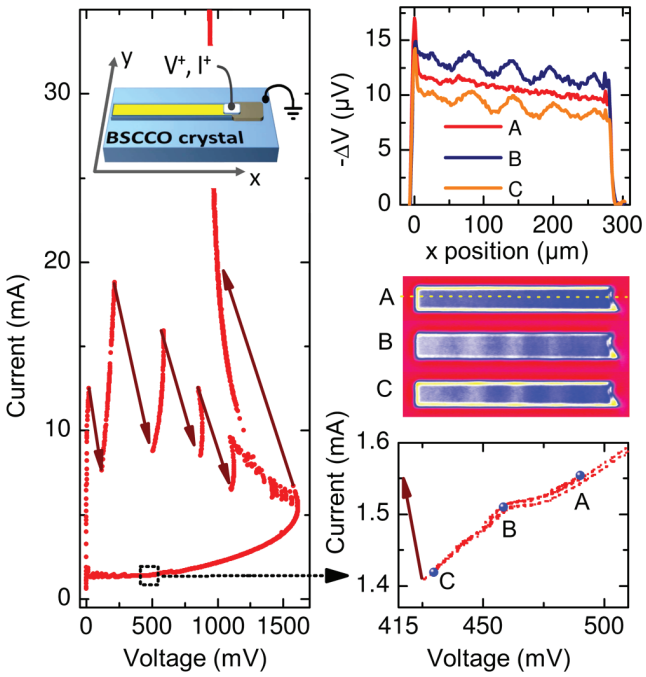

Figure 1.7: 40×330 μm^2 BSCCO mesa, at $T = 25$ K. Left: IVC on large current and voltage scales. Solid arrows denote jumps in the IVC; inset shows the geometry of the device. Right: enlargement of the IVC (bottom) in the region where LTSLM images (A–C; shown above) were recorded. Upper graph shows line scans from images A–C, along the long side of the mesa at half width, cf. dashed line in image A. Caption and figures from [51]. © 2009 by the American Physical Society.

microscopy, many temperature-dependent physical quantities can be visualized and there are numerous examples using an electron beam [53–59] or a laser [60–62], working after the same principle (cf. Fig. 1.6): The electron or laser beam is focused to a micrometer sized spot on the surface of the sample under investigation. This creates a locally heated zone with a temperature rise of a few K, typically several μm large in diameter and several hundreds of nm deep. However, the material under investigation can have a strong influence on these parameters. All temperature-dependent properties are slightly changed in the locally heated zone, leading to a change of the voltage measured across the whole sample. The beam is then scanned across the sample and the voltage change is recorded for each pixel, leading to so called voltage images. The correct interpretation of these images is the main challenge of this microscopy technique. In [51], standing-wave patterns were imaged in the bias regime where terahertz radiation was observed by Ozyuzer et al. [22]. Figure 1.7 depicts the corresponding IVC and LTSLM images of a 30×330 μm^2 mesa. As seen in the enlargement, the LTSLM images were taken just before a jump occurred in the IVC. Images B and C show clear wave structures, which were identified with cavity resonances as in previous studies on Nb junctions [54, 55] and IJJ stacks [57]. Further, the formation of a hot spot for higher input powers was revealed, see Fig. 1.8 for the corresponding IVC and LTSLM images of a 30×330 μm^2 mesa. As inferred from the detected signals, the mesa roughly had a homogeneous tem-

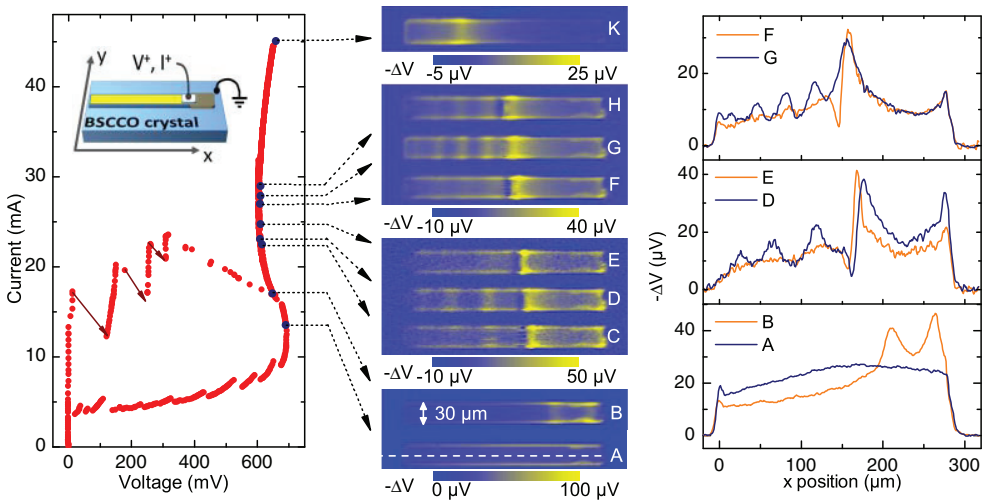

Figure 1.8: IVC and LTSLM data of a 30×330 μm^2 large BSCCO mesa at 50 K. Red solid arrows in the IVC denote switching processes, black arrows indicate bias points where LTSLM images A–K have been taken. Displayed on the right are line scans from images A, B, D–G along the long side of the mesa at half width, cf. white dashed line in image A. Caption and figures from [51]. © 2009 by the American Physical Society.

perature for low bias currents, elevated by a few K with respect to T_b, cf. LTSLM image A in Fig. 1.8. For currents exceeding a certain threshold, identifiably by a characteristic kink in the IVC, the sample is divided into a superconducting part and a part driven to above the superconducting transition temperature T_c, the hot spot, cf. e.g. LTSLM image B in Fig. 1.8. This phenomenon has been observed and analyzed earlier for low-T_c superconducting bridges [53, 63]. With increasing dc input power the hot spot grows, until the whole mesa is occupied, compare LTSLM images B–K in Fig. 1.8. In the presence of the hot spot, wave patterns could be observed in the superconducting part of the stack, as LTSLM images C, D, G and H in Fig. 1.8 show, strongly suggesting that terahertz emission should also appear in this high bias regime. An interaction between hot spot and terahertz waves was conjectured.

And indeed, terahertz emission in the presence of a hot spot could be detected with comparable frequencies and roughly the same output power as for the emission in the low bias regime [38, 64]. Especially important for applications is the stability and reversibility of terahertz emission in this regime, where no retrapping occurs. Our results can be found in **publication 1** and summarized in chapter 2.1. In addition, we showed via LTSLM, that terahertz emission and wave patterns do appear simultaneously. However, both phenomena also appeared independently of each other, the exact correlation between the phenomena is therefore not clear. The terahertz radiation occurring in this regime showed a large frequency tunability by voltage and bath temperature, which may partly be ascribed to the hot spot tuning the cavity by changing the size of the cold and therefore superconducting part of the mesa.

Wave patterns imaged via LTSLM in disk mesas further supported the interpreta-

tion as standing electromagnetic waves, since the patterns resemble expected cavity modes (cf. **publication 2**). The hot spot, forming in the center of the disk, probably creates an annular cavity for the terahertz waves, giving a good example for the interaction of hot spots and waves. Further examples for such an interaction as well as for hot-spot formation and manipulation are demonstrated in **publication 2** and summarized in chapter 2.2.
The linewidth of the terahertz waves emitted in the presence of a hot spot in the mesa is with typically 50 MHz one order of magnitude smaller than the lowest values detected without a hot spot. The smallest detected value was 23 MHz, making the mesas attractive for spectroscopy. Quite unusual, the linewidth in the high bias regime decreases with increasing bath temperature, which cannot be explained within standard models. A summary of these measurements is given in chapter 2.4, and the corresponding manuscript can be found in **publication 4**.
The strong influence of the hot spot on the terahertz emission demanded for a better theoretical understanding of the thermal physics taking place in the samples. Yurgens et al. [65, 66] were able to qualitatively reproduce the inhomogeneous temperature distribution in the mesas, in particular the hot spots, using three-dimensional finite-element simulations, taking into account a realistic sample geometry and realistic material properties. In **publication 5**, an understanding of the electrothermal behavior, including IVCs and temperature distributions, was obtained by applying the heat balance equation to a simple two-resistor or one-dimensional model. The c-axis electric conductivity of the quasi-particles could be identified as the main cause of electrothermal domain formation, i.e. the appearance of hot spots. This also clarified, that the first interpretation of the phenomenon as a result of the superconducting transition as in superconducting thin films in the spirit of [53, 63] was not correct. The LTSLM signals could be reproduced quantitatively, based on the change of the electrical conductivity in c-axis direction, using the temperature distributions from a three-dimensional model as in [65, 66] cf. chapter 2.5 for a summary of these results and **publication 5** for the manuscript.

As outlined in the preceding two paragraphs, terahertz emission occurs in two regimes: For low input power in the retrapping regime at almost constant temperature distribution and for larger input power in the presence of a hot spot. Recently, terahertz emission has also been detected from the inner branches of the IVC [45] and it is quite remarkable, that the emission frequencies range from 440 to 800 GHz generated by one sample, cf. Fig. 1.9 (a). A similar behavior was observed for an Au-BSCCO-Au structure, as shown in 1.9 (b). A significant amount of the observed frequencies does not match any cavity resonance, as determined by the authors. They therefore conclude, that cavity resonances are not necessarily involved in synchronizing the junctions and that another mechanism is needed. However, in their calculation of the resonance frequencies, they do not take the temperature dependence of the mode velocity into account [40, 51], which may already be sufficient to explain the observed discrepancy, if one keeps the strongly inhomogeneous temperature distribution within the stacks in mind.

Besides the experimental efforts to identify the terahertz emission mechanism, also from theoretical side endeavors have been made. In order to understand the

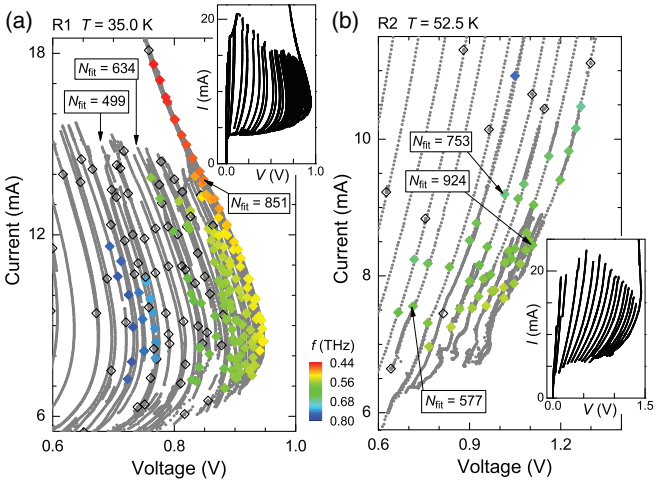

Figure 1.9: Terahertz radiation from the inner branches of the IVC of two IJJ stacks. Filled diamonds indicate emission from points in the IVC at frequencies coded by color. No radiation was detected at the open diamonds. Arrows indicate the fitted numbers of resistive junctions from fits to the Josephson relation. (a) Data of a rectangular $100 \times 140 \times 1.3$ μm^3 FIB-milled mesa. (b) Data of a rectangular $62 \times 332 \times 1.5$ μm^3 Au-BSCCO-Au structure. Insets: Full IVCs. Figures and modified caption from [45]. © 2012 by the American Physical Society.

electromagnetic behavior of a stack of IJJs, in principle, one has to consider the phase dynamics of each single JJ. This is appropriately described by a set of N coupled sine-Gordon equations [67–69]. However, solving more than 500 coupled non-linear equations demands a lot of time or extremely fast computers, so usually only 2 to maybe 50 equations are considered. The basic known dynamic solutions are collective small-amplitude oscillations of the phases (plasma oscillations), motion of fluxons and antifluxons (and combinations of those) and the McCumber (i.e. resistive) state, where the phase evolves linearly in time. An interplay of these solutions gives a broad variety of possible states for the IJJ stack [69]. The plasma oscillations create an electric field which corresponds to a standing wave pattern [68], and resonance occurs when $q\lambda/2 = w$ is met, with q being an integer, the plasma wavelength λ and the width (or length) w of the IJJ stack. The phase configuration in c-axis direction of the plasma oscillations is uniform.

For the occurrence of terahertz radiation, the oscillating supercurrents in each IJJ, generated by the ac-Josephson effect from the applied dc voltage, need to be locked to one common frequency. This frequency locking can be achieved with the excitation of an in-phase plasma mode in the stack. An alternative are solitonic solutions [70], e.g. when a rectangular fluxon lattice is realized. This however is hard to achieve, since the triangular lattice is favorable and strong external in-plane magnetic fields H are required [71, 72]. In addition to the in-phase plasma oscillation, a mechanism transferring energy from the dc voltage to the radiation is needed [73]. In other words, something has to excite the in-phase plasma mode. The Lorentz force, that has impact on fluxons of a configuration allowing them to enter a stack for $H = 0$, is such a mechanism.

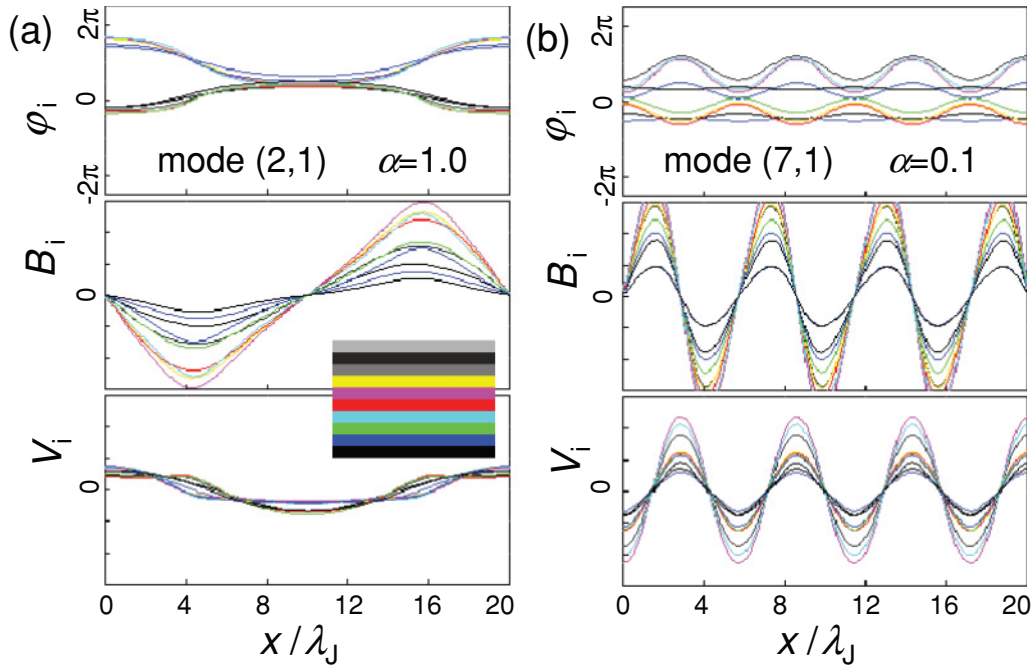

Figure 1.10: Snapshots of phases φ_i, magnetic inductions B_i, and ac component of voltages V_i at two different breather resonances for an overdamped (a) and underdamped (b) stack, i is the junction index. It is seen that the electromagnetic field forms standing-wave patterns in the stack. Excited cavity modes (m, n) are indicated in the figures. The resonances are coherently emitting modes with $n = 1$ and in-phase oscillations in all junctions. Figures and modified caption from [73]. © 2011 by the American Physical Society.

One suggestion for a phase configuration, that fulfills the described requirements, is a so-called π-kink state [74–84]. Here, the phase consists of four terms: The first term evolves linear in time for the ac-Josephson effect. The second term consists of static (time-independent) $(2m + 1)\pi$ phase kinks and anti-kinks (m is an integer), arranged periodically in c-axis direction and located in the center of the stack (interpretable as static semi-fluxons/antifluxons [73]). Third, there are plasma oscillations that are uniform along c-axis direction and lastly a constant term. Despite of the inhomogeneity in c-axis direction due to the kinks, the oscillating electric and magnetic fields are almost homogeneous in all junctions. Calculations demonstrate that energy is significantly transferred into radiation, showing that the π-kink state could be in principle responsible for terahertz emission. Another possible state with the needed in-phase plasma wave but without π-kinks was spotted by Tachiki et al. [85]. However, the corresponding phase distribution has not been published and the viability of this state with respect to terahertz emission from stacks of IJJs is unclear [86]. Breather-type solutions (bound pairs of self-oscillating fluxons/antifluxons), consisting of an ordered breather lattice, may also provide the needed mechanism [73, 87], cf. Fig. 1.10 for snapshots of the phases, magnetic inductions and ac voltages of such breather states for a stack of ten junctions.

In order to investigate the radiation properties, the simplification of only in-phase

motion of the phase differences along the c-axis direction has been considered (also called McCumber solution) [77, 88, 89]. In one study [90], also the Maxwell equations in free space and the feedback of their solution on the IJJ system are considered. A dipole-like far-field radiation pattern is found, not consistent with the measurements [35, 37]. In a subsequent study [91], the assumption of pure in-phase motion of the phase differences was dropped and solutions containing π- and 2π-kinks appear, somewhat similar to [74, 76]. The resulting far-field radiation pattern has a better match with experiments than [90]. Asai et al. [92] similarly considered in-phase motion of the phase differences and also solved the Maxwell equations outside the stack. Additionally, they considered regions of local suppression of the critical current, trying to mimic the hot spot. One finding is a uniform background phase oscillation in combination with two-dimensional wave patterns, which they interpret as a confirmation of the dual source mechanism proposed by Klemm et al. [47–49] and their calculated far-field radiation patterns. Further, the simulation yields a strong influence of the position of the hot spot on the appearance of odd modes.
Besides the fact, that the direct assumption of an in-phase mode omits the needed excitation mechanism, Nonomura [79] analyzed, that it strongly depends on the surface impedance Z, if the McCumber or the π-kink state is realized. The McCumber state is only realized for small Z and therefore the appearance of the π-kink state is preferred. A similar result is obtained in a stability analysis [93].
A different approach for synchronizing the IJJs is to add a shunt to the stack. This has been investigated longer ago for Josephson junction arrays in general [94–97]. In this spirit, Tachiki et al. [98] numerically analyzed a series of IJJs, described in the resistively and capacitively shunted junction (RCSJ) model, embedded in an LCR circuit [99] (slightly different to *shunted* by an LCR circuit, here L stands for an inductor, C for a capacitor and R for a resistor). In this model, synchronization can be achieved and a single peak radiation occurs in connection with a hump in the IVC. Lin et al. [100] investigated the synchronization in a one-dimensional array of RCSJ-like JJs coupled to a common load with respect to stability, also accounting for thermal noise. With this, they constructed a stability diagram of the in-phase phase oscillations in the IJJ stacks in dependence of bias current and McCumber parameter (i.e. hysteresis and shunting properties). Yurgens [66] considered a distributed load (a network of lumped resistors and capacitors) connected to the IJJ stack, representing the hot spot appearing for higher bias currents. This is illustrated in Fig. 1.11, where the simulated temperature distribution of the cross section through a mesa and its base crystal is depicted, and a sketch of the hot spot as distributed load is given in the inset. Describing the IJJs as a series of RCSJ-like JJs, Yurgens showed that it is in principle possible to achieve synchronization in this scenario. In experiment, no shunting elements have been added to the IJJ stacks artificially and it has not been analyzed, whether the environment of a stack (electrodes, substrate, wiring, etc.) is relevant for the synchronization of the IJJs with respect to shunting. However, especially considering the hot spot as a distributed load is of direct applicability, if one keeps the linewidth measurements [43] in mind, that showed a great difference for the presence or absence of the hot spot. Hence, shunting definitely plays an important role for terahertz radiation.
There are other approaches for achieving synchronization in IJJ stacks, that are not

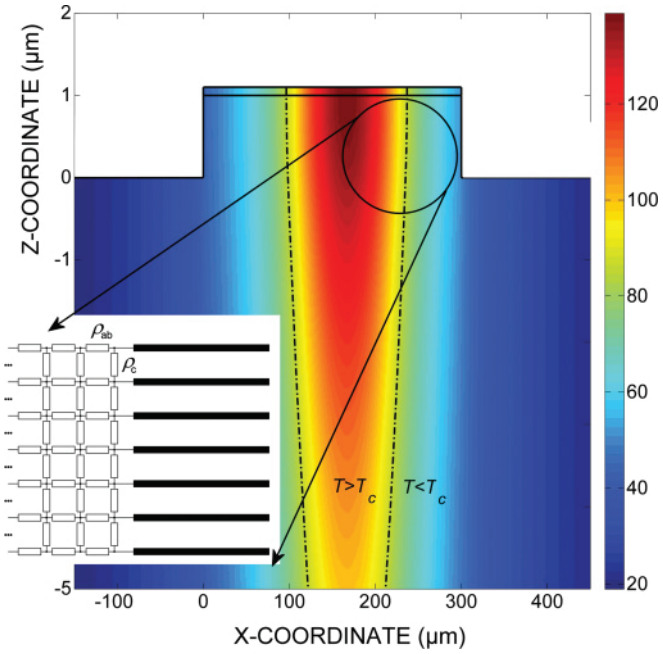

Figure 1.11: Temperature distribution across the vertical middle section of a mesa and the underlying single crystal at an injected current density $j = 1.33$ MA/m^2. The dashed-dotted lines mark the isotherm $T = T_c = 86$ K while the solid horizontal line marks the boundary between the mesa and the electrode. The inset schematically shows a simplified picture of the resistively shunted section of the mesa. The equivalent shunting circuitry is an infinite matrix of resistors representing the in- and out-of-plane resistivities. Figures and modified caption from [66]. © 2011 by the American Physical Society.

directly intended to explain the observed terahertz radiation. Notably, before the detection of coherent terahertz radiation from the large BSCCO IJJ stacks, Bulaevskii et al. [23] suggested to use much larger stacks than had been done so far. However, they suggested 4 μm wide, more than 300 μm long and 40 μm thick stacks (at the order of 10^4 junctions) with thick gold electrodes on top and bottom, differing from the sample design exhibiting terahertz radiation. In this scenario, synchronization is achieved through a feedback effect of the radiation itself. It has been further embellished in [101–104] and is still waiting for its experimental realization, even if it may have triggered the work by Ozyuzer et al. [22].
Another idea is to introduce a spatial modulation of the Josephson current in order to excite the cavity resonances [24]. This has to be done artificially, e.g. via a magnetic field [105] and, to the knowledge of the author, has also not been realized, yet.

Despite all efforts from experimental and theoretical side, the terahertz radiation mechanism has not been clearly identified up to now. Especially the question, which role cavity resonances play is not answered satisfactorily. Therefore, future efforts should focus on realizing an experiment that is able to give unambiguous evidence or dismissal for the existing models.

Chapter 2

Summary of publications

2.1 Publication 1: Coherent terahertz emission of intrinsic Josephson junction stacks in the hot spot regime

The discovery of hot spots, forming in the BSCCO IJJ mesas for relatively high input power, and the simultaneous appearance of wave patterns in LTSLM measurements suggested the occurrence of coherent terahertz emission also for high bias currents [51].
In **publication 1** we demonstrated, that coherent terahertz emission in the hot-spot regime indeed occurs. In order to do so, we established a terahertz interferometer at NIMS in Tsukuba (Japan), equipped with a Si bolometer for radiation detection, a helium flow cryostat as used for LTSLM in Tübingen, and a lamellar mirror interferometer [106, 107]. Several BSCCO mesas were fabricated based on photo lithography and argon ion etching. Some of those showed coherent terahertz emission in the hot spot regime and others in the low bias regime, however, never directly before a jump in the IVC as observed by Ozyuzer et al. [22]. Nevertheless, the output power and frequencies were comparable. Two of the mesas showing emission in coexistence with a hot spot in the mesa were investigated in detail and presented in this manuscript.
For the first sample, wave patterns could be observed by LTSLM in the emission regime in the presence of a hot spot, pointing to the importance of cavity resonances for synchronizing the IJJs. The second sample showed a frequency tunability ranging continuously from 450 to 750 GHz by choosing bath temperature and bias voltage, cf. Fig. 2.1 (a), demonstrating the potential for applications of these structures. Figure 2.1 (b) depicts the detected emission power vs bath temperature, peaking around 50 K, which is a peculiarity of this sample. No clear wave patterns were observed for this sample. In general, it was not possible to establish a direct correlation between the occurrence of emission and wave patterns as suggested by the first sample. The question of the role of wave patterns and their correct interpretation is therefore still open. The frequency measurements showed a setup-limited linewidth

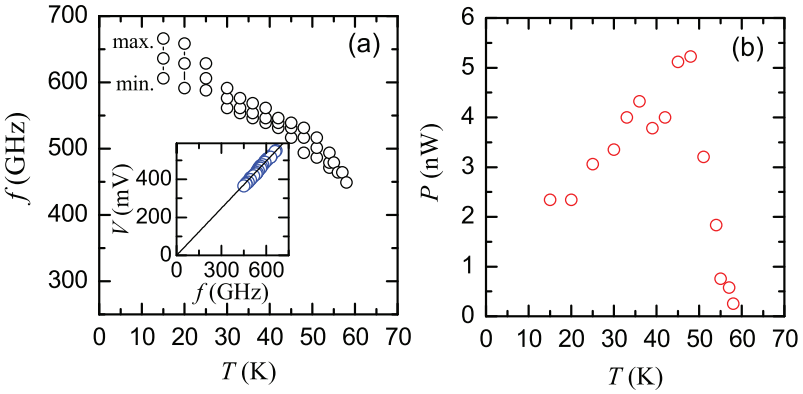

Figure 2.1: (a) Range of emission frequencies f due to voltage and bath temperature variation. The inset depicts the voltage across the mesa vs f, where the solid line is given by the function $V = Nf\phi_0$, with $N = 400$. The dependence of the detected emission power on T_b is depicted in (b). Figures and modified caption from **publication 1**. © 2010 by the American Physical Society.

of below 15 GHz, far too small for the expected quality factor of the cavity of a BSCCO mesa, pointing to an additional synchronization mechanism. The data suggested that the hot spot may possibly allow to vary the resonance frequency of the cavity by changing the in-phase mode velocity, as well as the size of the emitting cold part of the mesa, therefore playing an important role for terahertz emission.

2.2 Publication 2: Interaction of hot spots and terahertz waves in $Bi_2Sr_2CaCu_2O_8$ intrinsic Josephson junction stacks of various geometry

The appearance of wave patterns in LTSLM images in the terahertz emission regime, also in combination with hot spots has been shown in **publication 1**. It has not been resolved however, which role the wave patterns really play for terahertz emission and how they interact with hot spots. In **publication 2**, we present measurements on mesas of different geometries in order to improve the understanding of these issues.
(i) A disk-shaped mesa showed wave patterns in LTSLM measurements, that are expected for a circular cavity, complementing the previous observations in rectangular mesas. This further confirmed the interpretation of the patterns as electromagnetic cavity modes. Also terahertz emission could be detected in the bias regime where the wave patterns appeared, however an order of magnitude smaller than for rectangular mesas.
(ii) Surrounding a rectangular mesa with small detector mesas enhanced the understanding of hot-spot formation: The critical currents of the detectors vanished when being passed by the front of the growing hot spot due to increasing input power, monitored by LTSLM images. Hence, the suppression of superconductivity in the detectors served as a local temperature sensor, approving the interpretation of the

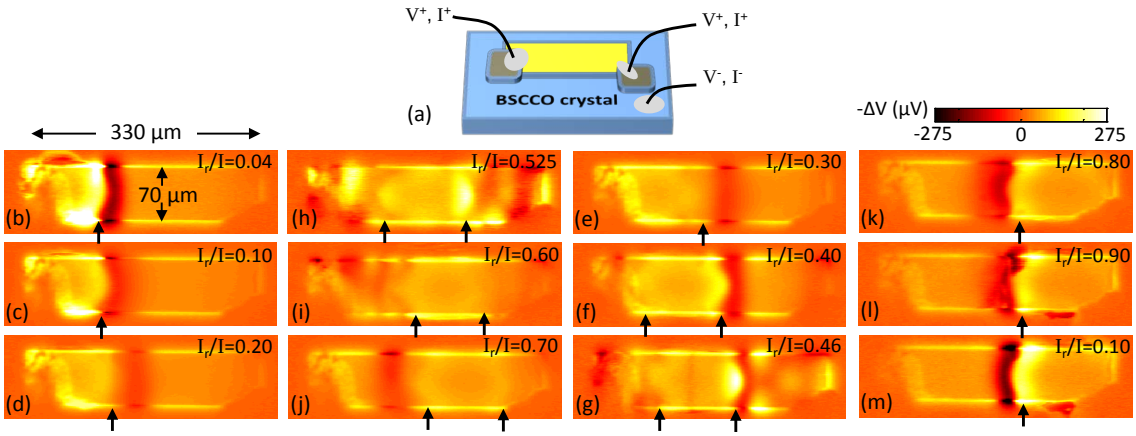

Figure 2.2: (a) Sketch of sample, equipped with two current injectors. (b)–(m) LTSLM images at $T = 18$ K for increasing ratios of the current I_r through the right injector to the total current I, as indicated in the images. Arrows indicate the edges of the hot spots. Figures and caption modified from **Publication 2**. © 2010 by the American Physical Society.

LTSLM signals in terms of hot spots.
(iii) Equipped with a current lead each on the left and right side, a rectangular mesa allowed to study the controllability of hot spots and wave patterns, see Fig. 2.2 (a) for a sketch of the sample. For a constant total bias current, different hot-spot localizations could be realized, controlled by the ratio of currents through the two injectors, compare Figs. 2.2 (b)–(m). In fact, the hot spot could be adjusted to virtually any position along the center line of the length of the mesa. Wave patterns appeared for certain hot-spot positions, either on the left (cf. Figs. 2.2 (h), (i)) or right (cf. Fig. 2.2 (g)) side of the mesa. This controllability over the hot-spot position and the appearance of wave patterns may serve as a valuable tool for the use of the mesas as terahertz emitters in applications.
(iv) In an arrow-shaped mesa, the hot spot nucleated at the arrow tip, and not close to the current injection point as for all structures investigated so far, showing that the nucleation point can also have geometric origin. This could be reproduced in three-dimensional finite-element simulations of the heat balance in such a sample geometry, cf. **publication 5**. In the three parts of the arrow independent wave patterns were –presumably– switched on and off by the hot spot, again acting as a control element for the wave patterns.

2.3 Publication 3: Terahertz emission from $Bi_2Sr_2CaCu_2O_{8+\delta}$ intrinsic Josephson junction stacks with all-superconducting electrodes

Up to this point, coherent terahertz emission from BSCCO IJJ stacks had mainly been detected from the mesa-type geometry with large dimensions, adopted from

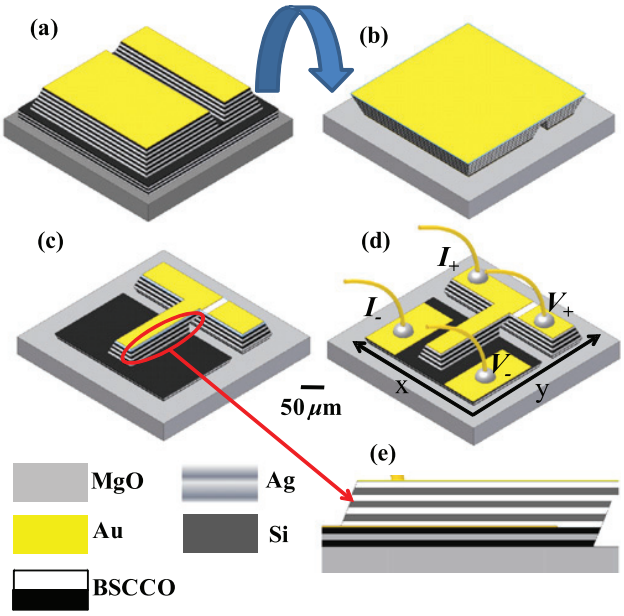

Figure 2.3: A schematic diagram of the critical steps in the fabrication process. (a) Two mesa-like structures sitting on top of a square were structured into a BSCCO crystal, which was glued to a Si substrate. (b) The patterned single crystal surface was glued onto a MgO substrate and turned upside-down. The Si substrate and remanent square pedestal was removed and an Au film was deposited. (c) A T-shaped structure was patterned, giving the IJJ stack its final shape. (d) Final state with electrodes. I_+, I_-, V_+ and V_- indicate current and voltage leads. (e) View parallel to the short side of the stack showing that the cross-section parallel to the long side of the stack approximates a parallelogram. Figure and modified caption from **Publication 3**. © 2012 IOP Publishing Ltd

Ozyuzer et al. [22]. For small stacks different sample designs had been developed, employing different fabrication techniques.

Publication 3 presents data from a sample fabricated using the double-sided technique [108, 109], however with dimensions $300 \times 50 \times 1.2\,\mu\text{m}^3$, that are adequate for terahertz emission. In this design, the IJJ stack is equipped with superconducting electrodes on top and bottom of the stack. The detected terahertz radiation of this sample was comparable in power and frequency to the mesa-type samples, showing that this fabrication technique is a promising alternative for sample preparation. The superconducting top electrode did not seem to influence the emission power significantly, as was expected from measurements on Au-BSCCO-Au structures [41, 48]. Several advantages arise with the double-sided fabrication: The superconducting electrodes avoid contact resistance and additional power dissipation produced by the Au leads that are usually employed. Degraded top junctions, which often occur in mesa-type samples, and typically strongly reduce the critical current density, are also avoided. Further, the fabrication process guarantees well-controlled uniformity in both junction number and lateral dimensions, which is especially important for fabricating array structures. Figure 2.3 (a)-(d) depicts sketches of the sample during the different steps of the fabrication process.

2.4 Publication 4: Linewidth dependence of coherent terahertz emission from $Bi_2Sr_2CaCu_2O_8$ intrinsic Josephson junction stacks in the hot-spot regime

Determining the linewidth Δf of the emitted terahertz radiation had been limited to several GHz by the FTIR spectrometers. Only one recent mixing experiment revealed a Δf of about 500 MHz for low bias currents [41]. The linewidth is an important quantity for applications and may give information on the synchronization mechanism. To be able to measure Δf, we started a collaboration with the Kotel'nikov Institute of Radio Engineering and Electronics in Moscow, which is equipped with a superconducting integrated receiver (SIR). The SIR can determine the linewidth of frequencies between 450 an 700 GHz to below 100 kHz [110–112]. The results of these measurements, elaborated in **publication 4**, show a very unusual linewidth behavior of the terahertz radiation from BSCCO IJJ stacks. First, for low bias currents, the lowest Δf was around 500 MHz, in agreement with [41]. A typical value was several GHz, and sometimes the 6 GHz bandwidth of the SIR

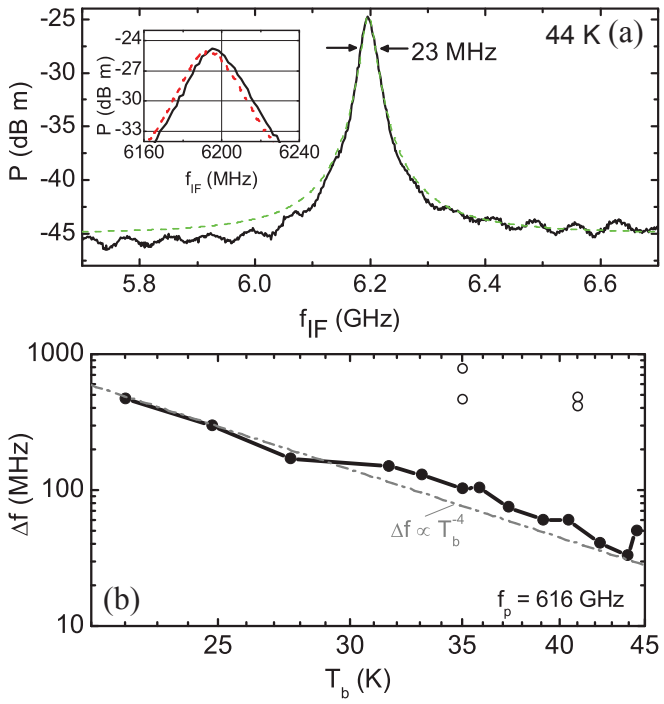

Figure 2.4: (a) SIR spectrum of the mixing output for I = 16.3 mA, V = 0.721 V in the high-bias regime at $T_b = 44$ K. The frequency of the local oscillator is $f_{LO} = 605.75$ GHz, the intermediate frequency $f_{IF} = 6.2$ GHz and the emission frequency $f_p = f_{LO} + f_{IF}$. The dashed line results from a Lorentzian fit with $\Delta f = 23$ MHz. Inset: Drift of the emission peak after 3 min. (b) Dependence of the linewidth on the bath temperature. Open circles are for low and solid ones for high bias. Figures and caption modified from **Publication 4**. © 2012 by the American Physical Society.

was exceeded. However, for high bias, when a hot spot is present in the stack, Δf was around 50 MHz, and the lowest value was 23 MHz, cf. Fig. 2.4 (a). These surprising results suggest, that the hot spot works as an active element in synchronizing the IJJs, significantly enhancing the emission properties. It also seems, that synchronization is not complete for low bias currents. The narrow minimum linewidth makes IJJ stacks interesting for applications such as e.g. terahertz spectroscopy. Second, the linewidth for high bias currents *decreases* with increasing bath temperature, roughly following $\Delta f \propto T_b^{-4}$ for the presented sample, cf. Fig. 2.4 (b). Other samples also show a decreasing Δf, but not with the T_b^{-4}-dependence. The cold, terahertz emitting part of a stack has a lower temperature for smaller T_b than for higher T_b, despite the non-homogeneous temperature distribution in the stack. Hence, the non-homogeneous temperature distribution cannot explain such a $\Delta f\,(T_b)$. No standard model one would apply (e.g. Nyquist noise) is capable of explaining the observed $\Delta f\,(T_b)$; an increasing Δf with T_b is always predicted. A possible explanation could be time-dependent hot-spot fluctuations or oscillations [113], that decrease with increasing T_b. Notably, the temperature gradient of the edge of the hot spot shows such a T_b-dependence. However, up to now we were not able to identify any traces of hot-spot oscillations or fluctuations in experiment.

2.5 Publication 5: Hot-spot formation in stacks of intrinsic Josephson junctions in $Bi_2Sr_2CaCu_2O_8$

The occurrence of hot spots in BSCCO IJJ stacks, as revealed via LTSLM [51], has not been understood and theoretically described in sufficient detail. Ascribing the voltage signals detected with LTSLM to a transition from a superconducting part to a part with a temperature $T > T_c$, as observed earlier for superconducting thin films, see e.g. [53, 58, 63], does not correctly reflect the experimental situation for BSCCO IJJ stacks. Yurgens et al. [66, 104] used finite element analysis (FEA) in three dimensions to solve the heat diffusion equation, and could indeed reproduce the hot spots qualitatively. However, a quantitative analysis was lacking, and the calculated IVCs did not feature characteristic kinks observed in experiment.
In **publication 5**, we eliminated these inconsistencies, and gave a clear picture of the electrothermal behavior of the samples. In general, the occurrence of hot spots is a well described phenomenon [113, 114] and evident in many materials. For terahertz emission, the IJJ stacks are operated in their resistive state, where the superconducting transition is not of importance for the current flow, since the electrical resistivity in c-axis direction ρ_c increases continuously when cooling the sample through T_c [115, 116]. However, ρ_c increases strongly with decreasing temperature in the relevant temperature range of 10–90 K. For such a $\rho_c\,(T)$-dependence the occurrence of hot spots is well-known in semiconducting structures [113, 114]. We therefore identified the hot spots with electrothermal domains, as they appear in semiconductors.
In the most simple way, the formation of such hot spots can be examined by modeling a mesa with two lumped, parallel resistors A and B, cf. Fig. 2.5 (a) and (b).

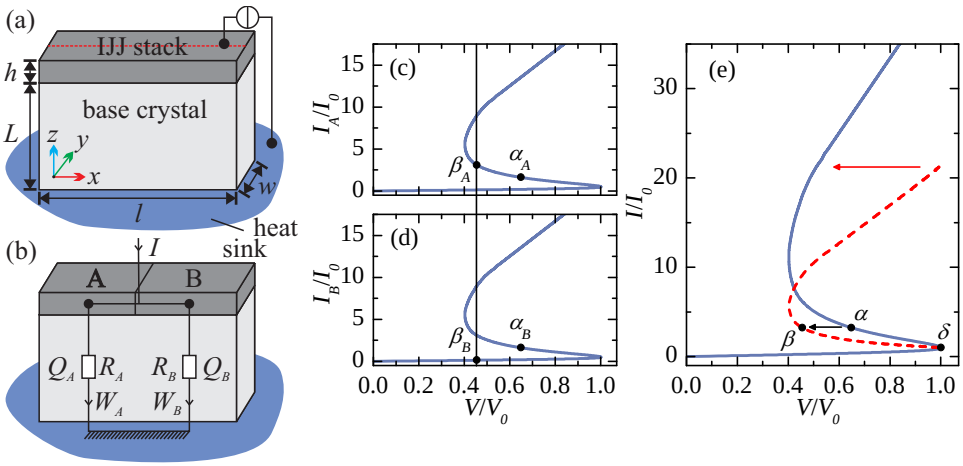

Figure 2.5: Discrete approximation for a mesa. (a) Dimensions of mesa and base crystal. (b) The mesa is replaced by two vertically cooled resistors R_A and R_B producing Joule heat Q_A and Q_B, which is vertically transported to a thermal bath via heat-transfer powers W_A and W_B. (c) and (d) display the IVCs of the two individual parts A and B, respectively. (e) IVC of the combined system. The axes are normalized to the current (voltage) of the point showing local maximal voltage V_0. The total current through the mesa at V_0 is I_0. The bias points indicated by Greek characters are discussed in the text. In (e), for the solid (blue) curve resistors A and B are at the same temperature, while for the dashed (red) curve their temperature differs, corresponding to hot-spot formation in the continuous case. Caption and figures modified from **publication 5**. © 2012 by the American Physical Society.

Taking realistic, temperature-dependent values for electrical and thermal conductivities into account, the IVC of a single, current-biased resistor is determined by the balance between Joule heating Q and heat transfer power W. The result is a curve that has a regime of negative differential resistance, see e.g. Fig. 2.5 (c). Each current value corresponds to a certain temperature of the resistor. For two such resistors in parallel, thermal bistability is possible in the regime of negative differential resistance, since $Q = W$ has more than one solution. Therefore, a branch exists in the IVC with equal temperatures of the resistors, see the blue curve in Fig. 2.5 (e), and a branch where the temperature differs (cf. red, dashed curve in Fig. 2.5 (e)). Rather than being in state α in Fig. 2.5 (e), the system favors state β for currents higher than δ. For the individual resistors this means, that e.g. resistor A switches from state α_A to β_A and resistor B from α_B to β_B, cf. Figs. 2.5 (c) and (d). Therefore, $T_{\beta_A} > T_{\beta_B}$, i.e. resistor A represents the hot spot. Such a simple model is capable of explaining the occurrence of hot spots and the shape of the IVC in a qualitative manner.

One obtains more details, when considering a one-dimensional, continuous model for the heat flow along the red, dashed line in Fig. 2.5 (a), neglecting variations in c-axis direction. The formation of hot spots and the branching in the IVC as seen in the two resistor model are reproduced. Further, one finds a realistic shape of the hot spot (i.e. a realistic temperature distribution) and its growth with increasing input power, as observed in experiment.

Lastly, we solved the three-dimensional heat diffusion equation with FEA, just as in

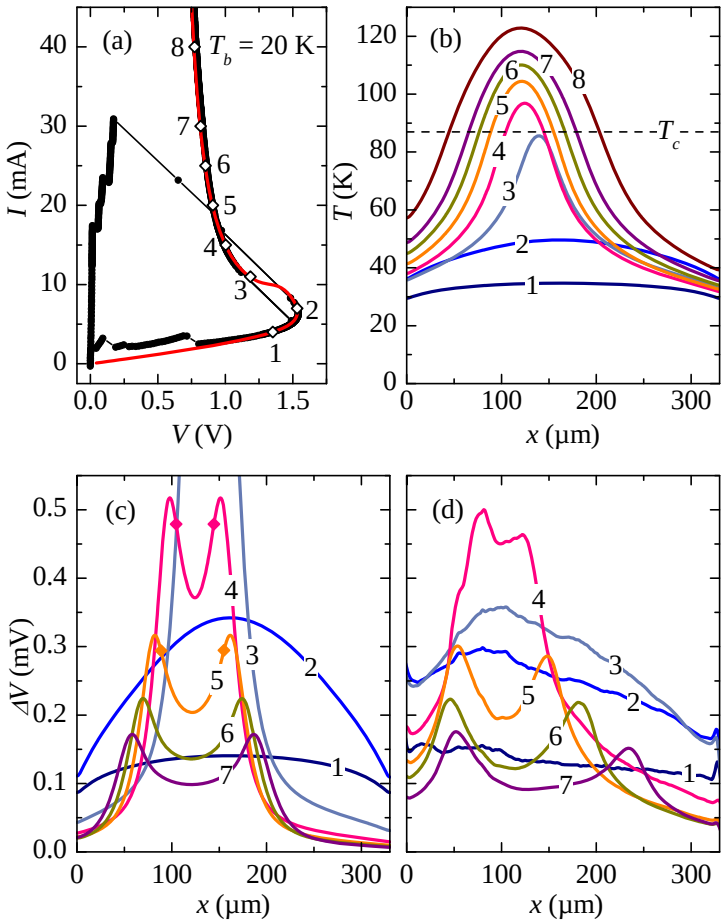

Figure 2.6: Comparison of three-dimensional simulation and experimental data for a mesa at $T_b = 20$ K. (a) Measured (black, solid circles) and simulated (red solid line) IVCs. In (b), simulated $T(x)$ profiles along the red, dashed line in Fig. 2.5 (a) for $z = 0.5h$ are shown. The diamonds in (a) indicate the corresponding bias points. The calculated and measured LTSLM signals $\Delta V(x)$ are shown in (c) and (d), respectively. Diamonds in (c) indicate the x position where $T = T_c$. Figures and caption modified from **publication 5**. © 2012 by the American Physical Society.

[66, 104], however, treating the physics in a more quantitative manner, accounting for the sample properties as good as possible. Data for a mesa at $T_b = 20$ K are shown in Fig. 2.6. A very good match between simulated and measured IVCs, cf. Fig. 2.6 (a), has been achieved by adjusting the sub-gap electrical resistivity accordingly. The resulting temperature distributions along the red, dashed line in Fig. 2.5 (a) for $z = 0.5h$, show how the hot spot evolves, cf. Fig. 2.6 (b). Notably, the maximum temperature of the hot spot may be above or below T_c. Based on these simulated temperature distributions, the detected LTSLM signals, shown in Fig. 2.6 (d), were now correctly attributed to the temperature dependence of ρ_c, and could be reproduced sufficiently precise by calculating the voltage response of the sample, see Fig. 2.6 (c). These temperature distributions provide a basis needed for the correct interpretation of other physics taking place in the samples, such as the ac Josephson currents.

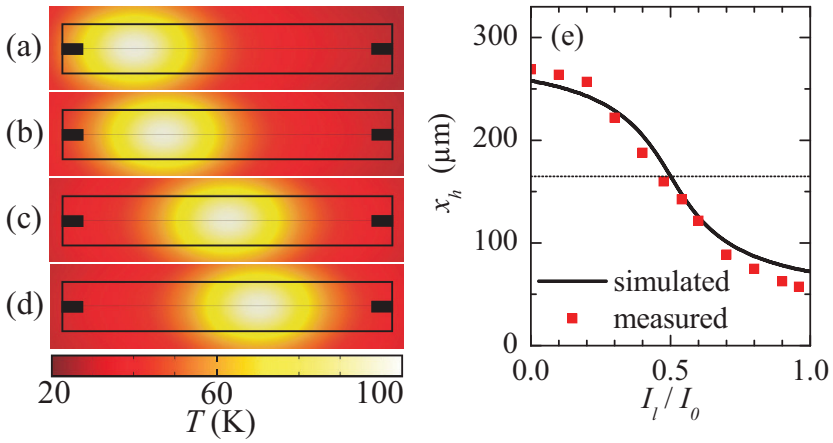

Figure 2.7: (a)–(d) Surface plots of hot-spot solutions, obtained by solving the three-dimensional heat diffusion equation with FEA for a mesa with two current injection points, indicated by black rectangles. The sum I_0 of the currents through the left (I_l) and right (I_r) injection points has been kept constant, and for the ratio I_l/I_0 values of (a) 1, (b) 0.7, (c) 0.5, and (d) 0.425 have been used. (e) The center position x_h of the hot spot vs current injection ratio for simulated and measured data. Figures and caption modified from **publication 5**. © 2012 by the American Physical Society.

Effects related to the point of hot-spot nucleation, described in **publication 2**, could be reproduced correctly with the FEA simulations, approving that the model established in the manuscript is capturing the relevant thermal physics. This is e.g. demonstrated in Fig. 2.7: Surface plots (Figs. 2.7 (a)–(d)) of the temperature distribution in a mesa with two current injection points show that the experimentally observed movement of the hot spot depending on the ratio of injected currents is reproduced; especially the center position of the hot spot vs injected current ratio is reproduced well, as depicted in Fig. 2.7 (e).

Summary and outlook

Summary

The successful first measurements on large BSCCO mesas at Tübingen University [51] were the starting point for this thesis. Since then, the major contribution of our work to the field was the finding and investigation of terahertz radiation in the presence of a hot spot in the IJJ stack, cf. **publication 1**. The radiation in this regime was discovered at about the same time by Minami et al. [64], however without putting it into context. Additionally, we could visualize via LTSLM wave patterns in the emission regime where a hot spot is present. These wave patterns, interpreted as standing electromagnetic waves in the cavity of the mesa, seem to be relevant for terahertz emission. However, their exact role has not been resolved, yet. The interaction between wave patterns and hot spots has been investigated in **publication 2**. Here, standing wave patterns could be imaged in a disk-shaped mesa, that are compatible with cavity resonance patterns. This confirmed the validity of their interpretation. We proved the existence of the hot spot and its growth with increasing input power by surrounding a rectangular mesa with several small detector junctions, serving as a local thermometer. The controllability and mobility of the hot spot could be demonstrated using two current injection leads installed at one mesa. At the same time the hot spot operated as a switch for wave patterns; this switching behavior was also shown in an arrow-shaped mesa.
In **publication 4**, we have determined the radiation linewidth Δf in the hot-spot regime for the first time. In this regime $\Delta f \approx 50$ MHz, which is roughly one order of magnitude smaller than without the hot spot, demonstrating the relevance of the hot spot for terahertz radiation. Remarkably, we found that the linewidth decreases with the bath temperature of the sample, which cannot be understood within standard models.
A consistent picture of the electrothermal physics of the BSCCO mesas has been presented in **publication 5**. Especially a detailed explanation and description of the formation of hot spots was given. This provides a good basis for understanding the electrodynamics of the IJJ stacks.
Finally, in **publication 3**, we demonstrated the applicability of a fabrication process originally used for small IJJ stacks to produce large BSCCO stacks that emit terahertz radiation. In particular, these samples are equipped with superconducting electrodes on top and bottom of the stack. This does not affect the output power of the terahertz radiation significantly, as it was expected from observations

on Au-BSCCO-Au sample structures. This fabrication method avoids degraded top junctions and top electrode contact resistance, reducing the local heating. It may also be of importance for building larger array structures.

Outlook

There are still many open questions regarding terahertz emission from IJJ stacks. Most important, the mechanism that provides synchronization of the junctions has not clearly been determined. There are potential candidates, such as the π-kink state, however unambiguous proof of their existence and relevance for terahertz radiation is still lacking. Probably related is the fact that wave patterns in LTSLM images and terahertz radiation appear together but also independently. Here, measurements with a LTSLM setup under construction at NIMS in Tsukuba may provide further information: With this system, detection of terahertz radiation and LTSLM imaging is possible simultaneously. First measurements indicate, that wave patterns appear just when terahertz radiation vanishes (when sweeping the current). An interpretation of this data has not been found, yet.
As we have adequately captured the electrothermal physics of the mesas in **publication 5**, this opens the way for combining the electrothermal physics with the phase dynamics in the stacks. That is solving coupled sine-Gordon equations together with the heat diffusion equation. It is to expect, that the non-homogeneous temperature distribution has an essential impact on the phase dynamics. Whether such a model correctly describes the system can be tested by checking, if the yielded linewidth of the terahertz radiation in presence of a hot spot decreases with increasing T_b, as has been observed in experiment.
Another important issue is the practical applicability of the IJJ stacks as terahertz emitters. For that, the output power has to be increased at least by one or two orders of magnitude. This task can be achieved in various ways. First of all, if the mechanism behind the terahertz radiation is understood, the samples can be adequately designed for high power output. Integration with other circuits, e.g. embedding the stacks into an antenna structure [117] is another option. In general, the structures have not been optimized with respect to impedance matching, a crucial aspect for high power generation of radiation. Already ongoing is research on the fabrication of array structures [41, 118]. The output power is expected to increase quadratically with the number of stacks and the operation of several synchronized stacks is therefore very promising. However, synchronization of two or more stacks has not been proven yet, and a way to realize this has still to be found. Also the realization of different approaches for synchronization of the IJJ stacks [23, 24] may be fruitful. In defiance of the limitations of terahertz radiation from BSCCO IJJ stacks, the practical applicability has already been proven: A terahertz imaging system employing a mesa as terahertz emitter has been built and used to image two Japanese Yen coins inside an envelope [119]. In addition, Turkoglu et al. [120] demonstrated, that room temperature detectors are sensitive enough for detecting the emitted terahertz waves. This shows, that the usage of BSCCO as terahertz emitter in applications is within reach.

Appendix: Acronyms and physical quantities

List of acronyms in alphabetic order

ac	Alternating current
BSCCO	$Bi_2Sr_2CaCu_2O_{8+\delta}$
CW	Continuous-wave
dc	Direct current
FEA	Finite element analysis
FIB	Focused ion beam
FTIR	Fourier transformation infrared spectroscopy
IJJ	Intrinsic Josephson Junction
IVC	Current-voltage characteristics
JJ	Josephson junction
LCR	Combination of an inductor, capacitor and resistor
LTSLM	Low-temperature scanning laser microscopy
NIMS	National Institute for Material Science (Tsukuba, Japan)
RCSJ	Resistively and capacitively shunted junction
SIR	Superconducting integrated receiver

List of physical quantities in alphabetic order

α, $\alpha_{A,B}$	State of a resistor
a	Radius of a disk mesa
β, $\beta_{A,B}$	State of a resistor
B_i	Magnetic induction of a Josephson junction with index i
δ	State of a resistor
Δf	Linewidth of the terahertz radiation
e	Elementary charge
f	Frequency of the terahertz radiation
f_1	Fundamental radiation frequency
f_{IF}	Intermediate frequency
f_{LO}	Local oscillator frequency
f_p	Frequency of the terahertz radiation
ϕ_0	Magnetic flux quantum
φ_i	Phase of a Josephson junction with index i
h	Planck constant or height of the mesa
H	External in-plane magnetic field
$I_{+,-}$	Current lead (positive or negative)
I_0	Total current through two injectors or current for maximum local voltage
I_l	Current through left injector
I_r	Current through right injector
j	Current density
λ	Plasma wavelength
m, n	Integer
N	Number of Josephson junctions in a stack
P	Output power of the terahertz radiation
q	Integer
$Q_{A,B}$	Joule heating of resistor A or B
$R_{A,B}$	Resistor A or B
T	Temperature
T_b	Bath temperature
T_c	Superconducting transition temperature
ρ_c	Electrical resistivity in c-axis direction
V	Voltage across a Josephson junction
$V_{+,-}$	Voltage lead (positive or negative)
V_0	Maximum local voltage
V_i	Voltage of a Josephson junction with index i
w	Width of a mesa
$W_{A,B}$	Heat transfer power of resistor A or B
x_h	Center position of the hot spot
Z	Surface impedance

Bibliography

[1] E. Spenke, Eine anschauliche Deutung der Abzweigtemperatur scheibenfoermiger Heissleiter, *Electr. Eng. (Archiv fuer Elektrotechnik)* **30**(11), 728 (1935).

[2] E. Spenke, Zur technischen Beherrschung des Waermedurchschlages von Heissleitern, *Wiss. Veröff. a. d. Siemens-Werken* **15**(1), 92 (1936).

[3] K. Sakai (Editor), Terahertz optoelectronics (Springer, Berlin, 2005).

[4] S. L. Dexheimer (Editor), Terahertz spectroscopy: principles and applications (CRC Press, 2008).

[5] Y.-S. Lee, Principles of Terahertz Science and Technology (Springer, New York, 2009).

[6] J. Federici and L. Moeller, Review of terahertz and subterahertz wireless communications, *J. Appl. Phys.* **107**(11), 111101, doi:10.1063/1.3386413 (2010).

[7] B. Ferguson and X.-C. Zhang, Materials for terahertz science and technology, *Nat. Mater.* **1**(1), 26, doi:10.1038/nmat708 (2002).

[8] J. F. Federici, B. Schulkin, F. Huang, D. Gary, R. Barat, F. Oliveira, and D. Zimdars, THz imaging and sensing for security applications–explosives, weapons and drugs, *Semicond. Sci. Technol.* **20**(7), S266, doi:10.1088/0268-1242/20/7/018 (2005).

[9] W. L. Chan, J. Deibel, and D. M. Mittleman, Imaging with terahertz radiation, *Rep. Prog. Phys.* **70**(8), 1325, doi:10.1088/0034-4885/70/8/R02 (2007).

[10] M. Tonouchi, Cutting-edge terahertz technology, *Nat. Photon.* **1**(2), 97, doi:10.1038/nphoton.2007.3 (2007).

[11] G. Gallerano and S. Biedron, Overview of Terahertz Radiation Sources, *Proceedings of the 2004 FEL Conference,* pages 216–221 (2004).

[12] M. Lee and M. C. Wanke, Searching for a Solid-State Terahertz Technology, *Science* **316**(5821), 64, doi:10.1126/science.1141012 (2007).

[13] M. Rodwell, M. Le, and B. Brar, InP Bipolar ICs: Scaling Roadmaps, Frequency Limits, Manufacturable Technologies, *Proc. IEEE* **96**(2), 271 , doi:10.1109/JPROC.2007.911058 (2008).

[14] C. Sirtori, Applied physics: Bridge for the terahertz gap, *Nature* **417**(6885), 132, doi:10.1038/417132b (2002).

[15] R. Kleiner, Applied Physics: Filling the Terahertz Gap, *Science* **318**(5854), 1254, doi:10.1126/science.1151373 (2007).

[16] J. Bednorz and K. Mueller, Possible high T_c superconductivity in the Ba-La-Cu-O system, *Z. Phys. B Con. Mat.* **64**, 189, doi:10.1007/BF01303701 (1986).

[17] R. Kleiner, F. Steinmeyer, G. Kunkel, and P. Müller, Intrinsic Josephson effects in $Bi_2Sr_2CaCu_2O_8$ single crystals, *Phys. Rev. Lett.* **68**(15), 2394, doi:10.1103/PhysRevLett.68.2394 (1992).

[18] M. Mößle, Josephson-Tunnel- und Transportmessungen an einzelnen CuO_2-Doppelebenen in $Bi_2Sr_2CaCu_2O_{8+x}$, Ph.D. thesis, Erlangen-Nürnberg University (2000).

[19] A. A. Yurgens, Intrinsic Josephson junctions: recent developments, *Supercond. Sci. Technol.* **13**(8), R85, doi:10.1088/0953-2048/13/8/201 (2000).

[20] R. Kleiner and P. Müller, Intrinsic Josephson effects in high-T_c superconductors, *Phys. Rev. B* **49**, 1327, doi:10.1103/PhysRevB.49.1327 (1994).

[21] I. E. Batov, X. Y. Jin, S. V. Shitov, Y. Koval, P. Müller, and A. V. Ustinov, Detection of 0.5 THz radiation from intrinsic $Bi_2Sr_2CaCu_2O_8$ Josephson junctions, *Appl. Phys. Lett.* **88**(26), 262504, doi:10.1063/1.2214157 (2006).

[22] L. Ozyuzer, A. E. Koshelev, C. Kurter, N. Gopalsami, Q. Li, M. Tachiki, K. Kadowaki, T. Yamamoto, H. Minami, H. Yamaguchi, T. Tachiki, K. E. Gray, W.-K. Kwok, and U. Welp, Emission of Coherent THz Radiation from Superconductors, *Science* **318**(5854), 1291, doi:10.1126/science.1149802 (2007).

[23] L. N. Bulaevskii and A. E. Koshelev, Radiation due to Josephson Oscillations in Layered Superconductors, *Phys. Rev. Lett.* **99**(5), 057002, doi:10.1103/PhysRevLett.99.057002 (2007).

[24] A. E. Koshelev and L. N. Bulaevskii, Resonant electromagnetic emission from intrinsic Josephson-junction stacks with laterally modulated Josephson critical current, *Phys. Rev. B* **77**(1), 014530, doi:10.1103/PhysRevB.77.014530 (2008).

[25] P. Thomas, J. Fenton, G. Yang, and C. Gough, Intrinsic c-axis transport in 2212-BSCCO, *Physica C* **341–348, Part 3**(0), 1547 , doi:10.1016/S0921-4534(00)01330-7 (2000).

[26] J. C. Fenton and C. E. Gough, Heating in mesa structures, *J. Appl. Phys.* **94**(7), 4665, doi:10.1063/1.1606860 (2003).

[27] K. Anagawa, Y. Yamada, T. Shibauchi, M. Suzuki, and T. Watanabe, 60 ns time scale short pulse interlayer tunneling spectroscopy for $Bi_2Sr_2CaCu_2O_{8+\delta}$, *Appl. Phys. Lett.* **83**(12), 2381, doi:10.1063/1.1612891 (2003).

[28] V. N. Zavaritsky, Intrinsic Tunneling or Joule Heating?, *Phys. Rev. Lett.* **92**, 259701, doi:10.1103/PhysRevLett.92.259701 (2004).

[29] A. Yurgens, D. Winkler, T. Claeson, S. Ono, and Y. Ando, A Reply to the Comment by V. N. Zavaritsky, *Phys. Rev. Lett.* **92**, 259702, doi:10.1103/PhysRevLett.92.259702 (2004).

[30] V. M. Krasnov, M. Sandberg, and I. Zogaj, *In situ* Measurement of Self-Heating in Intrinsic Tunneling Spectroscopy, *Phys. Rev. Lett.* **94**, 077003, doi:10.1103/PhysRevLett.94.077003 (2005).

[31] H. B. Wang, T. Hatano, T. Yamashita, P. H. Wu, and P. Müller, Direct observation of self-heating in intrinsic Josephson junction array with a nanoelectrode in the middle, *Appl. Phys. Lett.* **86**(2), 023504, doi:10.1063/1.1852077 (2005).

[32] B. Verreet, N. Sergeant, D. M. Negrete, M. Torstensson, D. Winkler, and A. Yurgens, Self-consistent estimations of heating in stacks of intrinsic Josephson junctions, *Supercond. Sci. Technol.* **20**(2), S48, doi:10.1088/0953-2048/20/2/S11 (2007).

[33] K. Kadowaki, H. Yamaguchi, K. Kawamata, T. Yamamoto, H. Minami, I. Kakeya, U. Welp, L. Ozyuzer, A. Koshelev, C. Kurter, K. Gray, and W.-K. Kwok, Direct observation of tetrahertz electromagnetic waves emitted from intrinsic Josephson junctions in single crystalline $Bi_2Sr_2CaCu_2O_{8+\delta}$, *Physica C* **468**(7-10), 634, doi:10.1016/j.physc.2007.11.090 (2008).

[34] K. E. Gray, A. E. Koshelev, C. Kurter, K. Kadowaki, T. Yamamoto, H. Minami, H. Yamaguchi, M. Tachiki, W. K. Kwok, and U. Welp, Emission of Terahertz Waves From Stacks of Intrinsic Josephson Junctions, *IEEE Trans. Appl. Supercond.* **19**(3), 886, doi:10.1109/TASC.2009.2017888 (2009).

[35] H. Minami, I. Kakeya, H. Yamaguchi, T. Yamamoto, and K. Kadowaki, Characteristics of terahertz radiation emitted from the intrinsic Josephson junctions in high-T_c superconductor $Bi_2Sr_2CaCu_2O_{8+\delta}$, *Appl. Phys. Lett.* **95**(23), 232511, doi:10.1063/1.3269996 (2009).

[36] L. Ozyuzer, Y. Simsek, H. Koseoglu, F. Turkoglu, C. Kurter, U. Welp, A. E. Koshelev, K. E. Gray, W. K. Kwok, T. Yamamoto, K. Kadowaki, Y. Koval, H. B. Wang, and P. Muller, Terahertz wave emission from intrinsic Josephson junctions in high- Tc superconductors, *Supercond. Sci. Technol.* **22**(11), 114009 (7pp), doi:10.1088/0953-2048/22/11/114009 (2009).

[37] K. Kadowaki, M. Tsujimoto, K. Yamaki, T. Yamamoto, T. Kashiwagi, H. Minami, M. Tachiki, and R. A. Klemm, Evidence for a Dual-Source Mechanism of Terahertz Radiation from Rectangular Mesas of Single Crystalline $Bi_2Sr_2CaCu_2O_{8+\delta}$ Intrinsic Josephson Junctions, *J. Phys. Soc. Jpn.* **79**(2), 023703, doi:10.1143/JPSJ.79.023703 (2010).

[38] H. B. Wang, S. Guénon, B. Gross, J. Yuan, Z. G. Jiang, Y. Y. Zhong, M. Grünzweig, A. Iishi, P. H. Wu, T. Hatano, D. Koelle, and R. Kleiner, Coherent Terahertz Emission of Intrinsic Josephson Junction Stacks in the Hot Spot Regime, *Phys. Rev. Lett.* **105**(5), 057002, doi:10.1103/PhysRevLett.105.057002 (2010).

[39] S. Guenon, M. Gruenzweig, B. Gross, J. Yuan, Z. G. Jiang, Y. Y. Zhong, M. Y. Li, A. Iishi, P. H. Wu, T. Hatano, R. G. Mints, E. Goldobin, D. Koelle, H. B. Wang, and R. Kleiner, Interaction of hot spots and terahertz waves in $Bi_2Sr_2CaCu_2O_8$ intrinsic Josephson junction stacks of various geometry, *Phys. Rev. B* **82**(21), 214506, doi:10.1103/PhysRevB.82.214506 (2010).

[40] T. M. Benseman, A. E. Koshelev, K. E. Gray, W.-K. Kwok, U. Welp, K. Kadowaki, M. Tachiki, and T. Yamamoto, Tunable terahertz emission from $Bi_2Sr_2CaCu_2O_{8+\delta}$ mesa devices, *Phys. Rev. B* **84**, 064523, doi:10.1103/PhysRevB.84.064523 (2011).

[41] T. Kashiwagi, M. Tsujimoto, T. Yamamoto, H. Minami, K. Yamaki, K. Delfanazari, K. Deguchi, N. Orita, T. Koike, R. Nakayama, T. Kitamura, M. Sawamura, S. Hagino, K. Ishida, K. Ivanovic, H. Asai, M. Tachiki, R. A. Klemm, and K. Kadowaki, High Temperature Superconductor Terahertz Emitters: Fundamental Physics and Its Applications, *Jpn. J. Appl. Phys.* **51**(1), 010113, doi:10.1143/JJAP.51.010113 (2012).

[42] I. Kakeya, Y. Omukai, T. Yamamoto, K. Kadowaki, and M. Suzuki, Effect of thermal inhomogeneity for terahertz radiation from intrinsic Josephson junction stacks of $Bi_2Sr_2CaCu_2O_{8+\delta}$, *Appl. Phys. Lett.* **100**(24), 242603, doi:10.1063/1.4727899 (2012).

[43] M. Li, J. Yuan, N. Kinev, J. Li, B. Gross, S. Guénon, A. Ishii, K. Hirata, T. Hatano, D. Koelle, R. Kleiner, V. P. Koshelets, H. Wang, and P. Wu, Linewidth dependence of coherent terahertz emission from $Bi_2Sr_2CaCu_2O_8$ intrinsic Josephson junction stacks in the hot-spot regime, *Phys. Rev. B* **86**, 060505, doi:10.1103/PhysRevB.86.060505 (2012).

[44] M. Tsujimoto, K. Yamaki, K. Deguchi, T. Yamamoto, T. Kashiwagi, H. Minami, M. Tachiki, K. Kadowaki, and R. A. Klemm, Geometrical Resonance Conditions for THz Radiation from the Intrinsic Josephson Junctions in $Bi_2Sr_2CaCu_2O_{8+\delta}$, *Phys. Rev. Lett.* **105**(3), 037005, doi:10.1103/PhysRevLett.105.037005 (2010).

[45] M. Tsujimoto, T. Yamamoto, K. Delfanazari, R. Nakayama, T. Kitamura, M. Sawamura, T. Kashiwagi, H. Minami, M. Tachiki, K. Kadowaki, and R. A. Klemm, Broadly Tunable Subterahertz Emission from Internal Branches of the Current-Voltage Characteristics of Superconducting $Bi_2Sr_2CaCu_2O_{8+\delta}$ Single Crystals, *Phys. Rev. Lett.* **108**, 107006, doi:10.1103/PhysRevLett.108.107006 (2012).

[46] H. Koseoglu, F. Turkoglu, Y. Simsek, and L. Ozyuzer, The Fabrication of THz Emitting Mesas by Reactive Ion-Beam Etching of Superconducting Bi2212 with Multilayer Masks, *J. Supercond. Nov. Magn.* **24**, 1083, doi:10.1007/s10948-010-0859-9 (2011).

[47] R. A. Klemm and K. Kadowaki, Output from a Josephson stimulated terahertz amplified radiation emitter, *J. Phys.: Condens. Matter* **22**(37), 375701, doi:10.1088/0953-8984/22/37/375701 (2010).

[48] R. Klemm and K. Kadowaki, Angular Dependence of the Radiation Power of a Josephson STAR-emitter, *J. Supercond. Nov. Magn.* **23**, 613, doi:10.1007/s10948-010-0719-7 (2010).

[49] R. A. Klemm, E. R. LaBerge, D. R. Morley, T. Kashiwagi, M. Tsujimoto, and K. Kadowaki, Cavity mode waves during terahertz radiation from rectangular $Bi_2Sr_2CaCu_2O_{8+\delta}$ mesas, *J. Phys.: Condens. Matter* **23**(2), 025701, doi:10.1088/0953-8984/23/2/025701 (2011).

[50] K. Yamaki, M. Tsujimoto, T. Yamamoto, A. Furukawa, T. Kashiwagi, H. Minami, and K. Kadowaki, High-power terahertz electromagnetic wave emission from high-T_c superconducting $Bi_2Sr_2CaCu_2O_{8+\delta}$ mesa structures, *Opt. Express* **19**(4), 3193, doi:10.1364/OE.19.003193 (2011).

[51] H. B. Wang, S. Guénon, J. Yuan, A. Iishi, S. Arisawa, T. Hatano, T. Yamashita, D. Koelle, and R. Kleiner, Hot Spots and Waves in $Bi_2Sr_2CaCu_2O_8$ Intrinsic Josephson Junction Stacks: A Study by Low Temperature Scanning Laser Microscopy, *Phys. Rev. Lett.* **102**(1), 017006, doi:10.1103/PhysRevLett.102.017006 (2009).

[52] S. Guénon, Cryogenic Scanning Laser Microscopy: Investigation of large BSCCO mesas and development of a polarizing microscope, Ph.D. thesis, Tuebingen University (2011).

[53] R. Eichele, L. Freytag, H. Seifert, R. Huebener, and J. R. Clem, Two-dimensional imaging of hotspots in superconducting bridges by low-temperature scanning electron microscopy, *J. Low Temp. Phys.* **52**, 449, doi:10.1007/BF00682126 (1983).

[54] B. Mayer, T. Doderer, R. P. Huebener, and A. V. Ustinov, Imaging of one- and two-dimensional Fiske modes in Josephson tunnel junctions, *Phys. Rev. B* **44**(22), 12463, doi:10.1103/PhysRevB.44.12463 (1991).

[55] S. G. Lachenmann, T. Doderer, R. P. Huebener, D. Quenter, J. Niemeyer, and R. Pöpel, Spatially resolved study of the dynamics of Josephson tunnel junctions, *Phys. Rev. B* **48**(5), 3295, doi:10.1103/PhysRevB.48.3295 (1993).

[56] R. Gross and D. Koelle, Low temperature scanning electron microscopy of superconducting thin films and Josephson junctions, *Rep. Prog. Phys.* **57**(7), 651, doi:10.1088/0034-4885/57/7/001 (1994).

[57] T. Clauss, T. Uchida, M. Mossle, D. Koelle, and R. Kleiner, Imaging of μm wavelength collective cavity resonances in $Bi_2Sr_2CaCu_2O_{8+x}$ intrinsic Josephson junction stacks under microwave irradiation, *Appl. Phys. Lett.* **85**(15), 3166, doi:10.1063/1.1806272 (2004).

[58] D. Doenitz, R. Kleiner, D. Koelle, T. Scherer, and K. F. Schuster, Imaging of thermal domains in ultrathin NbN films for hot electron bolometers, *Appl. Phys. Lett.* **90**(25), 252512, doi:10.1063/1.2751109 (2007).

[59] C. Guerlich, S. Scharinger, M. Weides, H. Kohlstedt, R. G. Mints, E. Goldobin, D. Koelle, and R. Kleiner, Visualizing supercurrents in ferromagnetic Josephson junctions with various arrangements of 0 and π segments, *Phys. Rev. B* **81**, 094502, doi:10.1103/PhysRevB.81.094502 (2010).

[60] M. Wagenknecht, H. Eitel, T. Nachtrab, J. B. Philipp, R. Gross, R. Kleiner, and D. Koelle, Laser Microscopy of Tunneling Magnetoresistance in Manganite Grain-Boundary Junctions, *Phys. Rev. Lett.* **96**, 047203, doi:10.1103/PhysRevLett.96.047203 (2006).

[61] H. B. Wang, B. Y. Zhu, C. Gürlich, M. Ruoff, S. Kim, T. Hatano, B. R. Zhao, Z. X. Zhao, E. Goldobin, D. Koelle, and R. Kleiner, Fast Josephson vortex ratchet made of intrinsic Josephson junctions in $Bi_2Sr_2CaCu_2O_8$, *Phys. Rev. B* **80**, 224507, doi:10.1103/PhysRevB.80.224507 (2009).

[62] R. Werner, A. Y. Aladyshkin, S. Guénon, J. Fritzsche, I. M. Nefedov, V. V. Moshchalkov, R. Kleiner, and D. Koelle, Domain-wall and reverse-domain superconducting states of a Pb thin-film bridge on a ferromagnetic $BaFe_{12}O_{19}$ single crystal, *Phys. Rev. B* **84**, 020505, doi:10.1103/PhysRevB.84.020505 (2011).

[63] W. J. Skocpol, M. R. Beasley, and M. Tinkham, Self-heating hotspots in superconducting thin-film microbridges, *J. Appl. Phys.* **45**(9), 4054, doi:10.1063/1.1663912 (1974).

[64] H. Minami, N. Orita, T. Koike, T. Yamamoto, and K. Kadowaki, Continuous and reversible operation of Bi2212 based THz emitters just below T_c, *Physica C* **470, Supplement 1**(0), S822 , doi:10.1016/j.physc.2010.01.016 (2010).

[65] A. Yurgens, M. Torstensson, and D. Winkler, In situ detection of radiation and heat balance in large Bi2212 mesas, *Physica C* **470**(19), 818 , doi:10.1016/j.physc.2010.02.086 (2010).

[66] A. Yurgens, Temperature distribution in a large $Bi_2Sr_2CaCu_2O_{8+\delta}$ mesa, *Phys. Rev. B* **83**(18), 184501, doi:10.1103/PhysRevB.83.184501 (2011).

[67] S. Sakai, P. Bodin, and N. F. Pedersen, Fluxons in thin-film superconductor-insulator superlattices, *J. Appl. Phys.* **73**(5), 2411, doi:10.1063/1.353095 (1993).

[68] R. Kleiner, Two-dimensional resonant modes in stacked Josephson junctions, *Phys. Rev. B* **50**(10), 6919, doi:10.1103/PhysRevB.50.6919 (1994).

[69] R. Kleiner, T. Gaber, and G. Hechtfischer, Stacked long Josephson junctions in zero magnetic field: A numerical study of coupled one-dimensional sine-Gordon equations, *Phys. Rev. B* **62**(6), 4086, doi:10.1103/PhysRevB.62.4086 (2000).

[70] R. Kleiner, T. Gaber, and G. Hechtfischer, Stacked long Josephson junctions in external magnetic fields – a numerical study of coupled one-dimensional sine-Gordon equations, *Physica C* **362**(1-4), 29, doi:10.1016/S0921-4534(01)00643-8 (2001).

[71] M.-H. Bae, H.-J. Lee, and J.-H. Choi, Josephson-Vortex-Flow Terahertz Emission in Layered High-T_c Superconducting Single Crystals, *Phys. Rev. Lett.* **98**(2), 027002, doi:10.1103/PhysRevLett.98.027002 (2007).

[72] G. Hechtfischer, R. Kleiner, K. Schlenga, W. Walkenhorst, P. Müller, and H. L. Johnson, Collective motion of Josephson vortices in intrinsic Josephson junctions in $Bi_2Sr_2CaCu_2O_{8+y}$, *Phys. Rev. B* **55**, 14638, doi:10.1103/PhysRevB.55.14638 (1997).

[73] V. M. Krasnov, Terahertz electromagnetic radiation from intrinsic Josephson junctions at zero magnetic field via breather-type self-oscillations, *Phys. Rev. B* **83**(17), 174517, doi:10.1103/PhysRevB.83.174517 (2011).

[74] S. Lin and X. Hu, Possible Dynamic States in Inductively Coupled Intrinsic Josephson Junctions of Layered High-T_c Superconductors, *Phys. Rev. Lett.* **100**, 247006, doi:10.1103/PhysRevLett.100.247006 (2008).

[75] X. Hu and S. Lin, Three-dimensional phase-kink state in a thick stack of Josephson junctions and terahertz radiation, *Phys. Rev. B* **78**, 134510, doi:10.1103/PhysRevB.78.134510 (2008).

[76] A. E. Koshelev, Alternating dynamic state self-generated by internal resonance in stacks of intrinsic Josephson junctions, *Phys. Rev. B* **78**, 174509, doi:10.1103/PhysRevB.78.174509 (2008).

[77] S. Lin and X. Hu, Phase dynamics in intrinsic Josephson junctions and their electrodynamics, *Phys. Rev. B* **79**(10), 104507, doi:10.1103/PhysRevB.79.104507 (2009).

[78] X. Hu and S. Lin, Cavity phenomena in mesas of cuprate high-T_c superconductors under voltage bias, *Phys. Rev. B* **80**, 064516, doi:10.1103/PhysRevB.80.064516 (2009).

[79] Y. Nonomura, Stationary phase-kink states and dynamical phase transitions controlled by surface impedance in terahertz wave emission from intrinsic Josephson junctions, *Phys. Rev. B* **80**, 140506, doi:10.1103/PhysRevB.80.140506 (2009).

[80] S.-Z. Lin and X. Hu, Kink State in a Stack of Intrinsic Josephson Junctions in Layered High–T_c Superconductors and Terahertz Radiation, *J. Supercond. Nov. Magn.* **23**, 1025, doi:10.1007/s10948-010-0673-4 (2010).

[81] S.-Z. Lin and X. Hu, Response and amplification of terahertz electromagnetic waves in intrinsic Josephson junctions of layered high- T_c superconductor, *Phys. Rev. B* **82**(2), 020504, doi:10.1103/PhysRevB.82.020504 (2010).

[82] S.-Z. Lin and X. Hu, Stability of the kink state in a stack of intrinsic Josephson junctions, *Physica C* **470, Supplement 1**(0), S201 , doi:10.1016/j.physc.2009.11.042 (2010).

[83] X. Hu and S.-Z. Lin, Phase dynamics in a stack of inductively coupled intrinsic Josephson junctions and terahertz electromagnetic radiation, *Supercond. Sci. Technol.* **23**(5), 053001, doi:10.1088/0953-2048/23/5/053001 (2010).

[84] S.-Z. Lin and X. Hu, In-plane dissipation as a possible synchronization mechanism for terahertz radiation from intrinsic Josephson junctions of layered superconductors, *Phys. Rev. B* **86**, 054506, doi:10.1103/PhysRevB.86.054506 (2012).

[85] M. Tachiki, S. Fukuya, and T. Koyama, Mechanism of Terahertz Electromagnetic Wave Emission from Intrinsic Josephson Junctions, *Phys. Rev. Lett.* **102**(12), 127002, doi:10.1103/PhysRevLett.102.127002 (2009).

[86] S. Lin and X. Hu, Comment on "Mechanism of Terahertz Electromagnetic Wave Emission from Intrinsic Josephson Junctions", *ArXiv e-prints* (2009).

[87] V. M. Krasnov, Radiative annihilation of a soliton and an antisoliton in the coupled sine-Gordon equation, *Phys. Rev. B* **85**, 134525, doi:10.1103/PhysRevB.85.134525 (2012).

[88] H. Matsumoto, T. Koyama, and M. Machida, Electromagnetic waves in single- and multi-Josephson junctions, *Physica C* **468**, 654 , doi:10.1016/j.physc.2007.11.030 (2008).

[89] H. Matsumoto, T. Koyama, M. Machida, and M. Tachiki, Theory of THz emission from the intrinsic Josephson junction, *Physica C* **468**, 1899 , doi:10.1016/j.physc.2008.05.158 (2008).

[90] T. Koyama, H. Matsumoto, M. Machida, and K. Kadowaki, In-phase electrodynamics and terahertz wave emission in extended intrinsic Josephson junctions, *Phys. Rev. B* **79**, 104522, doi:10.1103/PhysRevB.79.104522 (2009).

[91] T. Koyama, H. Matsumoto, M. Machida, and Y. Ota, Multi-scale simulation for terahertz wave emission from the intrinsic Josephson junctions, *Supercond. Sci. Technol.* **24**(8), 085007, doi:10.1088/0953-2048/24/8/085007 (2011).

[92] H. Asai, M. Tachiki, and K. Kadowaki, Three-dimensional numerical analysis of terahertz radiation emitted from intrinsic Josephson junctions with hot spots, *Phys. Rev. B* **85**, 064521, doi:10.1103/PhysRevB.85.064521 (2012).

[93] A. E. Koshelev, Stability of dynamic coherent states in intrinsic Josephson-junction stacks near internal cavity resonance, *Phys. Rev. B* **82**, 174512, doi:10.1103/PhysRevB.82.174512 (2010).

[94] A. K. Jain, K. K. Likharev, J. E. Lukens, and J. E. Sauvageau, Mutual phase-locking in Josephson junction arrays, *Phys. Rep.* **109**(6), 309 , doi:10.1016/0370-1573(84)90002-4 (1984).

[95] P. Hadley, M. R. Beasley, and K. Wiesenfeld, Phase locking of Josephson-junction series arrays, *Phys. Rev. B* **38**, 8712, doi:10.1103/PhysRevB.38.8712 (1988).

[96] K. Wiesenfeld, S. P. Benz, and P. A. A. Booi, Phase-locked oscillator optimization for arrays of Josephson junctions, *J. Appl. Phys.* **76**(6), 3835, doi:10.1063/1.357387 (1994).

[97] A. A. Chernikov and G. Schmidt, Conditions for synchronization in Josephson-junction arrays, *Phys. Rev. E* **52**, 3415, doi:10.1103/PhysRevE.52.3415 (1995).

[98] T. Tachiki and T. Uchida, Influence of thermal noise on terahertz-wave radiation from intrinsic Josephson junctions, *Physica C* **471**(21–22), 1206 , doi:10.1016/j.physc.2011.05.160 (2011).

[99] Z. Tiege, M. Jing, C. Hanlin, Z. Xinjie, F. Lan, and Y. Shaolin, The model of Josephson junction arrays embedded in resonant cavities and the phase-locking properties, *Physica C* **469**(13), 785 , doi:10.1016/j.physc.2009.04.012 (2009).

[100] S.-Z. Lin, X. Hu, and L. Bulaevskii, Synchronization in a one-dimensional array of point Josephson junctions coupled to a common load, *Phys. Rev. B* **84**, 104501, doi:10.1103/PhysRevB.84.104501 (2011).

[101] L. N. Bulaevskii, A. E. Koshelev, and M. Tachiki, Shapiro steps and stimulated radiation of electromagnetic waves due to Josephson oscillations in layered superconductors, *Phys. Rev. B* **78**, 224519, doi:10.1103/PhysRevB.78.224519 (2008).

[102] I. Martin, G. B. Halasz, L. N. Bulaevskii, and A. E. Koshelev, Shunt-capacitor-assisted synchronization of oscillations in intrinsic Josephson junctions stack, *J. Appl. Phys.* **108**(3), 033908, doi:10.1063/1.3467962 (2010).

[103] L. N. Bulaevskii, I. Martin, and G. B. Halász, Intrinsic lineshape of Josephson radiation from layered superconductors, *Phys. Rev. B* **84**, 014516, doi:10.1103/PhysRevB.84.014516 (2011).

[104] A. Yurgens and L. N. Bulaevskii, Temperature distribution in a stack of intrinsic Josephson junctions with their CuO-plane electrodes oriented perpendicular to supporting substrate, *Supercond. Sci. Technol.* **24**(1), 015003, doi:10.1088/0953-2048/24/1/015003 (2011).

[105] A. L. Rakhmanov, S. E. Savel'ev, and F. Nori, Resonant electromagnetic emission from intrinsic Josephson-junction stacks in a magnetic field, *Phys. Rev. B* **79**, 184504, doi:10.1103/PhysRevB.79.184504 (2009).

[106] H. Eisele, M. Naftaly, and J. R. Fletcher, A simple interferometer for the characterization of sources at terahertz frequencies, *Meas. Sci. Technol.* **18**(8), 2623, doi:10.1088/0957-0233/18/8/038 (2007).

[107] M. Naftaly, P. Dean, R. Miles, J. Fletcher, and A. Malcoci, A Simple Interferometer for the Analysis of Terahertz Sources and Detectors, *IEEE J. Sel. Top. Quantum Electron.* **14**(2), 443, doi:10.1109/JSTQE.2007.912915 (2008).

[108] H. B. Wang, P. H. Wu, and T. Yamashita, Stacks of intrinsic Josephson junctions singled out from inside $Bi_2Sr_2CaCu_2O_{8+x}$ single crystals, *Appl. Phys. Lett.* **78**(25), 4010, doi:10.1063/1.1379065 (2001).

[109] H. B. Wang, P. H. Wu, J. Chen, K. Maeda, and T. Yamashita, Three-dimensional arrays of BiSrCaCuO-2212 intrinsic Josephson junctions and zero-crossing Shapiro steps at 760 GHz, *Appl. Phys. Lett.* **80**(9), 1604, doi:10.1063/1.1456555 (2002).

[110] V. P. Koshelets and S. V. Shitov, Integrated superconducting receivers, *Supercond. Sci. Technol.* **13**(5), R53, doi:10.1088/0953-2048/13/5/201 (2000).

[111] K. V. Kalashnikov, A. V. Khudchenko, P. N. Dmitriev, V. P. Koshelets, and A. M. Baryshev, Phase-locking of Flux-Flow Oscillator by Harmonic Mixer based on SIS junction, in 21th International Symposium on Space Terahertz Technology (2010).

[112] K. Kalashnikov, A. Khudchenko, A. Baryshev, and V. Koshelets, Harmonic mixer based on superconductor-insulator-superconductor tunnel junction, *J. Commun. Technol. El.* **56**, 699, doi:10.1134/S106422691106009X (2011).

[113] A. V. Gurevich and R. G. Mints, Self-heating in normal metals and superconductors, *Rev. Mod. Phys.* **59**(4), 941, doi:10.1103/RevModPhys.59.941 (1987).

[114] A. F. Volkov and S. M. Kogan, Physical Phenomena in Semiconductors with Negative Differential Conductivity, *Sov. Phys. Uspekhi* **11**(6), 881, doi:10.1070/PU1969v011n06ABEH003780 (1969).

[115] A. Yurgens, D. Winkler, N. V. Zavaritsky, and T. Claeson, Relationship between the Out-Of-Plane Resistance and the Subgap Resistance of Intrinsic Josephson Junctions in $Bi_2Sr_2CaCu_2O_{8+\delta}$, *Phys. Rev. Lett.* **79**(25), 5122, doi:10.1103/PhysRevLett.79.5122 (1997).

[116] Y. I. Latyshev, T. Yamashita, L. N. Bulaevskii, M. J. Graf, A. V. Balatsky, and M. P. Maley, Interlayer Transport of Quasiparticles and Cooper Pairs in $Bi_2Sr_2CaCu_2O_{8+\delta}$ Superconductors, *Phys. Rev. Lett.* **82**, 5345, doi:10.1103/PhysRevLett.82.5345 (1999).

[117] H. Asai, M. Tachiki, and K. Kadowaki, Proposal of terahertz patch antenna fed by intrinsic Josephson junctions, *Appl. Phys. Lett.* **101**(11), 112602, doi:10.1063/1.4751846 (2012).

[118] N. Orita, H. Minami, T. Koike, T. Yamamoto, and K. Kadowaki, Synchronized operation of two serially connected Bi2212 THz emitters, *Physica C* **470, Supplement 1**(0), S786 , doi:10.1016/j.physc.2010.01.051 (2010).

[119] M. Tsujimoto, H. Minami, K. Delfanazari, M. Sawamura, R. Nakayama, T. Kitamura, T. Yamamoto, T. Kashiwagi, T. Hattori, and K. Kadowaki, Terahertz imaging system using high-T_c superconducting oscillation devices, *J. Appl. Phys.* **111**(12), 123111, doi:10.1063/1.4729799 (2012).

[120] F. Turkoglu, H. Koseoglu, Y. Demirhan, L. Ozyuzer, S. Preu, S. Malzer, Y. Simsek, P. Müller, T. Yamamoto, and K. Kadowaki, Interferometer measurements of terahertz waves from $Bi_2Sr_2CaCu_2O_{8+\delta}$ mesas, *Supercond. Sci. Technol.* **25**(12), 125004, doi:10.1088/0953-2048/25/12/125004 (2012).

Appended publications

Publication 1

Coherent Terahertz Emission of Intrinsic Josephson Junction Stacks in the Hot Spot Regime

H. B. Wang,[1] S. Guénon,[2] B. Gross,[2] J. Yuan,[1] Z. G. Jiang,[3] Y. Y. Zhong,[3] M. Grünzweig,[2] A. Iishi,[1] P. H. Wu,[3] T. Hatano,[1] D. Koelle,[2] and R. Kleiner[2]

[1]*National Institute for Materials Science, Tsukuba 3050047, Japan*

[2]*Physikalisches Institut-Experimentalphysik II and Center for Collective Quantum Phenomena, Universität Tübingen, Auf der Morgenstelle 14, D-72076 Tübingen, Germany*

[3]*Research Institute of Superconductor Electronics, Nanjing University, Nanjing 210093, China*

(Received 15 April 2010; published 28 July 2010; publisher error corrected 28 July 2010)

We report on THz emission measurements and low temperature scanning laser imaging of $Bi_2Sr_2CaCu_2O_8$ intrinsic Josephson junction stacks. Coherent emission is observed at large dc input power, where a hot spot and a standing wave, formed in the ''cold'' part of the stack, coexist. By changing bias current and bath temperature, the emission frequency can be varied by more than 40%; the variation matches the Josephson-frequency variation with voltage. The linewidth of radiation is much smaller than expected from a purely cavity-induced synchronization. Thus, an additional mechanism seems to play a role. Some scenarios, related to the presence of the hot spot, are discussed.

DOI: 10.1103/PhysRevLett.105.057002 PACS numbers: 74.50.+r, 74.72.−h, 85.25.Cp

Phase synchronization is one of the prerequisites to use Josephson junction arrays as tunable high frequency sources [1–4]. While Nb based junctions are limited to frequencies below 1 THz—with applications up to 600 GHz [5]—intrinsic Josephson junctions (IJJs) [6,7] in $Bi_2Sr_2CaCu_2O_8$ are, at least in principle, able to operate up to several THz. Stacks of many junctions can be made, e.g., by patterning mesa structures on top of single crystals. For many years, investigations focused on small structures consisting of some 10 IJJs, with lateral sizes of a few μm. Here, with few exceptions [8,9], the IJJs in the stack tended to oscillate out-of-phase or were not synchronized at all. Experimental and theoretical studies included the generation of synchronous Josephson oscillations by moving Josephson vortices [8–13], the use of shunting elements [14–16], the excitation of Josephson plasma oscillations via heavy quasiparticle injection [17,18] or the investigation of stimulated emission due to quantum cascade processes [19]. High-frequency emission of unsynchronized intrinsic junctions has been observed up to 0.5 THz [20]. For more details, see Ref. [2].

Recently, coherent off-chip THz radiation with an extrapolated output power of some μW was observed from stacks of more than 600 IJJs, with lateral dimensions in the 100 μm range [21–25]. Phase synchronization involved a cavity resonance oscillating along the short side of the mesa. This radiation was studied theoretically in a series of recent papers, either based on vortex-type or plasmonic excitations, coupled to cavity modes [26–36], or on nonequilibrium effects caused by quasiparticle injection [37].

While THz emission was obtained at relatively low bias currents and moderate dc power input [21–25], using low temperature scanning laser microscopy (LTSLM) we have shown that standing wave patterns, presumably associated with THz radiation, can be obtained at high input power where, in addition, a hot spot (i.e., a region heated to above the critical temperature T_c) forms within the mesa structure [38]. Hot spot and waves seem to be correlated. The purpose of the present work is to investigate THz emission in this high power regime in detail, combining THz emission measurements and LTSLM. Apart from further clarifying the role of the hotspot, we are specifically interested in the question whether *coherent* radiation can be achieved in spite of the high temperatures involved.

By photolithogaphy and ion milling, 330×50 μm^2 large mesa structures were patterned on top of $Bi_2Sr_2CaCu_2O_8$ single crystals [39]. Below we discuss two samples, with thicknesses of 1 μm (sample 1) and 0.7 μm (sample 2), corresponding to stacks of, respectively, 670 and 470 IJJs. Mesa and base crystal were contacted by Au wires fixed with silver paste. Insulating polyimide was used to surround the mesa edge at which an Au wire was attached. In order to provide a load line for stable operation, the mesas were biased using a current source and variable resistor in parallel to the mesa. Contact resistances (around 5 Ω) are subtracted in the data discussed below. THz emission measurements were performed in Tsukuba; the samples were subsequently shipped to Tübingen for LTSLM. In total we detected THz emission from seven (out of a total of twelve) mesas on five different crystals. In one case (sample 1) emission was detected both at low bias and in the (high bias) hot spot regime; a disk shaped sample [40] radiated close to the hot spot nucleation point. Five others radiated in the hot spot regime only. Thus, the hot spot, although not a necessary ingredient for THz emission, seems to help considerably in increasing the yield of radiating samples.

The LTSLM setup is described in Ref. [38]. In brief, the laser beam is scanned across the sample surface. Local heating by 2–3 K in an area of a few μm^2 and about 0.5 μm in depth causes a change ΔV of the voltage V across the mesa serving as the contrast for the LTSLM

image. Standing waves can be imaged due to the beam-induced local change of the quality factor, leading to a strong signal ΔV at antinodes and a weak signal at nodes, located at the mesa edge, if ΔV is dominated by the magnetic field. The edge of a hot spot leads to a strong signal, while ΔV is small in the interior of the hot spot and in the "cold" part of the mesa [38]. The THz emission setup, allowing for bolometric detection and Fourier spectrometry, is described in detail in Ref. [39]. We note that numbers quoted below refer to *detected* power, to be extrapolated to 4π using the 0.04 sr aperture of the setup.

We first discuss THz emission data of sample 1, measured at $T = 20$ K. Figure 1(a) shows by solid circles the current voltage characteristic (IVC), as measured in Tsukuba. Starting from zero current, groups of junctions become resistive for $I > 20$ mA. At $I = 30$ mA the whole stack switches to the resistive state. Lowering the bias in this state the IVC is continuous down to ~10 mA where another switch to a current of ~8 mA occurs. As revealed by LTSLM, this switch corresponds to the disappearance of the hot spot present at high bias. For 3 mA $< I <$ 10 mA the IVC is continuous until further switches and hystereses appear due to the retrapping to the zero voltage state of some of the IJJs in the stack. Note that, due to different environmental noise, the switching currents to the resistive state differ for the two IVCs. However, the outermost branch, which is of interest here, nearly coincides for both IVCs, allowing for a fair, although not perfect, comparison of LTSLM and emission measurements. Figures 1(b) and 1(c) show the emission power detected by the bolometer as a function of, respectively, I and V. The largest response occurs in the high power (hot spot) regime and covers a current range from 10 mA up to ~30 mA. Here, V ranges from 0.83 to 1.13 V. If all N IJJs in the stack are *frequency* locked and participate in radiation we expect that the Josephson relation $V/N = \Phi_0 f$ holds, where Φ_0 is the flux quantum and f is the emission frequency. The Fourier spectrum, at given bias, revealed a single sharp emission line (with a resolution limited $\Delta f \approx 12$ GHz linewidth) continuously shifting with V. Two spectra are shown in Fig. 1(d). From these data we infer $N = 676 \pm 5$ in very good agreement with the 1 μm thickness of the mesa. The maximum detected power was 6 nW, corresponding to roughly 2 μW when extrapolating to 4π, even without taking additional losses into account. Thus the emitted power is comparable to the one quoted in Ref. [21]. Sample 1 also showed a bolometric response at low bias [c.f., grey (orange) lines in Figs. 1(b) and 1(c)]. Here, the detected power (~0.4 nW) was too low for Fourier spectrometry.

The different peaks visible in the radiometer data of Figs. 1(b) and 1(c) are likely to correspond to different cavity modes excited in the mesa (a similar case is shown in Fig. 3 of Ref. [38]). For the present sample, only for a bias at the main emission peak the standing wave pattern appeared. Figure 1(e) shows five LTSLM images at the bias points indicated in Fig. 1(b). The bright circular feature visible in the left part of the mesa is the hot spot. In all

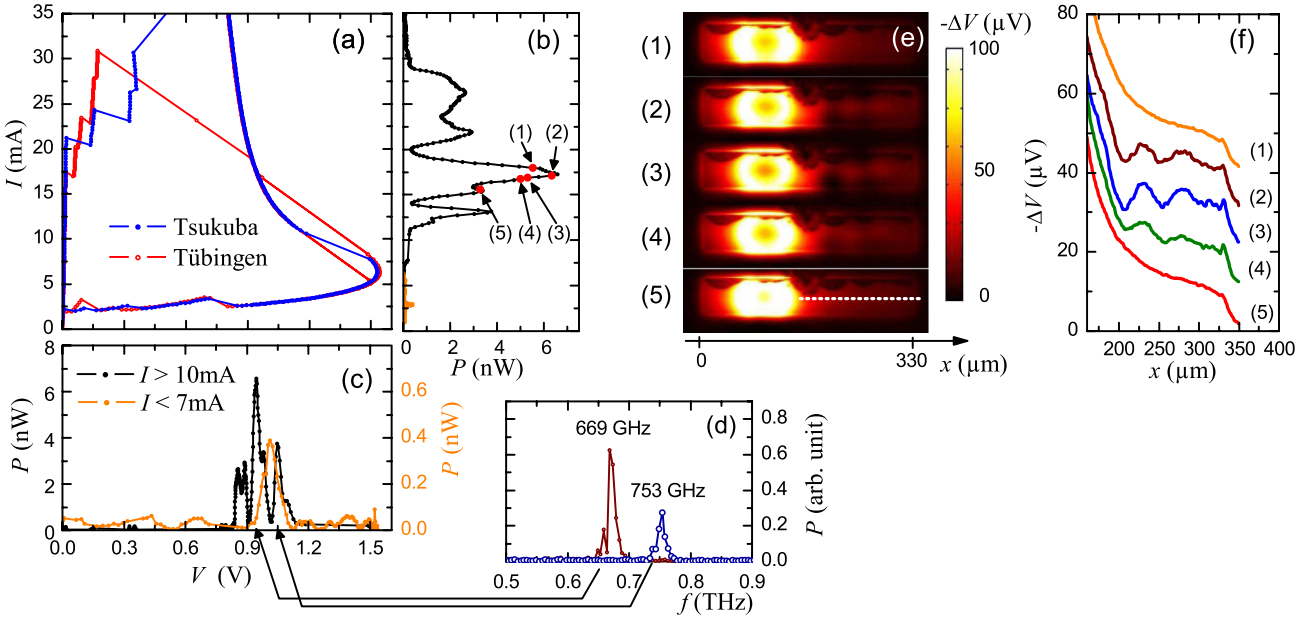

FIG. 1 (color online). Sample 1 at $T = 20$ K: IVCs (a) as measured in Tsukuba and in Tübingen. Emission power detected by the bolometer vs current (b) and voltage (c) at high bias ($I > 10$ mA) and low bias ($I < 7$ mA). Arrows labeled (1) to (5) indicate bias points of LTSLM images in (e). Fourier spectra (d) of emitted radiation taken at $V = 944$ mV, $I = 17.2$ mA (peak at 669 GHz), and $V = 1046$ mV, $I = 13.2$ mA (peak at 753 GHz). LTSLM images (e) and corresponding line scans (f) at the bias points indicated in (b). Line scans, taken along the center of the mesa, are shown only for the "cold" part of the mesa, c.f., dashed line in image (5) of graph (e). Adjacent line scans are vertically offset by 10 μV.

images there is a wavy dark feature at the upper edge of the mesa; this is caused by the polyimide covering the mesa edge. While, apart from the polyimide feature, LTSLM images (1) and (5) are smooth in the right part of the mesa, in images (2), (3), and (4) a wavy feature can be seen which is strongest along the center of the junction. Line scans in Fig. 1(f), taken in the right part of the mesa along the dashed line indicated in graph (5) of Fig. 1(e), show the wave feature in more detail. Maximum modulation is observed at bias point (3) which is close to the center of the main emission peak. Away from this bias, the wave amplitude decreases and becomes undetectable at bias points (1) and (5). This indicates a clear correlation between waves and emission. LTSLM did not reveal standing wave features outside the main emission peak (e.g., at the secondary emission peaks between 20 and 30 mA). However, this should not be interpreted as emission without waves, since, by experience, it is more difficult to see signals of waves than, e.g., of hot spots in LTSLM.

LTSLM images (2), (3), and (4) indicate that a standing wave, consisting of a half wave along the mesa width and about three half waves along its length, has been excited. From our data we infer wavelengths $\lambda_x \approx \lambda_y \approx 100\ \mu$m. Using $f = c(\lambda_x^{-2} + \lambda_y^{-2})^{1/2}$, with $f = 0.67$ THz, we find a mode velocity $c \approx 4.7 \times 10^7$ m/s, which is fully compatible with the *in-phase* mode velocity at the elevated temperatures (60–70 K) estimated for the cold part of the mesa [38,41]. Other (collective) mode velocities are by a factor of at least 2 lower. If the junctions would oscillate incoherently, the relevant mode velocity is the Swihart velocity $\bar{c} \approx 3 \cdot 10^5$ m/s, which is even lower. We thus conclude that all junctions oscillate in-phase.

We next discuss emission data of sample 2. IVCs, the bolometric response and Fourier spectrometer data are shown in Fig. 2. The largest emission was detected near a voltage of 456 mV [c.f., Figs. 2(b) and 2(c)]. Figure 2(d) shows Fourier spectra at $V = 440$ mV and $V = 451$ mV. From the emission peaks at, respectively, 531 and 554 GHz, we find the Josephson relation $V/N = \Phi_0 f$ to hold, with $N \approx 400$ (i.e., somewhat less than the 470 junctions expected from the mesa thickness). The 16 GHz linewidth is at the resolution limit. LTSLM revealed that a hot spot formed for $I > 25$ mA, covering about half of the mesa area for the bias where maximum emission was detected (increasing the current from 40 to 60 mA, the length of the cold part of the mesa decreased from about 200 to 150 μm). A standing wave pattern was vaguely visible, however, further analysis of the LTSLM data was prevented by a spurious strong response, presumably caused by additional IJJs switching to the resistive state when illuminated by the laser. Figure 3 shows emission data taken at different bath temperatures. The frequency range of detectable emission is shown in Fig. 3(a). Radiation was found between 15 and 58 K, with a maximum detected output power of about 5.5 nW near $T =$ 50 K [c.f., Fig. 3(b)]. At the lower temperatures, the emission frequencies varied continuously between 600 GHz and about 750 GHz; with increasing bath temperature the frequency of maximum emission power decreased, to about 450 GHz near 55 K; also, the frequency tunability by bias current decreased with increasing bath temperature, but still was on the order of 10% at 50 K. In the "low bias" case, the cavity resonance frequency is essentially fixed by the geometry of the mesa and may or may not be met by the frequency of the Josephson oscillations, set by the voltage V/N across each junction. In the hot spot regime (where V/N decreases with increasing bias current and bath temperature) the situation becomes more flexible (although, still, resonance is not possible for all cases).

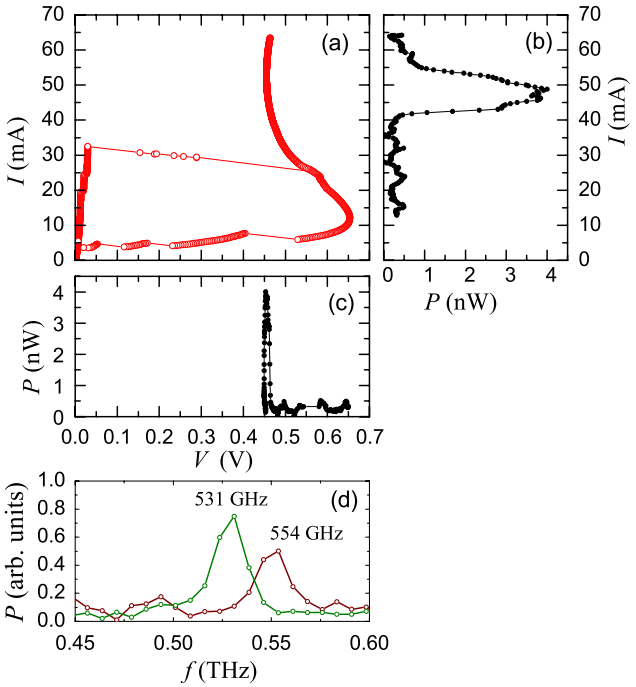

FIG. 2 (color online). Sample 2 at $T = 40$ K: IVCs (a), emission power vs current (b), and voltage (c). Panel (d) shows two spectra of the emitted power at $V = 440$ mV (peak at 531 GHz) and $V = 451$ mV (peak at 554 GHz).

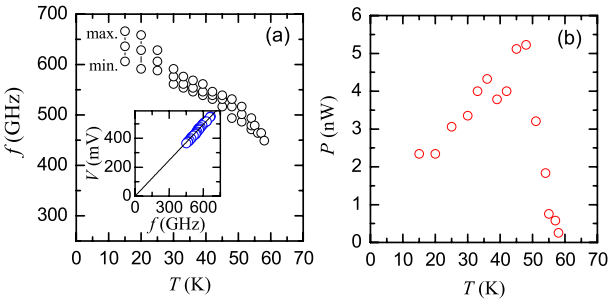

FIG. 3 (color online). Range of emission frequencies f (a) and detected emission power (b) of sample 2 vs bath temperature. Inset in (a) shows the voltage across the mesa as a function of f. Solid line in the inset is function $V = Nf\Phi_0$, with $N = 400$.

There are two factors contributing to this. First, the mode velocity c_1 decreases with increasing dc input power [38]. For example, at $T = 40$ K, over the resonance peak the input power varied from 18 to 26 mW; over such a range, at high temperatures, c_1 can decrease by some 20%–30%. Second, the hot spot changes the length L_c of the cold part of the mesa (at $T = 40$ K L_c changed by about 30% over the emission peak). Which of the two effects dominates depends on the effective temperature of the cold part and on the mode excited. In any case, the possibility to achieve resonance conditions over a comparatively wide frequency range allowed to test the Josephson relation $V/N = \Phi_0 f$, which we found to hold for all bias currents and temperatures, with $N = 400$ [c.f., inset of Fig. 3(a)].

The above results may show that, as in the low bias regime, also at high bias cavity modes are important for synchronizing the Josephson currents. However, there might be additional ingredients. For sample 1, the (resolution limited) 12 GHz linewidth of radiation is more than 50 times smaller than the oscillation frequency. For sample 2, $\Delta f/f < 0.03$ at $T = 40$ K. If, in the hot spot regime, Δf were determined by the quality factor Q of the cavity, one would require a $Q = f/\Delta f$ of at least 30–50. For a high Q cavity one would expect that clear resonant current steps are visible on the IVC which is not the case. For reference, one may analyze the IVCs of small-sized, few-junction stacks. For $T \approx 60$–70 K, these IVCs are only weakly hysteretic and Q is well below 10. The same will hold for the large mesas. One option for additional synchronization is that the hot spot interior effectively acts as a synchronizing element (RC or RLC shunt) [16,36,41,42]; another option is that (nonequilibrium) phenomena, in the spirit of Refs. [17–19,37], taking place at the hot spot edge, help in synchronizing the junctions, eventually leading to the small values of Δf observed. The fact that the Josephson-frequency-voltage relation holds rules out a purely quasiparticle related process, however, should not contradict a scenario of interacting Josephson and quasiparticle currents.

In summary, we have investigated THz emissison from intrinsic Josephson junction stacks by off-chip emission measurements and by low temperature scanning laser imaging. The stacks emit radiation coherently at high input power where a hot spot has formed. Here, standing wave patterns are observed pointing to the importance of cavity resonances for synchronization. By changing the mode velocity c_1, as well as the size of the cold part of the mesa, the hot spot allows one to vary the resonance frequency of the cavity. The linewidth of radiation, however, is too small to be determined by the cavity alone, pointing to an additional mechanism of synchronization.

We thank A. Yurgens, V. M. Krasnov, U. Welp, L. Ozyuzer, K. Kadowaki, I. Iguchi, K. Nakajima, and C. Otani for valuable discussions. Financial support by the JST/DFG strategic Japanese-German International Cooperative Program, and Grants-in-Aid for scientific research from JSPS is gratefully acknowledged.

[1] M. Darula, T. Doderer, and S. Beuven, Supercond. Sci. Technol. **12**, R1 (1999).
[2] X. Hu and S. Z. Lin, Supercond. Sci. Technol. **23**, 053001 (2010).
[3] F. Song *et al.*, Appl. Phys. Lett. **95**, 172501 (2009).
[4] I. Ottaviani *et al.*, Phys. Rev. B **80**, 174518 (2009).
[5] V. P. Koshelets and S. Shitov, Supercond. Sci. Technol. **13**, R53 (2000).
[6] R. Kleiner *et al.*, Phys. Rev. Lett. **68**, 2394 (1992).
[7] A. A. Yurgens, Supercond. Sci. Technol. **13**, R85 (2000).
[8] T. Clauss *et al.*, Appl. Phys. Lett. **85**, 3166 (2004).
[9] S. O. Katterwe and V. M. Krasnov, Phys. Rev. B **80**, 020502 (2009).
[10] R. Kleiner, Phys. Rev. B **50**, 6919 (1994).
[11] A. V. Ustinov and S. Sakai, Appl. Phys. Lett. **73**, 686 (1998).
[12] M. Machida *et al.*, Physica C (Amsterdam) **330**, 85 (2000).
[13] H. B. Wang *et al.*, Appl. Phys. Lett. **89**, 252506 (2006).
[14] H. B. Wang *et al.*, Appl. Phys. Lett. **77**, 1017 (2000).
[15] S. Madsen, G. Filatrella, and N. F. Pedersen, Eur. Phys. J. B **40**, 209 (2004).
[16] A. Grib and P. Seidel, Phys. Stat. Sol. (RRL) **3**, 302 (2009).
[17] K. Lee *et al.*, Phys. Rev. B **61**, 3616 (2000).
[18] E. Kume, I. Iguchi, and H. Takahashi, Appl. Phys. Lett. **75**, 2809 (1999).
[19] V. M. Krasnov, Phys. Rev. Lett. **97**, 257003 (2006).
[20] I. Batov *et al.*, Appl. Phys. Lett. **88**, 262504 (2006).
[21] L. Ozyuzer *et al.*, Science **318**, 1291 (2007).
[22] K. Kadowaki *et al.*, Physica C (Amsterdam) **468**, 634 (2008).
[23] L. Ozyuzer *et al.*, Supercond. Sci. Technol. **22**, 114009 (2009).
[24] H. Minami *et al.*, Appl. Phys. Lett. **95**, 232511 (2009).
[25] K. Kadowaki *et al.*, J. Phys. Soc. Jpn. **79**, 023703 (2010).
[26] L. N. Bulaevskii and A. E. Koshelev, Phys. Rev. Lett. **99**, 057002 (2007).
[27] A. E. Koshelev and L. N. Bulaevskii, Phys. Rev. B **77**, 014530 (2008).
[28] S. Lin and X. Hu, Phys. Rev. Lett. **100**, 247006 (2008).
[29] A. E. Koshelev, Phys. Rev. B **78**, 174509 (2008).
[30] X. Hu and S. Z. Lin, Phys. Rev. B **80**, 064516 (2009).
[31] R. A. Klemm and K. Kadowaki, arXiv:0908.4104.
[32] Y. Nonomura, Phys. Rev. B **80**, 140506 (2009).
[33] M. Tachiki, S. Fukuya, and T. Koyama, Phys. Rev. Lett. **102**, 127002 (2009).
[34] T. Koyama *et al.*, Phys. Rev. B **79**, 104522 (2009).
[35] S. Savel'ev *et al.*, Rep. Prog. Phys. **73**, 026501 (2010).
[36] N. Pedersen and S. Madsen, IEEE Trans. Appl. Supercond. **19**, 726 (2009).
[37] V. M. Krasnov, Phys. Rev. Lett. **103**, 227002 (2009).
[38] H. B. Wang *et al.*, Phys. Rev. Lett. **102**, 017006 (2009).
[39] See supplementary material at http://link.aps.org/supplemental/10.1103/PhysRevLett.105.057002 for details of sample preparation and the THz emission setup.
[40] S. Guénon *et al.*, arXiv:1005.2341.
[41] A. A. Yurgens (unpublished).
[42] M. Tachiki (unpublished).

Supplementary information to "Coherent THz emission of intrinsic Josephson junction stacks in the hot spot regime"

H.B. Wang,[1] S. Guénon,[2] B. Gross,[2] J. Yuan,[1] Z.G. Jiang,[3] Y.Y. Zhong,[3]
M. Grünzweig,[2] A. Iishi,[1] P.H. Wu,[3] T. Hatano,[1] D. Koelle,[2] and R. Kleiner[2]

[1] *National Institute for Materials Science, Tsukuba 3050047, Japan*
[2] *Physikalisches Institut – Experimentalphysik II and Center for Collective Quantum Phenomena, Universität Tübingen, Auf der Morgenstelle 14, D-72076 Tübingen, Germany*
[3] *Research Institute of Superconductor Electronics, Nanjing University, Nanjing 210093, China*

(Dated: June 10, 2010)

Contents

I. SAMPLE PREPARATION

For the experiments BSCCO single crystals were grown by the floating zone technique in a four lamp arc-imaging furnace. In the main paper we discuss results from two samples. Sample 1 was patterned on a crystal that was annealed in vacuum at 650 °C for 65 hours. It had a T_c of 86.6 K and a transition width ΔT_c of 1.5 K. Sample 2 was made on a crystal ($T_c = 87.6$ K, $\Delta T_c = 1.5$ K) annealed in vacuum at 600 °C for 72 hours. To provide good electrical contact the single crystals were cleaved in vacuum and a 30 nm Au layer was evaporated. Then, conventional photolithography was used to define the mesa size in the a-b plane (length 330 μm, width 50 μm for both samples). Ar ion milling yielded mesas with measured thicknesses of, respectively, 1 μm (sample 1) and 0.7 μm (sample 2) along the c-axis (corresponding to, respectively, stacks of 670 and 470 IJJs). Insulating polyimide was used to surround the mesa edge at which a Au wire was attached to the mesa by silver paste. Other Au wires were connected to the big single crystal pedestal as grounds. The voltage measured across the mesa includes the resistance of the contacting Au wires and the resistance between these wires and the mesa (4Ω for sample 1, 6.5Ω for sample 2). In the data discussed in the main paper this resistance is subtracted.

II. THE THZ EMISSION SETUP

The THz emission setup is shown schematically in Fig. 1 together with a sketch of the sample. The interferometer is similar to the one in Ref. 1, with the difference that a bolometer, with a 1 THz cut-off frequency, was used as a detector. The crystal is mounted in a continuous flow cryostat with a polyethylene window. The emitted radiation, chopped with a frequency of 13 Hz, is collected by a 90° off-axis parabolic mirror (2" diameter, focal length 100 mm) and deflected towards two lamellar split mirrors dividing the incoming radiation into two beams with almost the same intensity. A phase difference is introduced

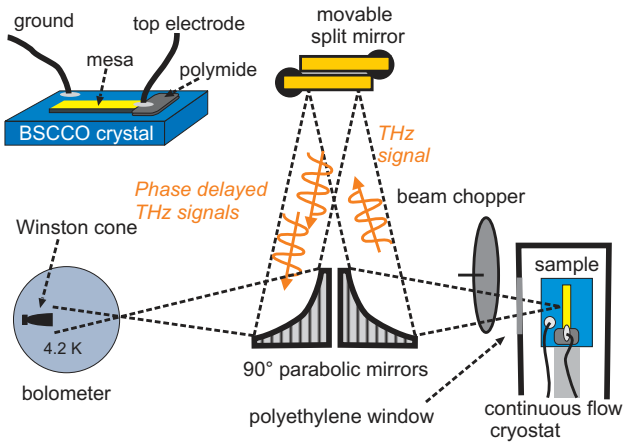

Figure 1: (color online). Schematic of the THz emission setup together with a sketch of the sample.

by moving one of these mirrors with a translation stage. Via a second parabolic mirror the radiation is deflected to the bolometer (gauged by using a Gunn oscillator for reference). A 1 THz cut-off type filter is used in front of the bolometer. The numbers we quote below are based on the *detected* power, ignoring additional losses (by a factor of 2–5) from the continuous flow cryostat window and the mirrors. The solid angle of our setup, defined by the aperture of the Winston cone in front of the bolometer, is 0.04 sr. The frequency resolution, depending on the maximum mirror displacement, is 10–15 GHz.

[1] H. Eisele, M. Naftaly, and J. Fletcher, Meas. Sci. Technol. **18**, 2623 (2007).

Publication 2

Interaction of hot spots and terahertz waves in $Bi_2Sr_2CaCu_2O_8$ intrinsic Josephson junction stacks of various geometry

S. Guénon,[1] M. Grünzweig,[1] B. Gross,[1] J. Yuan,[2] Z. G. Jiang,[3] Y. Y. Zhong,[3] M. Y. Li,[3] A. Iishi,[2] P. H. Wu,[3] T. Hatano,[2] R. G. Mints,[4] E. Goldobin,[1] D. Koelle,[1] H. B. Wang,[2,*] and R. Kleiner[1,†]

[1]*Physikalisches Institut, Experimentalphysik II and Center for Collective Quantum Phenomena, Universität Tübingen, Auf der Morgenstelle 14, D-72076 Tübingen, Germany*

[2]*National Institute for Materials Science, Tsukuba 3050047, Japan*

[3]*Research Institute of Superconductor Electronics, Nanjing University, Nanjing 210093, China*

[4]*The Raymond and Beverly Sackler School of Physics and Astronomy, Tel Aviv University, Tel Aviv 69978, Israel*

(Received 7 May 2010; revised manuscript received 16 September 2010; published 6 December 2010)

At high enough input power in stacks of $Bi_2Sr_2CaCu_2O_8$ intrinsic Josephson junctions a hot spot (a region heated to above the superconducting transition temperature) coexists with regions being still in the superconducting state. In the "cold" regions cavity resonances can occur, synchronizing the ac Josephson currents and giving rise to strong and stable coherent terahertz (THz) emission. We investigate the interplay of hot spots and standing electromagnetic waves by low-temperature scanning laser microscopy and THz emission measurements, using stacks of various geometries. Standing electromagnetic wave patterns and THz emission are observed for a disk-shaped sample. The growth of a hot spot with increasing input power is monitored by small detector junctions surrounding a large rectangular mesa. For two rectangular mesas equipped with two current injectors and one arrow-shaped structure we show that the standing wave can be turned on and off in various regions of the stack structure, depending on the hot-spot position. The results support the picture of the hot spot acting as a reflective termination of the cavity, formed by the cold part of the mesa.

DOI: 10.1103/PhysRevB.82.214506 PACS number(s): 74.50.+r, 74.72.−h, 85.25.Cp

I. INTRODUCTION

Josephson junctions are attractive for the generation of high-frequency electromagnetic radiation because the frequency of emission is tunable by the voltage across the device. A Nb-based Josephson flux flow device was used as a local oscillator in a highly optimized integrated superconducting receiver operating up to about 600 GHz.[1] In the oscillator a row of Josephson fluxons is created by applying a magnetic field parallel to the junction barrier. The fluxons move along the barrier layer exciting junction cavity resonances. The emission frequency corresponds to the cavity resonance frequency and is tunable by choosing different resonances. In this on-chip design the Josephson oscillator delivers a power of a few microwatt to a superconducting mixer. However, the *off-chip* output power obtained from more typical junctions is only in the nanowatt range. Thus, to obtain a reasonable power output, arrays of many junctions should be synchronized.[2–7] While Nb-based junctions are limited by the superconducting energy gap to frequencies below 1 THz, intrinsic Josephson junctions (IJJs) (Refs. 8–10) in $Bi_2Sr_2CaCu_2O_8$ (BSCCO) are, at least in principle, able to operate up to several terahertz (THz). Stacks of many junctions can be made, e.g., by patterning mesa structures on top of single crystals. For many years, investigations focused on small structures consisting of some 10 IJJs with lateral sizes of a few micron.[11–23] Here, the IJJs in the stack most often tended to oscillate out of phase or were not synchronized at all.

Recently, coherent off-chip THz radiation with an extrapolated output power of some microwatt was observed from stacks of more than 600 IJJs with lateral dimensions in the 100 μm range.[24] Phase synchronization involved a cavity resonance oscillating along the short side of the mesa. In contrast to many previous experiments no external magnetic field was applied to create Josephson fluxons. This finding triggered numerous experimental[25–36] and theoretical studies,[5,37–50] the latter being based on either Josephson vortex-type or plasmonic excitations, coupled to cavity modes,[5,37–46,49,50] on synchronization via shunting networks[48,51,52] or on nonequilibrium effects caused by quasiparticle injection.[47]

Many of the experimental results were obtained at relatively low-bias currents through the mesa and moderate dc power input (<1 mW).[24–28,34–36] Under such conditions there is no severe self-heating of the mesa, and the THz emission observed presumably can be described by more or less standard Josephson physics and electrodynamics. On the other hand, one also observes strong THz emission at high input power, where self-heating is severe.[32,33] Basically all junctions in the stack oscillate coherently also in this high-bias regime, which has the advantage of allowing a stable and reproducible bias. By contrast, at low bias some of the junctions in the mesa can switch between the resistive state and the zero voltage state, causing multibranched hysteretic current-voltage characteristics.

For 330-μm-long rectangular mesa structures of widths between 30 and 80 μm low-temperature scanning laser microscopy (LTSLM) revealed that in the high-bias regime a hot spot,[53,54] i.e., a region heated to above the critical temperature T_c, forms.[31,32] It effectively separates the stack into a "cold" region, which is superconducting, and a hot part, which is in the normal state. The temperature of the cold part was estimated to be of order 50–70 K.[31,32,51] At certain values of bias current, where also the THz emission is strongest, the hot spot is accompanied by standing-wave patterns. One

TABLE I. Parameters of the samples investigated: shape, in-plane dimensions, thickness, critical temperature, transition width, and annealing conditions. Sample 2 in addition was surrounded by 10 μm wide, quadratic mesa structures consisting of 15–20 IJJs.

Sample	Shape	In-plane dimensions	Thickness (μm)	T_c (K)	ΔT_c (K)	Annealing conditions
1	Disk	200 μm diameter	0.9	86.6	1.5	600 °C, vacuum, 65 h
2	Rectangular	330×70 μm^2	0.5	87.6	1.5	600 °C, vacuum, 72 h
3	Rectangular	330×80 μm^2	1	83	1.5	600 °C, 1 atm, 99% Ar, 1% O_2, 48 h
4	Rectangular	330×70 μm^2	0.8	86.8	1.1	600 °C, 1 atm, 99% Ar, 1% O_2, 48 h
5	Arrow	Subsections 300×50 μm^2	1	87.6	1.5	600 °C, vacuum, 72 h

thus faces THz generation in a highly nonequilibrium situation. The underlying physics may differ from the low-bias case, requiring detailed investigation.

In the low-bias case the emission frequency is essentially fixed by the mesa geometry. By contrast, in the high-bias regime it can be varied by up to 40% by changing the bias current and the bath temperature.[32] The variation matches the Josephson-frequency voltage relation, showing that Josephson currents are at least a major source of the emission observed. Two factors contribute to the tunability at given bath temperature. First, it was found that, when increasing the bias current, the mode velocity of the cavity resonance decreases.[31] Second, the size of the hot spot grows with increasing bias current and, correspondingly, the size of the cold part of the mesa shrinks. Assuming that electromagnetic waves are reflected at the hot-spot boundary one faces a cavity with variable size and mode velocity and thus variable resonance frequency. Unfortunately, in the experiments reported in Refs. 31 and 32 these two factors were varied by only one quantity, namely, the bias current injected into the mesa.

In this paper we present a study of mesa structures of different geometry, in order to provide more information on hot-spot and wave formation and to examine possibilities to manipulate both hot spot and waves in a controlled way. For a rectangular mesa the standing-wave patterns visible in LTSLM basically consist of a sequence of straight stripes. It is hard to decide whether the electric or the magnetic part of the cavity mode is imaged. One might even argue that the stripes do not originate from an electromagnetic cavity mode. By contrast, a cylindrical mesa produces nontrivial resonance patterns.[41] In Sec. III A we will show LTSLM and THz emission data for such a structure. As we will see, the pattern observed is fully compatible with an electromagnetic standing wave. The data indicate that the magnetic part of the cavity mode is imaged. Regarding hot-spot formation, the case of the BSCCO mesa structures is quite different from the "standard case" in thin-film bridges, where one observes hot spots as an interplay between the zero-voltage superconducting state below T_c and the resistive state above T_c.[53,54] Here, typically, current flow is along a thin-film layer. In our case we have to consider a stack of tunnel junctions biased in their *resistive state* also below T_c. For conventional superconducting tunnel junctions, instead of hot-spot formation, the appearance of superconducting regions with suppressed energy gap upon strong current injection has been discussed.[55–59] One should thus address this scenario as an alternative, i.e., one should consider the case where the "hot-spot" area observed in LTSLM is still superconducting. In Sec. III B we will discuss data for a rectangular mesa which is surrounded by small detector mesas. The critical currents of these detector mesas approach zero when the front of the hot spot passes by. This is consistent with the hot-spot interpretation but hard to explain in the suppressed gap state scenario. We then turn to rectangular mesa structures that were contacted by two current injection points (Sec. III C). This configuration allowed to change the hot-spot position and to switch on and off standing-wave patterns in different sections of the mesa at nearly constant input power. The results support the picture of a variable-size cavity adjusted by the hot-spot position. Finally, in Sec. III D we will show data for an arrow-shaped mesa. Although equipped with only one current injector the geometry allowed to independently excite standing waves in various segments of the arrow, further confirming the picture of variable-size cavities terminated by the hot spot.

The paper is organized as follows. In Sec. II samples are characterized and the measurement techniques are described. Data for the different mesa structures are presented in Sec. III. Conclusions are given in Sec. IV.

II. SAMPLE PREPARATION AND MEASUREMENT TECHNIQUES

For the experiments BSCCO single crystals were grown by the floating zone technique in a four lamp arc-imaging furnace. Annealing conditions and the superconducting transition temperatures of the crystals used are listed in Table I. To provide good electrical contact the single crystals were cleaved in vacuum and a 30 nm Au layer was evaporated. Then, conventional photolithography and Ar ion milling was used to prepare mesas of various shapes and thicknesses. Insulating polyimide was used to surround the mesa edges at which Au wires were attached to the mesa by silver paste. Other Au wires were connected to the big single-crystal pedestal as grounds. Note that, since the large base crystals are not atomically flat, the foot of the mesa and the ground will, in general, be located in different CuO_2 layers. Consequently there can be a few additional IJJs of large size but not well-defined properties; partially, these layers are etched during ion milling, partially, they are shunted by the Au layer. While the parasitic IJJs contribute only marginally to the current-voltage characteristics (IVCs) of the mesas they can, at suf-

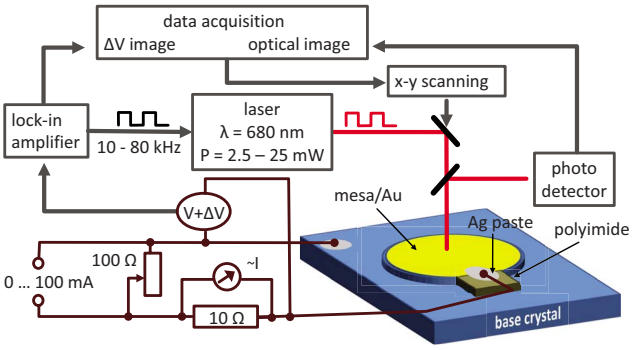

FIG. 1. (Color online) The LTSLM imaging system together with a sketch of a disk-shaped mesa.

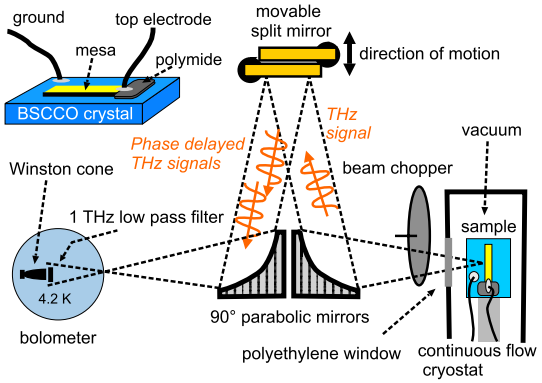

FIG. 2. (Color online) Schematic of the THz emission setup together with a sketch of a rectangular mesa contacted on its right edge.

ficiently high bias, strongly contribute to the LTSLM signal. Examples will be given.

Below we discuss results from five samples, cf. Table I. Sample 1 was disk shaped with a diameter of 200 μm and a thickness of 0.9 μm, corresponding to a stack of 600 IJJs. The mesa was contacted near its outer edge, as sketched in Fig. 1. The 330×70 μm^2 large and 0.5-μm-thick rectangular sample 2 was contacted on the right edge, cf. inset in Fig. 6(a). It was surrounded by much smaller, 10-μm-wide, square-shaped mesa structures consisting of 15–20 IJJs. To fabricate the detector mesas a U-shaped "mesa" was etched together with the main mesa. This structure surrounds the main mesa and is visible as a dark stripe in the inset of Fig. 6(a). Further etching of this structure yielded the small mesa structures. Subsequently the small mesas and the main mesa were contacted with a Au layer. The distance of the small mesas (used for thermometry) to the main mesa was 10 μm. The rectangular samples 3 and 4 were 330 μm long, 1 μm thick and, respectively, 80 μm and 70 μm wide. They were contacted at two edges, cf. Figs. 7(a) and 8(a). The arrow-shaped sample 5, cf. Fig. 9, consisted of three 330 μm long and 50 μm wide rectangular subsections rotated by 60° relative to each other and connected at one end (the top of the arrow). The mesa thickness was 1 μm. It was contacted at the end of the main stem of the arrow.

In order to provide a load line for stable operation, the mesas were biased using a current source and variable resistor in parallel to the mesa, see Fig. 1. The voltage measured across the mesa includes the resistance of the contacting Au wires and the resistance between these wires and the mesa. In the data discussed below this resistance (typically around 5 Ω) is subtracted.

LTSLM measurements were performed in Tübingen. For sample 1 additional THz emission measurements were performed in Tsukuba. The LTSLM setup is shown schematically in Fig. 1. The beam of a 25 mW laser diode (wavelength 680 nm) is modulated at frequencies between 10 and 80 kHz, deflected by a scanning unit and focused onto the sample surface. The incoming laser power was typically attenuated by a factor of 10 using optical attenuators. Furthermore, the gold layer covering the mesa surface reflects at least 90% of the laser light, resulting in an absorbed CW laser power of order 100 μW. The laser spot size is 1–2 μm. Simulations, performed using COMSOL simulation software, revealed that the laser spot locally heats by 2–3 K an area of a few square micron and about 0.5 μm in depth.[31] In this area both the in-plane and out-of-plane critical supercurrent densities and resistivities change, causing a global change $\Delta V(x,y)$ in the voltage V across the mesa. Here, x and y denote the in-plane position of the laser spot. $\Delta V(x,y)$ is detected using lock-in techniques and serves as the contrast for the LTSLM image. Below, when quoting ΔV, for simplicity we will omit the coordinates (x,y). Using the reflected laser light also optical images can be generated.

In general, an LTSLM image of a mesa will show some background signal arising, e.g., from the overall reduction in the c axis resistivity with increasing temperature. On top of that standing waves can be imaged due to the beam-induced local change in the quality factor, leading to a strong signal ΔV at antinodes and a weak signal at nodes. One observes the time-averaged intensity of either the electric or the magnetic field component. Which component dominates may depend on both the bias and the bath temperature. For Nb tunnel junctions the response was shown to primarily arise from the magnetic field component.[60] For IJJ stacks the situation is less clear; however, below we will show an example (sample 1) where the LTSLM response was most likely due to the magnetic field. Regarding the hot spot there is a strong signal ΔV when the laser beam illuminates its edge, i.e., the superconducting/normal boundary.[31,61] By contrast, ΔV is small in the interior of the hot spot and in the cold part of the mesa. A typical signature of the hot spot is that its size grows with increasing dc power IV dissipated in the sample. Here, I denotes the dc current through the mesa. For wide mesas having widths of 70 μm or more, the hot spot is circular and, when its diameter is large enough, is seen as a ring-shaped structure.[31] For narrower mesas the hot spot often is "one dimensional," i.e., its boundaries form straight lines parallel to the short side of the mesa.[31,32] Below, examples for both cases will be shown.

The THz emission setup is shown schematically in Fig. 2 together with a sketch of a rectangular mesa. The interferometer is similar to the one in Ref. 62 with the difference that in our case a bolometer is used as a detector. The crystal is mounted in vacuum on the cold finger of a continuous flow He cryostat. A polyethylene window is used which is trans-

parent at the frequencies of interest. The emitted radiation, chopped with a frequency of 13 Hz, is collected by a 90° off-axis parabolic mirror (2″ diameter, focal length 100 mm) and deflected toward two lamellar split mirrors dividing the incoming radiation into two beams with almost the same intensity. A phase difference is introduced by moving one of these mirrors with a translation stage. Via a second parabolic mirror the radiation is deflected to the bolometer. A 1 THz low-pass filter is used in front of the Winston cone. This setup can be used in two modes. In the first mode the emitted power of the mesa is recorded for different bias currents. The mirror is in the neutral position (i.e., no phase difference is introduced) for this purpose. In the second mode the autocorrelation function (emitted power vs mirror position) is acquired, which is mapped into a spectrum using fast Fourier transformation. The numbers we quote below are based on the *detected* power, ignoring additional losses (by a factor of 2–5) from the continuous flow cryostat window and the mirrors. The solid angle of our setup, defined by the aperture of the Winston cone in front of the bolometer, is 0.04 sr. The frequency resolution, depending on the maximum mirror displacement, is 10–15 GHz.

III. RESULTS

A. Standing waves, hot-spot formation, and THz emission in a disk-shaped mesa

We first discuss data of disk-shaped sample 1 which had a radius a of 100 μm. Disk-shaped mesa structures have been analyzed theoretically and considered promising for THz emission in Ref. 41. THz emission from such a structure is reported in Ref. 35. In our context we are, on one hand, interested in imaging the corresponding wave patterns. On the other hand the question arises whether or not hot-spot formation is supporting cavity modes in this geometry.

In the disks, the c axis electric field component is given by the time derivative of a term $\tilde{P}$ describing Josephson plasma oscillations at frequency ω and having the form $\tilde{P}(r,t)=Ag_{mn}(r)\sin(\omega t+\varphi)$ with some amplitude A and some initial phase φ. In cylindrical coordinates (ρ,ϕ) the function $g_{mn}(r)=J_m(\chi^c_{mn}\rho/a)\cos(m\phi)$, where χ^c_{mn} is the nth zero of the first derivative of Bessel function J_m. The in-plane magnetic field is proportional to the curl of $\tilde{P}\cdot e_z$ with the out-of-plane unit vector e_z. The resonance frequency is given by $c'\chi^c_{mn}/2\pi a$ with the mode velocity c'.

Figure 3(a) shows by blue dots connected by a solid line the IVC of sample 1, as measured during LTSLM at $T=19$ K (the IVC shown by green dots connected by a dotted line will be discussed below in the context of THz emission measurements). For bias currents between 22 and 25 mA there are instabilities on the resistive branch indicative of hot-spot formation.[31] In addition, some of the junctions may switch between the resistive state and the zero voltage state. Indeed one can trace out several different branches in this region by sweeping the bias current back and forth. Figures 3(b)–3(f) show LTSLM images taken at different bias points. The bias lead, attached on the left side of the disk, as sketched in the inset of Fig. 3(a), is visible in all LTSLM

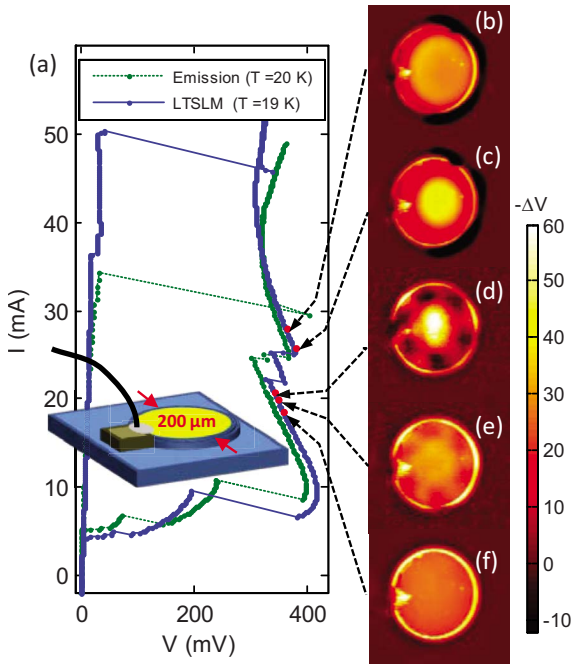

FIG. 3. (Color online) (a) IVCs, taken for LTSLM (blue dots connected by solid line) and for THz emission measurements (green dots connected by dotted line) and [(b)–(f)] LTSLM images of disk-shaped sample 1. Bias points where the images have been taken are indicated by arrows. Inset in (a) shows a sketch of the disk including the contacting lead.

images. Further, there is a strong edge signal arising because the mesas edges are not covered by gold; as a consequence, the laser-beam-induced temperature rise at the edge is larger than in the mesa interior. Apart from the signal caused by the wire and the edge effects, for currents below 19 mA the images are smooth, with $\Delta V<0$. Figure 3(f) shows an example. At $I=19.4$ mA a cartwheel-like pattern appears, having 6 "spokes," cf. Fig. 3(e). In the center of the disk as well as on the spokes ΔV does not differ much to the case of Fig. 3(f). In between the spokes $|\Delta V|$ is lower than the background, i.e., a positive signal is added. At $I=21$ mA, in addition to the cartwheel-like pattern a strong negative signal appears in the center of the disk, cf. Fig. 3(d). This signal grows with increasing bias current, cf. Figs. 3(c) and 3(b), and is indicative of a hot spot. As already mentioned, in LTSLM the *edge* of a hot spot produces the strongest response. Thus, the actual hot region in Fig. 3(d) is presumably still very small and the bright spot shows the transition region to the cold part of the mesa. In Fig. 3(c) $|\Delta V|$ still has maximum near the center of the disk while in Fig. 3(b) a dip appears near the center; the hot-spot signal becomes ring shaped.

The cartwheel-like pattern was visible for bias currents between 19 and 22 mA and is indicative of an $m=3$, $n=1$ cavity mode having six nodes in azimuthal direction. Here, $\chi^c_{mn}=4.2$. In Fig. 4 we compare the measured patterns [Figs. 4(a) and 4(b)] to calculated cavity modes [Figs. 4(c) and 4(d)]. In Fig. 4(c) we have plotted the square of the amplitude of the electric field component, Fig. 4(d) shows the corresponding plot for the magnetic field. For the compari-

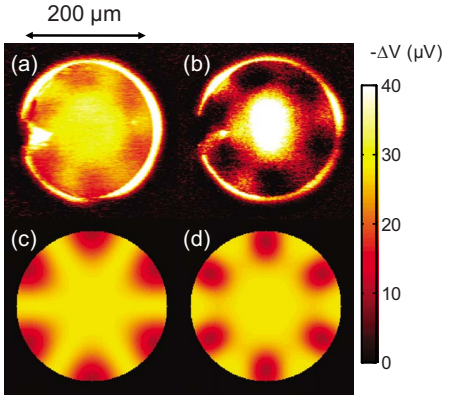

FIG. 4. (Color online) [(a) and (b)] LTSLM images, as measured at $I=19.4$ mA and $I=21$ mA, respectively, in comparison to the calculated distributions of the squares of (c) electric field and (d) magnetic field of the $m=3$, $n=1$ cavity mode. Color scale for the theoretical plots is made such that zeroes appear bright (yellow) and maxima appear dark (red).

son to the LTSLM data the color scale of the theoretical plots is chosen such that the zeroes of the standing waves appear in bright (yellow) color while the maxima are dark (red). For the magnetic field pattern, Fig. 4(d), one notes that the center region is hexagon shaped while the darkest regions are centered inside the disk. By contrast the electric field pattern, Fig. 4(c), is star shaped in the center of the disk while the maxima (dark regions) appear close to the outer perimeter. Figure 4(a) is an enlargement of Fig. 3(e), plotted on an enhanced color scale. The center part of the wave feature resembles the hexagon-shaped central structure of the magnetic field part of the cavity resonance. In Fig. 4(a) the dark regions seem to be located closer to the outer perimeter than in Fig. 4(d). However, the strong edge signal in LTSLM complicates the analysis of structures appearing close to the outer perimeter. Thus, we consider the structures appearing in the inner part of the disk more relevant and conclude that the magnetic field part of the cavity mode has been imaged in Fig. 4(a). In the LTSLM image Fig. 4(b), which is an enlargement of Fig. 3(d), the dark sections are more clearly located inside the disk and the hexagon structure is still visible in spite of the bright hot-spot feature. We thus conclude that also here the magnetic field has been imaged. Note that in the presence of a hot spot located in the center of the disk the superconducting part may be viewed as an *annular* mesa with an inner radius a_i corresponding to the hot-spot radius. The resonance mode imaged still corresponds to a $m=3$ mode. Since the $m=3$ mode has a zero in the center of the disk, for a small hot spot the standing-wave pattern visible in LTSLM outside the hot-spot region will not differ much from the case without hot spot. For a ring-shaped mesa the resonance frequencies are given by $c'\chi_{mn}/2\pi a$, where the coefficient χ_{mn} depends on the ratio a_i/a, cf. Eq. (15) in Ref. 41. Depending on n and m the resonance frequencies can either increase or decrease as a function of a_i/a. For the special case of a $m=3$, $n=1$ mode, χ_{31} is almost constant for $a_i/a < 0.3$; for $a_i/a=0.3$, $\chi_{31}=4.18$. For larger ratios of a_i/a, χ_{31} starts to decrease, having, e.g., a value of 3.75 for $a_i/a=0.6$. For the case of Fig. 3(d), $a_i/a \ll 1$, and thus $\chi_{mn} \approx \chi^c_{mn}$.

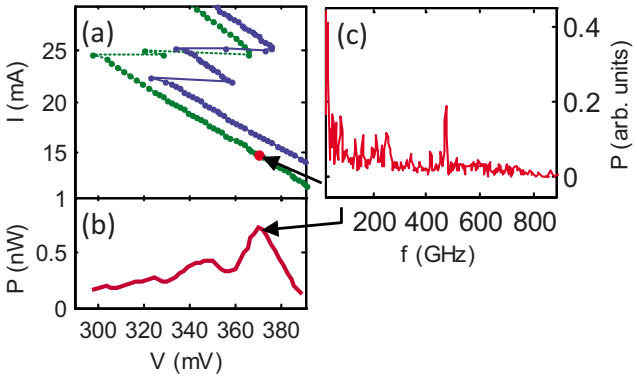

FIG. 5. (Color online) THz emission from sample 1: (a) enlargement of the IVC of Fig. 4(a) in the current and voltage range where emission has been detected; (b) detected emission power vs voltage across mesa; and (c) Fourier spectrum at a bias of 14.9 mA and 370 mV.

Next we analyze the THz emission detected from sample 1. Figure 5(a) shows an enlargement of the IVC of Fig. 3(a) for the current and voltage range where emission has been found (the same range where the cavity resonance was seen in LTSLM; note, however, that the IVCs measured in Tübingen and in Tsukuba slightly differ from each other, making it difficult to precisely assign LTSLM images and emission data. Emission peaks appear in the voltage range 330–380 mV, cf. Fig. 5(b), with a maximum *detected* power of about 0.8 nW. Extrapolated over 4π this yields a total power of order 0.25 μW which is actually almost an order of magnitude below the radiation power detected for rectangular stacks.[24,32] Figure 5(c) shows a Fourier spectrum of this radiation, with the sample biased at 14.9 mA and 370 mV [corresponding to LTSLM image Fig. 3(e), where no hot spot has formed yet]. The radiation peak occurs at $f=472$ GHz. Using the Josephson relation, $f=NV/\Phi_0$ with the flux quantum Φ_0, we infer a junction number $N=380$, which corresponds to only about 60% of the 600 junctions contained in the mesa, as estimated from its 0.9 μm thickness. Thus, not all junctions participate in radiation. Finally, from the $m=3$, $n=1$ mode observed and from the emission frequency we find a mode velocity of $c' \approx 7 \times 10^7$ m/s, which is the value to be expected when the junctions oscillate in phase and the temperature is not too high.[31,32] In Fig. 5(b) a second emission peak is visible at $V \approx 350$ mV. It might be attributed to the situation of Fig. 3(d) when the hot spot has nucleated and the cold part of the disk forms an annular structure. As discussed above, for a small hot-spot radius the cavity resonance frequency is almost the same as for the disk, assuming a constant mode velocity. On the other hand, with increasing temperature in the mesa, the mode velocity c' decreases[31,32] and thus effectively lowers the resonance frequency, consistent with the observed double peak structure in Fig. 5(b). For bias currents $I>25$ mA neither THz emission nor standing-wave patterns were detectable.

B. Hot-spot formation monitored by detector stacks

Sample 2 consists of a rectangular 330×70 μm^2 large and 0.5-μm-thick main mesa which is surrounded by small

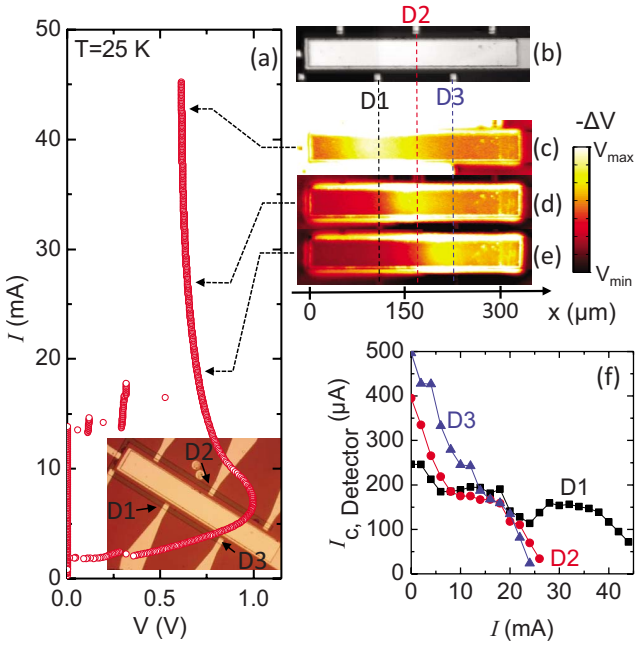

FIG. 6. (Color online) (a) IVC at $T=25$ K of sample 2 (main mesa) with optical image taken by the (b) laser microscope, [(c)–(e)] LTSLM images and (f) the critical current of detector junctions D1, D2, and D3 vs bias current through main mesa. Inset in (a) shows an optical image of sample 1, taken by a conventional microscope. Color bar for (c)–(e) denotes maximum and minimum values of $-\Delta V$. (c) $V_{max}=100$ μV, (d) 200 μV, and (e) 320 μV. $V_{min}=-50$ μV for all images.

mesas, cf. inset of Fig. 6(a). These mesas are separated by 10 μm from the main mesa. Three of them (denoted D1, D2, and D3) worked. We suppose that the gold leads connecting the other detectors were broken during the fabrication process. An optical image, taken during LTSLM, of the main mesa and the surrounding detector mesas is shown in Fig. 6(b). The working detector mesas are indicated. The current I through the main mesa is injected from its right side. Originally the small mesas were intended to detect THz emission from the main mesa which, however, did not radiate. A possible reason is that the mesa was unusually thin (0.5 μm). Still, the detectors were usable to estimate the temperature of the base crystal for different values of bias current through the main mesa. For this mesa, one observes a hot spot nucleating near the right end of the mesa; the hot-cold boundary forms a straight bright line moving to the left with increasing I. Figure 6(a) shows the IVC of the main mesa, measured at $T=25$ K. LTSLM image Fig. 6(e) is taken at $I=18.6$ mA. The right part of the mesa produces a negative response having a maximum near $x\approx 200$ μm. Here, the edge of the hot spot is located. In Fig. 6(d), taken at $I=28.8$ mA, this maximum has moved to the left and is located near $x\approx 150$ μm. Finally, in Fig. 6(c), taken at $I=42.4$ mA, the edge has moved to $x\approx 90$ μm. In Fig. 6(c) there is also a strong response from *outside* the main mesa, roughly coinciding with the U-shaped mesa forming the base of the detector mesas [the dark structure in the inset of Fig. 6(a)]. We attribute this signal to parasitic IJJs shared by the main mesa and the U-shaped line. Such junctions are formed if, during ion milling, in the moat between the "U" and the main mesa less material has been removed than outside the U. A strong response ΔV can occur when the heating by the laser beam drives these junctions to their resistive state. Figure 6(f) shows the critical current I_c of the three detector junctions as a function of the current through the main mesa. As can be seen from Fig. 6(e), for $I=18.6$ mA the hot-spot edge, seen as the bright stripe inside the mesa, has just passed detector D3. I_c of this detector goes to zero at the not much higher current $I\approx 22$ mA, where I_c of detectors D1 and D2 are still finite. At $I=26.8$ mA the front of the hot spot has passed detector D2, cf. Fig. 6(d), consistent with the observation that I_c of this detector vanishes at $I\approx 25$ mA. Finally, I_c of detector D1 approaches zero near $I=45$ mA. For comparison, the front of the hot spot passes this detector for $I\approx 43$ mA, cf. Fig. 6(c). Exactly this behavior can be expected if, on one hand, the hot-spot feature observed indeed is a region heated to above T_c and, on the other hand the hot-spot region extends outside the main mesa. By contrast, the fact that I_c of a given detector falls to zero when being passed by the front of the hot spot is hard to understand if one assumes that the hot-spot region is below T_c and, e.g., corresponds to some nonequilibrium state with a suppressed superconducting gap. We thus conclude that our hot-spot interpretation is correct. For completeness we note that I_c of detector D1 has a minimum near $I=25$ mA. This feature is most likely an artifact caused by noise.

Still one should give some arguments how hot-spot formation occurs in the mesa geometry. The 3D heat flow equations have been solved numerically in Ref. 51, using COMSOL simulation software. The BSCCO crystal was assumed to be glued to a sapphire substrate, and a 100-nm-thick Au layer covering the mesa was assumed as the contacting electrode. The electrical and thermal properties of BSCCO and the various contacting layers were taken into account as close as possible. In the absence of heating, a linear IVC was assumed for the IJJs both above and below T_c. These calculations reproduced the appearance of a negative differential resistance region in the IVCs at high-bias case. With respect to the hot-spot formation they are in qualitative agreement with the LTSLM findings, although the temperature profile of the hot spot was roughly Gaussian shaped and thus relatively smooth. Further, the simulated hot spot appeared in the center of the mesa. In our experiments the hot spot often forms in the vicinity of the bias lead, although not at the attachment point itself. Qualitatively, this can be understood by considering a multiple role of this lead. First, it injects a current I into the upper layers of mesa. From here the current distributes both along and perpendicular to the CuO_2 layers. The interlayer current density will have a maximum in the vicinity of the lead, providing local heating in the resistive state. Additional local heating, growing quadratically with I, arises from the contact resistance between the bias lead and the mesa. By contrast, the lead also acts as a current-independent local heat sink. At low bias, Joule heating due to the applied current is not essential. With increasing bias Joule heating increases and will eventually lead to hot-spot formation near but not exactly at the lead.

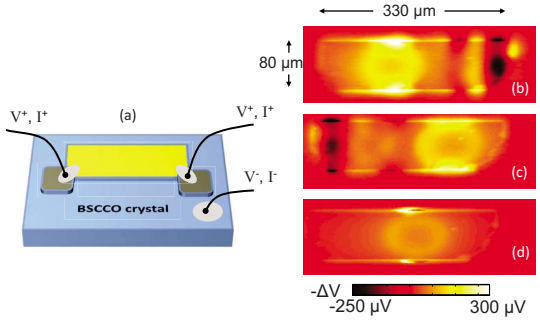

FIG. 7. (Color online) (a) Sketch of sample 3 and LTSLM data at $T=40$ K for various biasing conditions: (b) bias from left, (c) bias from right, and (d) symmetric bias. In the sketch, the yellow area symbolizes the Au layer covering the mesa. The dark squares at the lower mesa edges correspond to the insulating polyimide layer the gray dots symbolize the silver paste used to attach the contacting wires.

C. Manipulating hot spots and waves using two injection leads

In a number of experiments on rectangular mesas we observed that the hot spot often—although not always—nucleates near the current injection point. An obvious generalization is to use more than one current injection point to feed a given current I into the sample. If the injection points are very far from each other one may simply expect the formation of several hot spots near the injection points. On the other hand, for not too large mesas a single hot spot might form at a position that depends on the ratio of injected currents. If so, the size of the cold part of the mesa and consequently wave formation should depend on the ratio of injected currents. Below we show data for two 330-μm-long rectangular mesas that were contacted at two opposite edges. We start with data obtained from a 80-μm-wide mesa (sample 3), cf. Fig. 7(a). In Figs. 7(b)–7(d) we show LTSLM images taken at $T=40$ K at a bias current of 30.4 mA. For image in Fig. 7(b) the current has been injected at the left contact. Here, the hot spot appears as a circular structure in the left half of the mesa and there is a clear standing-wave pattern in the right half of the stack. For the image in Fig. 7(c) the current has been injected from the right side. The hot spot now appears in the right half of the mesa and the wave is situated in the left part. Finally, Fig. 7(d) shows a symmetric situation where the current has been injected from both edges; half of the total current of 30.4 mA flows through each contact. Here, the hot spot is centered in the mesa and no wave appears. For these measurements we have varied the current injection points at fixed total bias current. The voltage across the sample, and thus the Josephson frequency, slightly changed for the three bias conditions, from 0.59 V when biasing from left, to 0.58 V when biasing from the right, and to 0.6 V for the symmetric bias. In the case of symmetric bias the injection leads were used both for voltage measurement and current injection; the resulting contact resistance is subtracted from the voltage quoted. To check whether this change in voltage is the dominant quantity for the (dis)appearance of the standing wave we have investigated hot-spot and wave formation for the symmetric bias and the bias-from-left configuration over a wide current range. As expected for a hot spot, its size increased with increasing input power. Regarding wave signals it turned out that, for the symmetric bias, we could not achieve a wave pattern at all. For the other configuration the wave appeared over a wide current range, from about 28–45 mA. Here, the voltage varied between 0.51 and 0.63 V, i.e., over a much larger range than for the case of Figs. 7(b)–7(d).

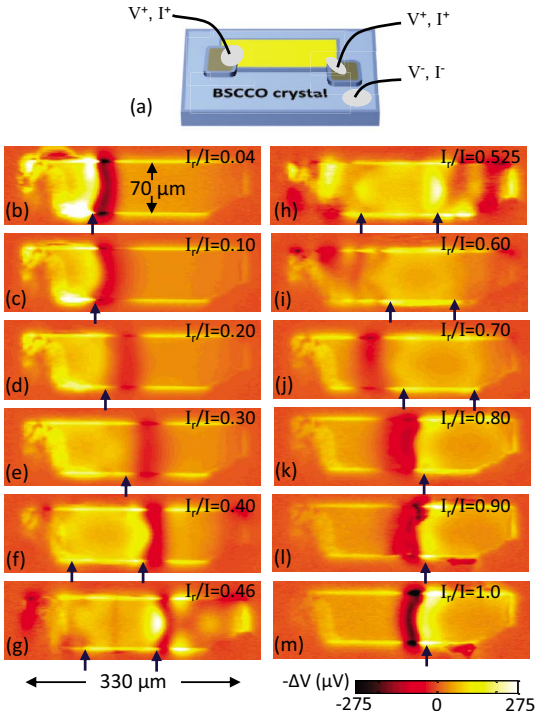

FIG. 8. (Color online) Sketch of sample 4, equipped with two current injectors (a) and (b) to (m) LTSLM data at $T=18$ K for various ratios of the current I_r through the right injector to the total current I. The ratios I_r/I are indicated in the graphs. Vertical arrows in LTSLM images indicate edges of hot spots.

In Fig. 8 we show data for a 70-μm-wide mesa (sample 4). Accidentally, on the left edge the silver paste used to fix the current lead extends significantly into the mesa, as sketched in Fig. 8(a). On the right side the silver paste covers only the lower corner of the mesa. For this sample the asymmetry in the two bias currents was varied in small steps. Figures 8(b)–8(m) show LTSLM images at $T=18$ K. The total current was fixed at 38 mA. In the graphs the ratio I_r/I of the current through the right injector to the total current is indicated. For $I_r/I=0.04$ the hot spot is located on the left side of the mesa, see Fig. 8(b). In the graph, its edge is marked by an arrow. For $I_r/I=0.1$ the hot-spot position seems to be unchanged, see Fig. 8(c). By contrast, when increasing I_r/I toward symmetric bias, the hot-spot location moves toward the center of the mesa, see Figs. 8(d)–8(g). The shift seems to occur continuously. This also holds for ratios I_r/I between 0.5 and 0.9, as shown in Figs. 8(h)–8(l). No further change in the hot-spot position is visible between $I_r/I=0.9$ [Fig. 8(l)] and $I_r/I=1$ [Fig. 8(m)]. Note that, for I_r/I between 0.4 and 0.7 both the left and right edges of the hot spots are located inside the mesa, leaving two cold re-

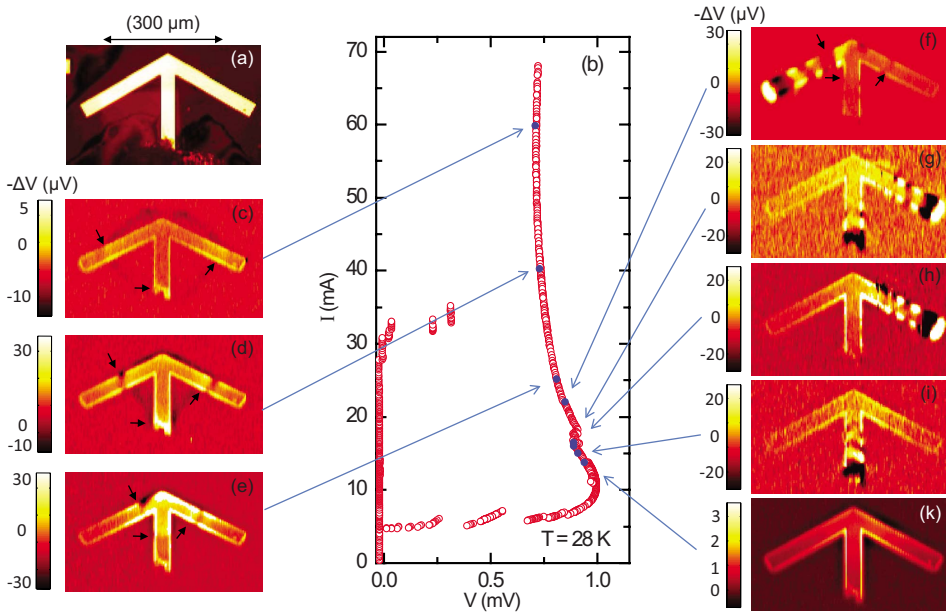

FIG. 9. (Color online) (a) Optical image, (b) current voltage characteristic, and [(c)–(k)] LTSLM images of the arrow-shaped sample 1, as measured at $T=28$ K. [(c)–(f)] Black arrows in images indicate edge of hot spot.

gions near the mesa edges. Further, in Fig. 8(g) a wavelike structure is visible in the right part of the mesa, although less clear as for sample 3 in Fig. 7(b). In Fig. 8(h) there seems to be an additional wave structure in the left part of the mesa which remains visible in Fig. 8(i) where the wave structure in the right part of the mesa has disappeared.

From our experiments on samples 3 and 4 we conclude that the hot-spot position can be varied more or less continuously by using different injection points. The experiments also support the picture that one of the roles of the hot spot simply is to adjust the size of the cavity, i.e., the cold part of the mesa. Thus, by using two or more injectors THz emission can be turned on and off in a more or less controlled way. We note, however, that for this purpose injectors should be patterned more reliably than just attaching wires by silver paste. This is feasible using standard lithographic techniques.

D. Hot-spot and wave formation in an arrow-shaped mesa

The last structure we discuss in this paper is an arrow-shaped mesa (sample 5), see Fig. 9(a). The structure, initially produced together with a "Y"-shaped mesa to study wave splitting at intersections, provides further insights into hot-spot nucleation points and wave formation.[63] The arrow was contacted on the foot of the arrow. The contact is visible in Fig. 9(a) and the LTSLM images, Figs. 9(c)–9(k). An IVC of the arrow, taken at a bath temperature of 28 K, is shown in Fig. 9(b). Starting from zero current the IJJs in the mesa switch to their resistive states at currents I between 30 and 35 mA. When lowering the current from high bias one observes an instability for currents between 18 and 16 mA that is indicative for the disappearance of a hot spot present at high bias. The LTSLM images are taken in the resistive state of all junctions. For currents decreasing from 60 to 25 mA one observes a diamond-shaped loop centered around the top of the arrow but extending far out of the mesa. At $I=60$ mA, cf. Fig. 9(c), the loop is visible as a bright stripe *inside* each arm of the mesa, as indicated by arrows in Fig. 9(c). Outside the actual mesa structure the feature is continued by a positive (black) signal ΔV. At $I=40$ mA, cf. Fig. 9(d), the loop has decreased in diameter. On the tip of the arrow it appears close to the mesa edge while it still extends significantly beyond the mesa in between the three arms. At $I=25$ mA, cf. Fig. 9(e), the feature has reduced basically to the tip of the arrow. *Inside* the mesa the feature shows the same behavior that we typically see for the hot-spot boundary in narrow mesas, i.e., a stripe moving with growing input power. The fact that the structure visibly continues outside the mesa is, similar to the case of sample 2, understood best if one assumes that there are additional parasitic IJJs at the foot of the mesa, contributing to the voltage measured and acting as sensors for the hot/cold boundary of the hot spot. Independent of this explanation the data on one hand show that the hot spot extends beyond the actual mesa, in agreement with the data presented for sample 2. On the other hand, we see that the hot spot forms at the tip of the arrow rather than close to the current injection point.

When lowering the current, between 24 and 15 mA standing-wave patterns appear in various parts of the mesa. Near $I=22$ mA a wave pattern is visible in the left part of the arrow [Fig. 9(f)]. At $I=16.4$ mA a wave pattern appears in the right part of the arrow and the shaft [Fig. 9(g)], at $I=16.0$ mA the wave is visible only in the right part of the arrow [Fig. 9(h)] and at $I=15.0$ mA the wave appears only in the shaft [Fig. 9(i)]. For currents below 15 mA the LTSLM images were smooth and neither hot spot nor wave features appeared, see Fig. 9(k). Thus, in a narrow current range the arrow acted as a switch, generating standing waves in different arms of the structure. This property, which might be interesting for integrated layouts involving several mesa struc-

tures, can be understood if one assumes that a hot spot is located at the tip of the arrow. It separates the arrow effectively into three cavities which can become resonant or not, depending on the position of the hot-spot edges adjusting the size of the cavities. In Fig. 9(f) the diamond-shaped loop representing the hot spot is still vaguely visible. For Figs. 9(g)–9(i) we cannot tell. However, these images have been taken very close to the instability in the IVC (kink at 18 mA), making it likely that there is either still a small hot spot or at least a zone very close to T_c effectively separating the three cavities.

IV. CONCLUSIONS

In this paper we presented LTSLM and THz emission measurements on four different mesa geometries. These measurements improve the understanding of hot-spot and wave formation in intrinsic Josephson junction stacks. Concerning the standing waves the nontrivial geometry of a disk-shaped mesa, as opposed to rectangular structures studied previously, further confirmed the interpretation of the patterns observed as electromagnetic cavity modes. Despite the fact that most of the junctions were in the resistive state, the emitted power was almost one order of magnitude below the power emitted by the best rectangular structures studied. This may indicate that disk structures, although valuable for fundamental studies, are not superior to rectangular mesas with respect to THz oscillators. Concerning hot-spot formation, using a rectangular mesa with nearby detector mesas we found that the critical currents of the detectors vanished when being passed by the front of the hot spot. This is consistent with the hot-spot interpretation of the feature observed in LTSLM but would be hard to explain if the hot-spot region were still superconducting and corresponds to, e.g., a region of suppressed superconducting gap. Our intention with the two other geometries—a rectangular mesa equipped with two current injectors and an arrow-shaped structure—was to check whether the hot spot and the wave formation could be controlled. Using two current injectors we have realized, for constant total bias current, different hot-spot locations depending on the ratio of currents through the two injectors. For certain hot-spot positions waves appeared in either the left or the right part of the mesa. In the arrow-shaped structure-independent wave formation was observed in the three parts of the arrow, that were presumably separated and changed in size by a hot spot located at the tip of the arrow. While often the hot spot nucleates near the current injection point, this geometry also showed that nucleation centers can have different (geometric) origin, i.e., the tip of the arrow in the present case.

These results point out ways to control hot-spot and THz wave formation in the high-bias regime. However, the reproducibility of the device properties needs further improvement. For example, not all samples radiate and, for the radiating samples, we cannot precisely predict the emission frequency range. The hot-spot formation results from a delicate balance between the dissipated power and heat flowing (or escaping) through the electrical leads and various thin-film layers involved. Thus, the precise thermal properties differ not only for different mesas but even depend on the setup. In addition, suitable models of hot-spot nucleation, THz generation and the interaction between hot spots and wave are lacking. Our results may have shown that one of the roles of the hot spot is to form an adjustable end of the cavity formed by the cold part of the mesa. In LTSLM the width of the hot/cold transition region typically has a width of 20–30 μm. This width, which may be resolution limited, is well below the typical wavelengths of the cavity modes excited (around 100 μm). Thus, changes in conductance between the hot and cold parts seem to be abrupt enough to lead to electromagnetic wave reflection at the hot-spot edge. One can further assume that, in the presence of a standing wave, the cold part of the mesa experiences additional heating at the positions of the wave antinodes, contributing to the heat balance of the whole mesa. This should cause backaction to the hot-spot position and may lead to some extent to a "self-alignment" of the hot-spot position relative to the wave. There may be additional interactions between the hot spot and the THz waves. For example, the hot part of the mesa could act as an external shunt, helping in synchronizing the junctions in the stack. Also, nonequilibrium processes at the hot-spot edge may contribute to synchronization. Some discussion in the context of the linewidth of the terahertz emission observed is given in Ref. 32. Solving at least some of these issues is the task for the near future.

ACKNOWLEDGMENTS

We thank A. Yurgens, V. M. Krasnov, U. Welp, L. Ozyuzer, K. Kadowaki, I. Iguchi, K. Nakajima, and C. Otani for valuable discussions. Financial support by the strategic Japanese-German International Cooperative Program of the JST and the DFG, by the German Israeli Foundation via research under Grant No. G-967-126.14/2007, and by Grants-in-Aid for scientific research from JSPS is gratefully acknowledged.

*wang.huabing@nims.go.jp
†kleiner@uni-tuebingen.de

[1] V. P. Koshelets and S. Shitov, Supercond. Sci. Technol. **13**, R53 (2000).
[2] P. A. A. Booi and S. P. Benz, Appl. Phys. Lett. **68**, 3799 (1996).
[3] P. Barbara, A. B. Cawthorne, S. V. Shitov, and C. J. Lobb, Phys. Rev. Lett. **82**, 1963 (1999).
[4] M. Darula, T. Doderer, and S. Beuven, Supercond. Sci. Technol. **12**, R1 (1999).
[5] X. Hu and S. Z. Lin, Supercond. Sci. Technol. **23**, 053001 (2010).
[6] F. Song, F. Müller, R. Behr, and M. Klushin, Appl. Phys. Lett.

95, 172501 (2009).
[7] I. Ottaviani, M. Cirillo, M. Lucci, V. Merlo, M. Salvato, M. G. Castellano, G. Torrioli, F. Mueller, and T. Weimann, Phys. Rev. B **80**, 174518 (2009).
[8] R. Kleiner, F. Steinmeyer, G. Kunkel, and P. Müller, Phys. Rev. Lett. **68**, 2394 (1992).
[9] R. Kleiner and P. Müller, Phys. Rev. B **49**, 1327 (1994).
[10] A. A. Yurgens, Supercond. Sci. Technol. **13**, R85 (2000).
[11] R. Kleiner, Phys. Rev. B **50**, 6919 (1994).
[12] G. Hechtfischer, R. Kleiner, A. V. Ustinov, and P. Müller, Phys. Rev. Lett. **79**, 1365 (1997).
[13] G. Hechtfischer, W. Walkenhorst, G. Kunkel, K. Schlenga, R. Kleiner, P. Müller, and H. L. Johnson, IEEE Trans. Appl. Supercond. **7**, 2723 (1997).
[14] K. Lee, W. Wang, I. Iguchi, M. Tachiki, K. Hirata, and T. Mochiku, Phys. Rev. B **61**, 3616 (2000).
[15] M. Machida, T. Koyama, A. Tanaka, and M. Tachiki, Physica C **330**, 85 (2000).
[16] T. Clauss, T. Ushida, M. Mößle, D. Koelle, and R. Kleiner, Appl. Phys. Lett. **85**, 3166 (2004).
[17] S. Madsen, G. Filatrella, and N. F. Pedersen, Eur. Phys. J. B **40**, 209 (2004).
[18] H. B. Wang, S. Urayama, S. M. Kim, S. Arisawa, T. Hatano, and B. Y. Zhu, Appl. Phys. Lett. **89**, 252506 (2006).
[19] V. M. Krasnov, Phys. Rev. Lett. **97**, 257003 (2006).
[20] I. Batov, X. Jin, S. Shitov, Y. Koval, P. Müller, and A. Ustinov, Appl. Phys. Lett. **88**, 262504 (2006).
[21] A. Grib, M. Mans, J. Scherbel, M. Büenfeld, F. Schmidl, and P. Seidel, Supercond. Sci. Technol. **19**, S200 (2006).
[22] M. H. Bae, H.-J. Lee, and J.-H. Choi, Phys. Rev. Lett. **98**, 027002 (2007).
[23] S. O. Katterwe and V. M. Krasnov, Phys. Rev. B **80**, 020502 (2009).
[24] L. Ozyuzer *et al.*, Science **318**, 1291 (2007).
[25] K. Kadowaki *et al.*, Physica C **468**, 634 (2008).
[26] L. Ozyuzer *et al.*, Supercond. Sci. Technol. **22**, 114009 (2009).
[27] H. Minami, I. Kakeya, H. Yamaguchi, T. Yamamoto, and K. Kadowaki, Appl. Phys. Lett. **95**, 232511 (2009).
[28] K. Kadowaki, M. Tsujimoto, K. Yamaki, T. Yamamoto, T. Kashiwagi, H. Minami, M. Tachiki, and R. A. Klemm, J. Phys. Soc. Jpn. **79**, 023703 (2010).
[29] C. Kurter *et al.*, IEEE Trans. Appl. Supercond. **19**, 428 (2009).
[30] K. E. Gray, L. Ozyuzer, A. E. Koshelev, C. Kurter, C. Kadowaki, T. Yamamoto, H. Minami, H. Yamaguchi, M. Tachiki, W.-K. Kwok, and U. Welp, IEEE Trans. Appl. Supercond. **19**, 886 (2009).
[31] H. B. Wang, S. Guénon, J. Yuan, A. Iishi, S. Arisawa, T. Hatano, T. Yamashita, D. Koelle, and R. Kleiner, Phys. Rev. Lett. **102**, 017006 (2009).
[32] H. B. Wang *et al.*, Phys. Rev. Lett. **105**, 057002 (2010).
[33] H. Minami, N. Orita, T. Koike, T. Yamamoto, and K. Kadowaki, Physica C (to be published).
[34] N. Orita, H. Minami, T. Koike, T. Yamamoto, and K. Kadowaki, Physica C (to be published).
[35] M. Tsujimoto, K. Yamaki, K. Deguchi, T. Yamamoto, T. Kashiwagi, H. Minami, M. Tachiki, K. Kadowaki, and R. A. Klemm, Phys. Rev. Lett. **105**, 037005 (2010)..
[36] K. Yamaki, M. Tsujimoto, T. Yamamoto, H. Minami, and K. Kadowaki, Physica C (to be published).
[37] L. N. Bulaevskii and A. E. Koshelev, Phys. Rev. Lett. **99**, 057002 (2007).
[38] A. E. Koshelev and L. N. Bulaevskii, Phys. Rev. B **77**, 014530 (2008).
[39] A. E. Koshelev, Phys. Rev. B **78**, 174509 (2008).
[40] S. Lin and X. Hu, Phys. Rev. Lett. **100**, 247006 (2008).
[41] X. Hu and S. Z. Lin, Phys. Rev. B **80**, 064516 (2009).
[42] R. A. Klemm and K. Kadowaki, J. Phys.: Condens. Matter **22**, 375701 (2010).
[43] Y. Nonomura, Phys. Rev. B **80**, 140506 (2009).
[44] M. Tachiki, S. Fukuya, and T. Koyama, Phys. Rev. Lett. **102**, 127002 (2009).
[45] T. Koyama, H. Matsumoto, M. Machida, and K. Kadowaki, Phys. Rev. B **79**, 104522 (2009).
[46] N. Pedersen and S. Madsen, IEEE Trans. Appl. Supercond. **19**, 726 (2009).
[47] V. M. Krasnov, Phys. Rev. Lett. **103**, 227002 (2009).
[48] A. Grib and P. Seidel, Phys. Status Solidi (RRL) **3**, 302 (2009).
[49] S. Savel'ev, V. A. Yampol'skii, A. L. Rakhmanov, and F. Nori, Rep. Prog. Phys. **73**, 026501 (2010).
[50] H. Matsumoto, T. Koyama, and M. Machida, Physica C **470**, 1485 (2010).
[51] A. A. Yurgens arXiv:1005.2932v1 (unpublished).
[52] M. Tachiki, K. Ivanovic, K. Kadowaki, and T. Koyama, (unpublished).
[53] W. J. Skocpol, M. R. Beasley, and M. Tinkham, J. Appl. Phys. **45**, 4054 (1974).
[54] A. V. Gurevich and R. G. Mints, Rev. Mod. Phys. **59**, 941 (1987).
[55] R. C. Dynes, V. Narayanamurti, and J. P. Garno, Phys. Rev. Lett. **39**, 229 (1977).
[56] K. E. Gray and H. W. Willemsen, J. Low Temp. Phys. **31**, 911 (1978).
[57] I. Iguchi and D. N. Langenberg, Phys. Rev. Lett. **44**, 486 (1980).
[58] H. Akoh and K. Kajimura, Phys. Rev. B **25**, 4467 (1982).
[59] R. Gross, D. B. Schmid, and R. P. Huebener, J. Low Temp. Phys. **62**, 245 (1986).
[60] S. G. Lachenmann, T. Doderer, R. P. Huebener, D. Quenter, J. Niemeyer, and R. Pöpel, Phys. Rev. B **48**, 3295 (1993).
[61] R. Eichele, L. Freytag, H. Seifert, R. P. Huebener, and J. R. Clem, J. Low Temp. Phys. **52**, 449 (1983).
[62] H. Eisele, M. Naftaly, and J. Fletcher, Meas. Sci. Technol. **18**, 2623 (2007).
[63] Similar to the arrow also the Y was contacted at its lower edge. The assumption was that the hot spot will nucleate near this contact; if the waves originate from the hot-spot edge, both structures would have allowed to study if and how the wave splits at the intersections. In experiment the Y did not work. For the arrow structure the hot spot formed at the tip of the arrow, producing the results discussed in the text.

Publication 3

Supercond. Sci. Technol. **25** (2012) 075015 (5pp) doi:10.1088/0953-2048/25/7/075015

Terahertz emission from $Bi_2Sr_2CaCu_2O_{8+\delta}$ intrinsic Josephson junction stacks with all-superconducting electrodes

J Yuan[1], M Y Li[1,2], J Li[1,3], B Gross[4], A Ishii[1], K Yamaura[1,3], T Hatano[1], K Hirata[1], E Takayama-Muromachi[1,3], P H Wu[2], D Koelle[4], R Kleiner[4] and H B Wang[1,2]

[1] National Institute for Materials Science, Tsukuba 3050047, Japan
[2] Nanjing University, Nanjing 210093, People's Republic of China
[3] Hokkaido University, Sapporo, Hokkaido 060-0810, Japan
[4] Physikalisches Institut and Center for Collective Quantum Phenomena in LISA$^+$ Universität Tübingen, Auf der Morgenstelle 14, D-72076 Tübingen, Germany

E-mail: Kleiner@uni-tuebingen.de and WANG.Huabing@nims.go.jp

Received 8 February 2012, in final form 2 May 2012
Published 15 June 2012
Online at stacks.iop.org/SUST/25/075015

Abstract
Terahertz (THz) emission has been recently detected from intrinsic Josephson junction (IJJ) stacks made of the high critical temperature superconductor $Bi_2Sr_2CaCu_2O_{8+\delta}$ (BSCCO). The most employed structure is a mesa standing on a big pedestal of a single crystal with a thin gold layer as its top electrode. In this work, a large ($300 \times 50 \times 1.2\ \mu m^3$) IJJ stack with superconducting electrodes was fabricated and studied. The stack consisted of $N \approx 800$ IJJs. It was prepared with a double-sided fabrication process, and significant THz emission was detected. The output power is comparable to the emission power detected from mesa structures, obviously not weakened by the superconducting upper electrode. The observation of THz emission from the double-sided structure suggests that off-chip THz emission from IJJs can be obtained not only from mesa structures and, most importantly, that the emission power can be potentially enhanced in integrated multi-stack radiation sources.

(Some figures may appear in colour only in the online journal)

1. Introduction

Terahertz (THz) technology has attracted increasing attention for a wide range of applications in detecting and imaging, such as high-altitude telecommunications, public security, food quality control and environmental monitoring [1, 2]. Although many techniques like femtosecond laser pulses, quantum cascade lasers, synchrotron light, backward wave oscillators, etc, have been introduced to generate THz electromagnetic waves, their high cost and complexity limits applications. The lack of cost-effective and active devices results in the 'THz gap' problem [3]. According to the theory of the ac Josephson effect, a Josephson junction can work as a dc-voltage to high-frequency current converter, with 1 mV corresponding to 483 GHz. This provides the basis of superconducting high-frequency detectors and tunable radiation sources. However, the radiation frequency f of Josephson junctions is limited by the superconducting energy gap, which restricts the operation of conventional junctions down to 700 GHz or less. Moreover, the low output power, in the picowatt to nanowatt range, limits the applicability of a single junction. Intrinsic Josephson junctions (IJJs) in BSCCO [4] can overcome both problems. They can be operated at THz frequencies and stacking of many IJJs is possible. Recently, coherent off-chip THz radiation with an extrapolated output power of some microwatt was observed from stacks (mesa structures) of

more than 600 IJJs with lateral dimensions in the 100 μm range [5]. For comparison, the Josephson length $\lambda_J \approx 0.5$ μm. It was assumed that the mesa forms an electromagnetic cavity and the Josephson oscillations in the individual junctions are synchronized by the alternating electromagnetic field stored in the cavity resonance. This finding triggered numerous experimental [6–16] and theoretical [17–35] studies to understand the mechanism of emission and to improve the performance of the radiation source.

Since there is no applicable single stack emitter, it is naturally expected to increase the output power by integrating several stacks into one device. If this is done with mesa structures one faces several problems: (1) mesas are typically contacted by normal conducting Au leads, leading to a finite contact resistance and additional power dissipation [36, 37]; (2) the mesa surface is often degraded, leading to surface junctions with a strongly reduced critical current density [37, 38]; (3) due to the mesa etching process the mesas have a trapezoidal cross-section, leading to a gradient in the critical currents of the IJJs [8]. These properties make it hard to achieve complete synchronization within a stack. Synchronization is even harder between different stacks. In our previous work, a double-sided fabrication process was applied in the preparation of small ($\sim$10 μm^2) IJJ stacks consisting of some ten junctions, as well as junction stack arrays [39, 40]. In this work well-controlled uniformity in both lateral dimension and junction number was demonstrated. We adopt this technique now to fabricate large IJJ stacks. The development of large stacks in a double-sided structure is a promising way to integrate radiation sources and perhaps also to address the issue of the mechanism of THz emission.

2. Experimental details

In the present experiment, the single crystals were grown by a floating zone technique in a four-lamp arc imaging furnace. They were annealed in a temperature range of 600–650 °C in an Ar 99%, O_2 1% atmosphere for 48–72 h. The crystals were slightly underdoped with a superconducting transition temperature (T_c) of 83–87 K.

The double-sided fabrication process for small IJJ stacks is described in detail in [39]. Here we outline some critical steps, shown in figure 1, to emphasize the modifications required to produce large stacks.

First, the ($\approx$50 μm thick) BSCCO single crystals were glued on a Si substrate with epoxy. A 30–40 nm thick Au thin film was deposited soon after the final cleaving step. A 600 $\times$ 600 μm^2 large square was patterned on the upper surface and etched by ion milling, leaving a mesa (about 2.0 μm thick) sitting on the BSCCO pedestal. A slit, 10 μm wide and 1.5 μm deep, was fabricated through the square mesa with its direction parallel with one boundary; two mesa-like structures sitting on top of the original square are formed during this step (see figure 1(a)). Then, the patterned single crystal surface was glued onto a MgO substrate and turned upside-down. The Si substrate was removed together with most of the BSCCO pedestal and the remnant pedestal was removed by an adhesive tape. Then a 30–40 nm thick Au thin

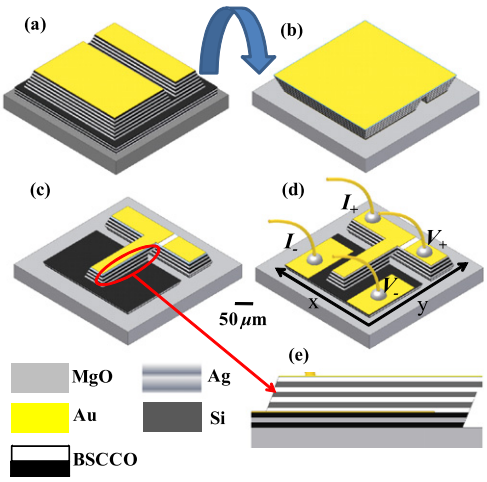

Figure 1. (a)–(d) A schematic diagram of the critical steps in the fabrication process. I_+, I_-, V_+ and V_- in (d) indicate current and voltage leads. (e) View parallel to the short side of the stack showing that the cross-section parallel to the long side of the stack approximates a parallelogram.

film was evaporated on this freshly cleaved surface. The link between the two mesas underneath is about 0.5 μm thick (see figure 1(b)). Next, a T shaped structure was patterned on this surface, with its cross bar located above one of the mesas created by the slit. The stem of the T crosses the slit and is mainly located on top of the other mesa. After ion milling the cross bar forms the bank contacting the upper surface of the IJJ stack. The stack itself is formed by the lower part of the stem (see figure 1(c)). Finally, four gold electrodes were made for current–voltage (I–V) measurements. The electrodes were connected to gold wires by silver paste, as shown in figure 1(d). The final structure contains an IJJ stack about 300 $\times$ 50 μm^2 in size, as sketched in figure 1(d). Its thickness is about 1.2 μm, corresponding to a stack of $\approx$800 IJJs, and it is connected to the ($\approx$0.3 μm thick) leads by BSCCO layers. Note that, because in this double-sided fabrication process Ar ion beams of opposite direction are used to etch different walls of the stack (the sample does not rotate during ion milling), its cross-section parallel to the long side forms a parallelogram rather than a trapezoid, see figure 1(e). The cross-section parallel to the short side is still trapezoidal. The angle between the Ar ion beam and the mesa surface is 45°, and the beam is along the long side of the stack. Under this condition, the steepness of the long-side wall of the stack (about 45°, as checked by atomic force microscopy (AFM)) is steeper than that obtained by a vertical beam (it is about 35° for our process). Overall, the junction areas become more uniform.

The samples were mounted in a continuous He flow cryostat. A four-terminal method was employed in the I–V measurement, as indicated in figure 1(d). In order to have stable operation, the junctions were biased using a current source driven by batteries. Emission data and frequency spectra were measured in a self-made interferometer using a Si bolometer for THz detection (see figure 2). The direction of detection is perpendicular to the BSCCO *ab* planes. The

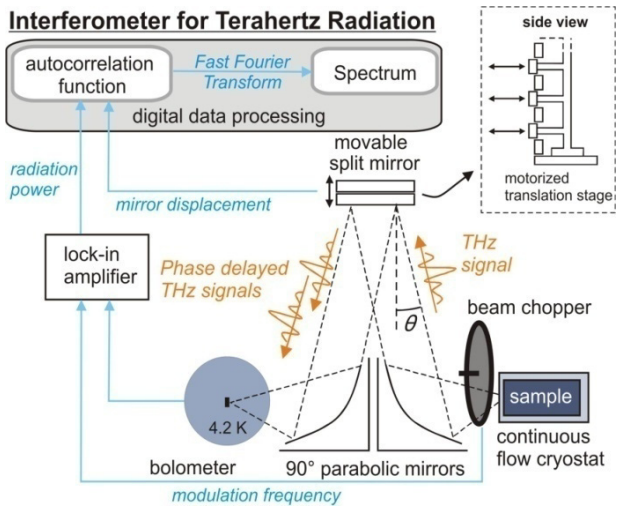

Figure 2. Schematic diagram of the experimental setup for THz detection.

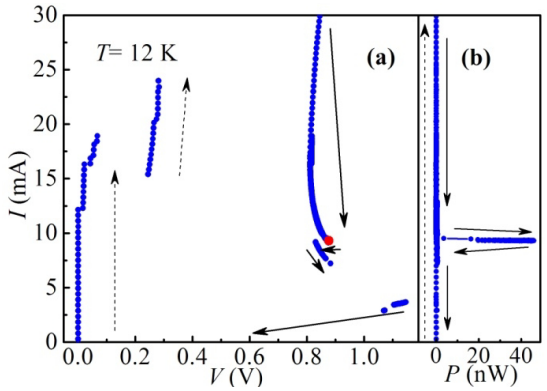

Figure 3. Experimental data with a double-sided IJJ stack at $T = 12$ K. (a) dc current–voltage curve; (b) emission power detected by bolometer versus current through the stack. Arrows indicate the direction of the current sweep. The red point in (a) indicates the bias point where the largest emission was detected.

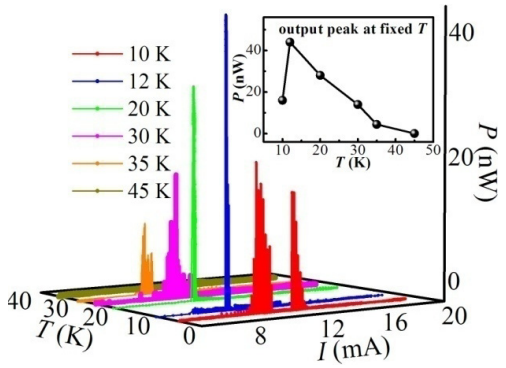

Figure 4. THz emission power versus bias current at various temperatures. The inset shows the temperature dependence of the emission peak with maximal output power.

light path from the emitter to the Si bolometer is about 1 m. The solid angle of our setup, defined by the aperture of the Winston cone in front of the bolometer, is 0.04 solid radians. The THz emission power from the double-sided stack was detected during the I–V scans and recorded simultaneously. Numbers for the emission power given below refer to the power detected by the bolometer. The frequency spectrum was obtained with the junctions being biased at fixed current. The details of the setup have been described elsewhere [10].

3. Results and discussion

Figure 3(a) shows an I–V curve of the double-sided sample at 12 K. Increasing I from zero one finds various jumps to resistive branches until, at $I \approx 25$ mA, the whole stack switches to the resistive state. When decreasing I in this fully resistive state one finds a region of negative differential resistance, very similar to the case of conventional mesa structures. Note that since the stack is connected with two superconducting electrodes, there is no contact resistance or strongly degraded surface junctions involved in the I–V measurements. We still observe some branches where switching occurs at reduced bias current, but the effect is much less pronounced than in mesa structures.

Figure 3(b) shows the detected THz signal versus I. A strong signal was observed in the fully resistive state of the stack at $I = 9.3$ mA, i.e. in the back-bending region of the I–V curves. The maximum detected emission power is about 45 nW, comparable to the emission power obtained from conventional mesa structures. At least for mesas the emission power is strongly angle dependent, with a maximum near 30° away from the c-axis [11, 15]. For simplicity, ignoring this angle dependence and integrating over the half-space above the substrate plane we find an integrated power of roughly 5 μW.

Figure 4 shows the current dependence of the detected emission power at various temperatures. The THz emission signal appeared in the fully resistive state and was observed in the temperature range from 10 to 45 K. Depending on temperature one or more emission peaks appeared. The largest one is at $T = 12$ K, i.e. close to the lower boundary of the temperature region where THz emission can be detected.

As to the emission frequency at the main output peak, the performance of the emitter is shown in figure 5. At the maximum radiation points, the voltage across the stack and emission signals are stable, allowing for measurements of the frequency spectrum by the interferometer. Graph (a) shows the spectrum at $T = 12$ K, $I = 9.3$ mA, and $V = 0.877$ V, where the maximum emission power was detected. The peak frequency is $f_p = 0.53$ THz, with a linewidth of 10 GHz, which is limited by the resolution of our setup (also at other temperatures the detected linewidths were resolution limited). According to the Josephson relation $V/N = \Phi_0 f$, we can calculate the junction number $N = 794$, close to the value estimated from the fabrication process. Graph (b) shows N versus T for various temperatures between 10 and 45 K. For temperatures of 12, 20 and 45 K, N is close to the value of 800 expected from the thickness of the stack. At $T = 10$ K N is slightly higher but within the error bars. At $T = 30$ and 35 K we seem to have lost some junctions. Graph (c) shows f_p versus T. The frequency interval where emission was

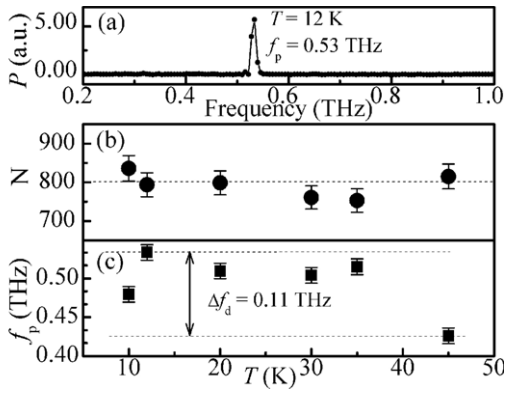

Figure 5. (a) Frequency spectrum of the detected emission at $T = 12$ K, $I = 9.3$ mA and $V = 0.877$ V, compare with figure 3(a). (b) Junction number (N) versus temperature. The dashed line indicates $N = 800$ expected from the thickness of the stack. (c) Peak frequency versus temperature.

observable is $\Delta f_d = 0.11$ THz. Note that the lowest values of f_p occur at, respectively the lowest and highest temperatures. The reason for this is unclear to us.

The observed maximum emission power is comparable to the emission power obtained from conventional mesa structures [5, 10, 11]. It was reported that a thick top upper electrode would hinder THz radiation from an IJJ stack [41]. This apparently is not the case, a finding which may trigger further understanding in the mechanism of generating coherent THz radiation from BSCCO IJJ stacks.

In the data shown above, the largest emission signals have been detected at high bias current. In fact, here the electrothermal behavior is different from that at low bias, where there is only little overheating of the stack. In the high bias regime, Joule heating leads to a non-homogeneous temperature distribution in the stack which may be well above the bath temperature in certain parts. As has been shown for mesa structures, above a certain current a hotspot (a region heated to a temperature above T_c) can form, typically near the point of current injection [6, 9, 10, 31, 41]. The position and size of the hotspot varies as the bias current changes, which will adjust some physical parameters in the stack. For instance, the hotspot can vary the resonance frequency of the cavity by changing the mode velocity and the size of the cold part of the mesa. In this way, the efficiency of synchronization from the cavity can be tuned by the hot spot. Often—although not always—the strongest emission is observed in this hotspot regime. As will be discussed elsewhere [42], a hotspot also appears in the double-sided structures. Here, heating is determined by the intrinsic properties of the single crystal itself, rather than being influenced by normal conducting contacts to the IJJ stack. As a consequence, the hotspot formation is very reproducible for stacks of a given geometry, a property which we believe is relevant for controlled THz emission. Further, as already mentioned, in the conventional fabrication process the shape of the mesa structure is usually a trapezoidal platform. The nonuniformity in junction area is a problem for synchronizing a large number of junctions [13]. In the double-sided fabrication process the nonuniformity in junction area is reduced, since two sides of the stack form a parallelogram, as shown in figure 1. This might help to fabricate more uniform, thick IJJ stacks for a powerful emitter.

However, the main advantage of the double-sided fabrication process is that various superconducting elements can be integrated in an all-superconducting structure. From the schematic diagram of figure 1 one can see that the electrodes on the other bank of the slit can be patterned into various elements such as antennas, additional stacks or other structures. It has been shown previously that arrays of stacks with superconducting interconnections, middle electrodes to a stack, antennas, or other integrated circuits can be realized from a single BSCCO crystal [39, 40, 43, 44]. This should have advantages compared to structures where different elements are connected by normal metal wires, e.g. by reducing resistive losses.

4. Conclusions

To conclude, we have successfully fabricated large size double-sided BSCCO IIJ stacks. In this way, the junction number in the stack can be well controlled and superconducting leads to the stack can be made. THz radiation comparable in power and frequency to conventional mesa structures was obtained. It seems that these double-sided IJJ THz emitter structures are helpful in making integrated radiation sources based on intrinsic Josephson junctions in high T_c superconductors. The result that THz emission from BSCCO stacks is not weakened by a thick superconducting upper electrode possibly triggers further understanding of THz emitters in IJJ stacks.

Acknowledgments

Financial support by the strategic Japanese–German International Cooperative Program of the JST and the DFG, and by Grants-in-Aid for scientific research from JSPS is gratefully acknowledged.

References

[1] Tonouchi M 2007 *Nature Photon.* **1** 97
[2] Lee M and Wanke M C 2007 *Science* **316** 64
[3] Ferguson B and Zhang X C 2002 *Nature Mater.* **1** 26
[4] Kleiner R, Steinmeyer F, Kunkel G and Muller P 1992 *Phys. Rev. Lett.* **68** 2394
[5] Ozyuzer L *et al* 2007 *Science* **318** 1291
[6] Wang H B, Guénon S, Yuan J, Iishi A, Arisawa S, Hatano T, Yamashita T, Koelle D and Kleiner R 2009 *Phys. Rev. Lett.* **102** 017006
[7] Minami H, Kakeya I, Yamaguchi H, Yamamoto T and Kadowaki K 2009 *Appl. Phys. Lett.* **95** 232511
[8] Ozyuzer L *et al* 2009 *Supercond. Sci. Technol.* **22** 114009
[9] Guénon S *et al* 2010 *Phys. Rev.* B **82** 214506
[10] Wang H B *et al* 2010 *Phys. Rev. Lett.* **105** 057002
[11] Tsujimoto M, Yamaki K, Deguchi K, Yamamoto T, Kashiwagi T, Minami H, Tachiki M, Kadowaki K and Klemm R A 2010 *Phys. Rev. Lett.* **105** 037005
[12] Koseoglu H, Turkoglu F, Simsek Y and Ozyuzer L 2011 *J. Supercond. Novel Magn.* **24** 1083–6

[13] Benseman T M, Koshelev A E, Gray K E, Kwok W K, Welp U, Kadowaki K, Tachiki M and Yamamoto T 2011 *Phys. Rev.* B **84** 064523
[14] Yamaki K, Tsujimoto M, Yamamoto T, Furukawa A, Kashiwagi T, Minami H and Kadowaki K 2011 *Opt. Express* **19** 3193
[15] Kashiwagi T *et al* 2012 *Japan. J. Appl. Phys.* **51** 010113
[16] Tsujimoto M *et al* 2012 *Phys. Rev. Lett.* **108** 107006
[17] Bulaevskii L N and Koshelev A E 2007 *Phys. Rev. Lett.* **99** 057002
[18] Koshelev A E 2008 *Phys. Rev.* B **78** 174509
[19] Lin S Z and Hu X 2008 *Phys. Rev. Lett.* **100** 247006
[20] Krasnov V M 2009 *Phys. Rev. Lett.* **103** 227002
[21] Klemm R A and Kadowaki K 2010 *J. Phys.: Condens. Matter* **22** 37
Klemm R A and Kadowaki K 2010 *J. Supercond. Novel Magn.* **23** 613
[22] Nonomura Y 2009 *Phys. Rev.* B **80** 140506
[23] Tachiki M, Fukuya S and Koyama T 2009 *Phys. Rev. Lett.* **102** 127002
[24] Koyama T, Matsumoto H, Machida M and Kadowaki K 2009 *Phys. Rev.* B **79** 104522
[25] Pedersen N F and Madsen S 2009 *IEEE Trans. Appl. Supercond.* **19** 726–9
[26] Savel'ev S, Yampol'skii V A, Rakhmanov A L and Nori F 2010 *Rep. Prog. Phys.* **73** 026501
[27] Hu X and Lin S Z 2010 *Supercond. Sci. Technol.* **23** 053001
[28] Zhou W, Wang C and Chen Q H 2010 *Phys. Rev.* B **82** 184514
[29] Koshelev A E 2010 *Phys. Rev.* B **82** 174512
[30] Tachiki M, Ivanovic K and Kadowaki K 2011 *Phys. Rev.* B **83** 014508
[31] Yurgens A 2011 *Phys. Rev.* B **83** 184502
[32] Lin S Z, Hu X and Bulaevskii L 2011 *Phys. Rev.* B **84** 104501
[33] Slipchenko T M, Kadygrob D V, Bogdanis D, Yampol'skii V A and Krokhin A A 2011 *Phys. Rev.* B **84** 224512
[34] Krasnov V M 2011 *Phys. Rev.* B **83** 174517
[35] Asai H, Tachiki M and Kadowaki K 2012 *Phys. Rev.* B **85** 064521
[36] Doh Y J, Lee H J and Chang H S 2000 *Phys. Rev.* B **61** 3620
[37] Doh Y J, Kim J H, Kim K T and Lee H J 2000 *Phys. Rev.* B **61** R3834
[38] Li S X, Qiu W, Han S, Wei Y F, Zhu X B, Gu C Z, Zhao S P and Wang H B 2007 *Phys. Rev. Lett.* **99** 037002
[39] Wang H B, Wu P H, Chen J, Maeda K and Yamashita T 2002 *Appl. Phys. Lett.* **80** 1604
[40] Wang H B, Wu P H and Yamashita T 2001 *Appl. Phys. Lett.* **78** 4010
[41] Kakeya I, Omukai Y, Yamamoto T, Kadowaki K and Suzuki M 2011 *Superconducting Centennial Conf. (Den Haag, Sept. 2011)*
[42] Gross B *et al* 2012 unpublished
[43] Wang H B, Hatano T, Yamashita T, Wu P H and Muller P 2005 *Appl. Phys. Lett.* **86** 023504
[44] Wang H B, Chen J, Wu P H, Yamashita T, Vasyukov D and Müller P 2003 *Supercond. Sci. Technol.* **16** 1375

Publication 4

PHYSICAL REVIEW B **86**, 060505(R) (2012)

Linewidth dependence of coherent terahertz emission from $Bi_2Sr_2CaCu_2O_8$ intrinsic Josephson junction stacks in the hot-spot regime

Mengyue Li,[1,2] Jie Yuan,[2,3,*] Nickolay Kinev,[4] Jun Li,[2,5] Boris Gross,[6] Stefan Guénon,[6] Akira Ishii,[2] Kazuto Hirata,[2] Takeshi Hatano,[2] Dieter Koelle,[6] Reinhold Kleiner,[6] Valery P. Koshelets,[4] Huabing Wang,[1,2,†] and Peiheng Wu[1]

[1]*Research Institute of Superconductor Electronics, Nanjing University, Nanjing 210093, China*

[2]*National Institute for Materials Science, Tsukuba 3050047, Japan*

[3]*Department of Applied Physics, Wuhan University of Science and Technology, Wuhan 430081, China*

[4]*Kotel'nikov Institute of Radio Engineering and Electronics, Moscow 125009, Russia*

[5]*Hokkaido University, Hokkaido 0600810, Japan*

[6]*Physikalisches Institut and Center for Collective Quantum Phenomena in LISA$^+$, Universität Tübingen, D-72076 Tübingen, Germany*

(Received 3 April 2012; revised manuscript received 20 July 2012; published 8 August 2012)

We report on measurements of the linewidth Δf of terahertz radiation emitted from intrinsic Josephson junction stacks, using a Nb/AlN/NbN integrated receiver for detection. Previous resolution-limited measurements indicated that Δf may be below 1 GHz—much smaller than expected from a purely cavity-induced synchronization. While at low bias we found Δf to be not smaller than ∼500 MHz, at high bias, where a hot spot coexists with regions which are still superconducting, Δf turned out to be as narrow as 23 MHz. We attribute this to the hot spot acting as a synchronizing element. Δf *decreases* with increasing bath temperature, a behavior reminiscent of motional narrowing in NMR or electron spin resonance (ESR), but hard to explain in standard electrodynamic models of Josephson junctions.

DOI: 10.1103/PhysRevB.86.060505 PACS number(s): 74.50.+r, 74.72.−h, 85.25.Cp

Terahertz generation utilizing stacks of intrinsic Josephson junctions (IJJs) in the high-transition-temperature (high-T_c) cuprate $Bi_2Sr_2CaCu_2O_{8+\delta}$ (BSCCO) has been a hot topic in recent years, both in terms of experiment[1–11] and theory.[12–39] Typical emission frequencies f_p are 0.4–1 THz, with a maximum output power of tens of microwatts emitted into free space.[10] The IJJ stacks are usually patterned as mesas on top of BSCCO single crystals and contain 500–2000 IJJs. A large fraction of these IJJs oscillate coherently. There are good indications that the synchronization has to do with electric fields utilizing the mesa as a cavity: (i) f_p increases inversely proportional to the junction width[1,10] or fulfills the resonance condition for cylindrical mesas[4,6] and (ii) low-temperature scanning-laser microscopy imaged standing waves at bias points close to terahertz emission maxima.[2,4,5] On the other hand, (iii) the linewidth Δf of terahertz radiation—so far mostly resolution limited to some gigahertz—is much lower than the estimated linewidth of the cavity resonances[5,38] and thus one cannot simply assume that the IJJs are slaved by the cavity. (iv) In some cases terahertz emission lines were fairly tunable or they occurred at positions not compatible with cavity resonances.[10] A recent mixing experiment[10] has revealed a Δf as low as ∼0.5 GHz at low bias, raising even more questions about the mechanism of synchronization.

In the IJJ stacks, operated at a bath temperature T_b well below T_c, there are two emission regimes. At moderate input power ("low-bias regime") there is only little heating and the temperature distribution in the mesa is roughly homogeneous and close to T_b. At high input power ("high-bias regime") a hot spot (an area heated to above T_c) forms inside the mesa, leaving the "cold" part of the mesa for terahertz generation by the Josephson effect. The hot spot seems to take part in synchronization.[4,5,31,33]

To measure Δf and thus to gain more insight into the mechanism of synchronization, we have used a Nb/AlN/NbN superconducting integrated receiver (SIR)[40] for detecting terahertz emission from an IJJ mesa containing ∼600 junctions; see Fig. 1.

The $330 \times 50\,\mu m^2$ wide and 0.9-μm-thick mesa was patterned on a BSCCO single crystal ($T_c \approx 82$ K), as described elsewhere.[2,4,5] Mesa and base crystal were contacted by Au wires fixed with silver paste. Contact resistances (∼1 Ω) have been subtracted in the data discussed below. "Conventional" terahertz emission measurements were performed in Tsukuba, using a Fourier spectrometer and a Si bolometer, as described in Ref. 5. Measurements with the SIR were performed in Moscow. The SIR comprises, on a single chip, a planar antenna combined with a superconductor-insulator-superconductor (SIS) mixer, a superconducting flux-flow oscillator (FFO) acting as local oscillator (LO), and a SIS harmonic mixer (HM) for the FFO phase locking. The frequency of the LO is continuously tunable from 350 to 750 GHz, while the SIS mixer is effectively matched to the planar antenna between 450 and 700 GHz, limiting the SIR operation range. A frequency resolution of the SIR well below 100 kHz has been confirmed.[41]

Figure 2 shows a typical set of data at $T_b = 40$ K. The current-voltage curve (IVC) of the mesa is shown in Fig. 2(a). Upon increasing bias current I, near $I \sim 25$ mA, one observes jumps (gray line of IVC) where the IJJs switch into their resistive state. When lowering I from ∼40 mA (black line) all junctions are resistive. Switchback occurs below 3.65 mA. The outermost branch, where the emission data are taken, exhibits the typical back bending arising from strong heating.[33] The high-bias regime embraces the region of negative differential resistance on this branch. Figures 2(b) and 2(c) show the broadband terahertz emission power P_{bol}, simultaneously detected with the IVC by a bolometer, vs (b) current I and (c) voltage V across the mesa. In panel (b) one observes a broad (with respect to I) emission peak in the high-bias regime and a sharper one at low bias which, for

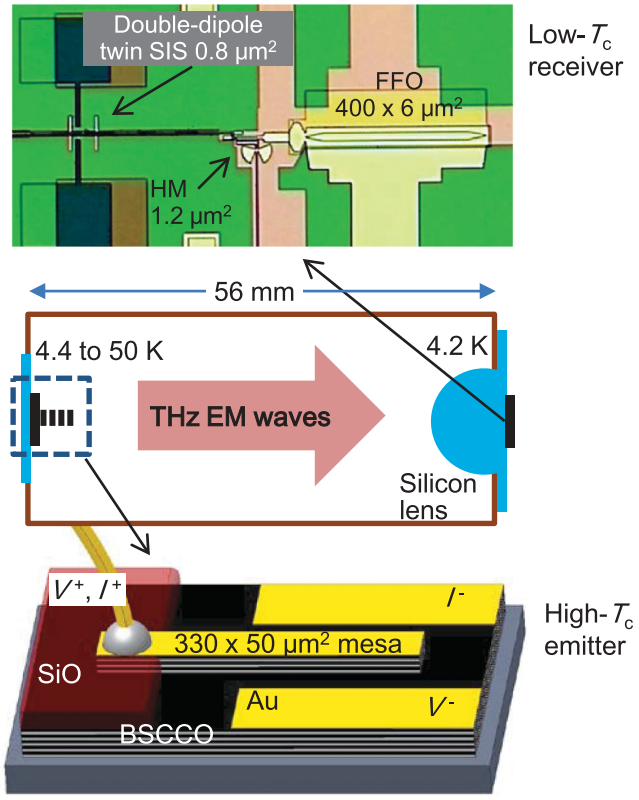

FIG. 1. (Color online) Setup for detection of terahertz emission from intrinsic Josephson junctions (sketched at bottom). Top: central part of the superconducting integrated receiver (SIR) chip with a double-dipole antenna, a twin superconductor-insulator-superconductor (SIS) mixer and a harmonic mixer (HM) for flux-flow oscillator (FFO) phase locking. For thermal shielding an infrared filter (2-mm-thick GoreTex film) was installed between the BSCCO oscillator and the SIR.

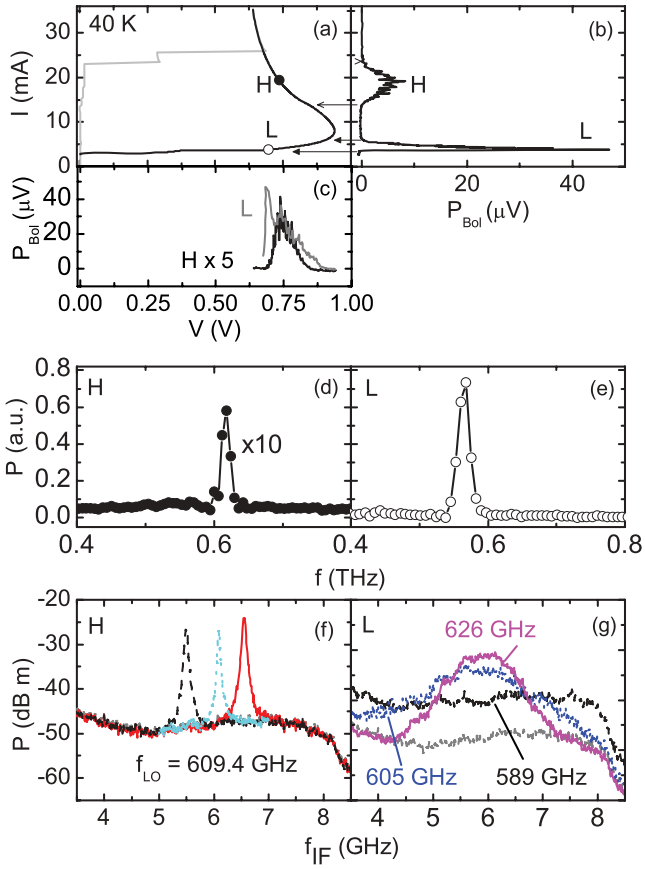

FIG. 2. (Color online) Results of the terahertz emission experiment at 40 K: (a) IVC of the IJJ stack. Terahertz emission power vs current (b) and voltage (c). (d), (e) Fourier spectra of emitted radiation taken at points H and L in panel (a). Spectra of the mixing output of the SIR for (f) three bias points in the high-bias regime and (g) for three bias points in the low-bias regime. In (g) f_{LO} was adjusted for each bias to bring the intermediate frequency (IF) signal, with $f_{IF} = f_p - f_{LO}$, to the center of the spectrum analyzer. f_{LO} values are indicated in the graph. Gray line indicates background noise.

this particular mesa, was more intense than the high-bias peak. P_{bol} vs. V, Fig. 2(c), shows a smooth peak for the high-bias regime, with a full-width-at-half-maximum in voltage of about 75 mV (black line). In contrast, the low-bias signal (gray line) seems to exhibit structure, indicating different groups of oscillating IJJs.[42] Emission spectra, measured using a Fourier spectrometer, are shown in Figs. 2(d) and 2(e). Spectrum (d) has been taken at point H in (a) where $V = 736$ mV, $I = 19.43$ mA. The emission peak is at $f_p = 618$ GHz, corresponding to $N = V/(f_p\Phi_0) \approx 575$ oscillating IJJs, with a ∼1% uncertainity arising from correcting for the contact resistance. Φ_0 is the flux quantum. The (resolution-limited) linewidth of the emission peak is ∼15 GHz. Figure 2(e) shows a spectrum for bias point L where $V = 697$ mV, $I = 3.76$ mA. The emission peak, having a width also near the resolution limit, is at $f_p = 594$ GHz, corresponding to $N \sim 567$.

The SIR measurements, showing the emitted radiation at the intermediate frequency (IF) $f_{IF} = f_p - f_{LO}$, were performed near points H [Fig. 2(f)] and L [Fig. 2(g)]. For $T_b = 32$ K and 44 K we have followed the voltage dependence of the emission peaks for frequencies between 560 and 737 GHz and found the Josephson relation $f_p = V/(N\Phi_0)$ to be fulfilled, with $N = 570 \pm 5$ in both cases. In Fig. 2(f) the LO frequency of the SIR is $f_{LO} = 609.4$ GHz. We show three measurements where V was increased from ≈724.7 mV in steps of 0.6 mV. There is a single emission peak which shifts with increasing voltage. Δf of the two outermost peaks is ∼60 MHz, while the center one is even sharper, $\Delta f \sim 40$ MHz. In contrast, the linewidths seen in the low-bias regime [see Fig. 2 (g)] are much larger and often exceeded the 6-GHz bandwidth of the IF amplifier. The lowest values are ∼0.5 GHz, in agreement with previous measurements.[10]

Figure 3 shows the most narrow line ($\Delta f = 23$ MHz) we have obtained in the high-bias regime. Data were taken at $T_b = 44$ K, $I = 16.3$ mA, and $V = 0.721$ V. From $f_{LO} = 605.75$ GHz and $f_{IF} = 6.2$ GHz we find $f_p = 611.95$ GHz and $N \approx 570$. This value for Δf is already quite close to the limit value that can be phase locked by a regular room-temperature semiconductor phase-locked-loop (PLL) system with regulation bandwidth of about 20 MHz, presently limited by the delay in the cable between the oscillator inside the cryostat and the PLL system (this limitation can be overridden by use of a cryogenic PLL system

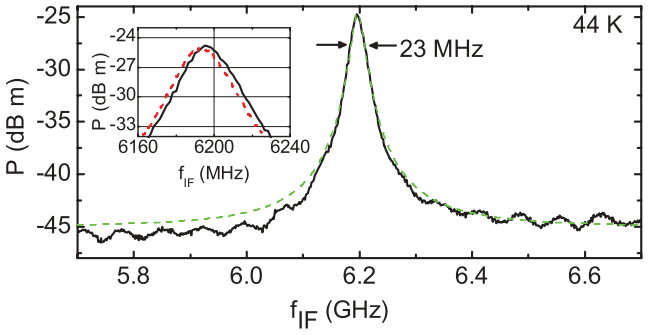

FIG. 3. (Color online) Spectrum (most narrow emission line obtained) of the mixing output of the SIR for $I = 16.3$ mA, $V = 0.721$ V in the high-bias regime at $T_b = 44$ K. The LO frequency is $f_{\rm LO} = 605.75$ GHz; $f_{\rm IF} = 6.2$ GHz. Dashed line is a Lorenzian fit with $\Delta f = 23$ MHz. Inset shows drift of emission peak within 3 min.

with regulation bandwidth >40 MHz[43]). We also investigated the stability of the terahertz emission line. The inset of Fig. 3 shows two measurements, taken at a 3-min interval. The 3-MHz drift observed was smooth and unidirectional and even lower than the typical 3-min drift (∼10 MHz) of a free-running Nb-based FFO. We also note that the emission lines observed at high bias have Lorentzian shape; see the dashed line in Fig. 3. Recent three-dimensional (3D) simulations[39] based on the sine-Gordon equation and taking a hot spot into account yielded an asymmetric Fano shape in contrast to our experimental data.

If Δf of the high-bias terahertz emission signal were set by a cavity resonance, its quality factor $Q = f/\Delta f$ would have to amount some 10^4, which is more than unrealistic for an IJJ stack.[28,38,44] At least for small mesas, cavity resonances become overdamped for $T > 60$ K.[44] For $T \sim 40$ K we expect $Q \ll 50$. The low value of Δf implies that when changing the bias current in Fig. 2(c), a sharp emission line "moves" through the $\Delta V = 75$-mV-wide emission peak. The ratio $V/\Delta V \sim 10$ of this peak would indeed be compatible with the notion of a cavity resonance.

In Fig. 4(a) we show by black circles Δf vs T_b. Strikingly, Δf *decreases* with increasing T_b by about a factor 15 and, roughly, $\Delta f \propto T_b^{-4}$; see the gray line in Fig. 4(a). For comparison we have also added for two temperatures low-bias data for f_p near 616 GHz. In this regime it was difficult to obtain systematic data points, because at most temperatures only a broadband (>6 GHz) signal appeared in the SIR output. This further indicates that at low bias phase lock is incomplete. Noting that T_b may not be the best variable for our system, in Fig. 4(b) we also show Δf vs the dc input power $P_{\rm dc} = IV$, where for V we have used the measured value, not corrected for contact resistance. Low-bias data are shown by open squares. The black circles show the same high-bias data as Fig. 4(a); Δf increases with increasing $P_{\rm dc}$. Note that the smallest $P_{\rm dc}$ is at high T_b and the highest $P_{\rm dc}$ is at the lowest T_b. However, this does not imply that the sample is hotter at low T_b. Simulations of the temperature distribution, performed analogously to the calculations in Ref. 33, yielded temperatures of the cold part of the mesa which are some 10–15 K above T_b but still increase with increasing T_b. For the hot part we find peak temperatures $T_{\rm h}$ in the range 80–110 K, with the highest value indeed at the

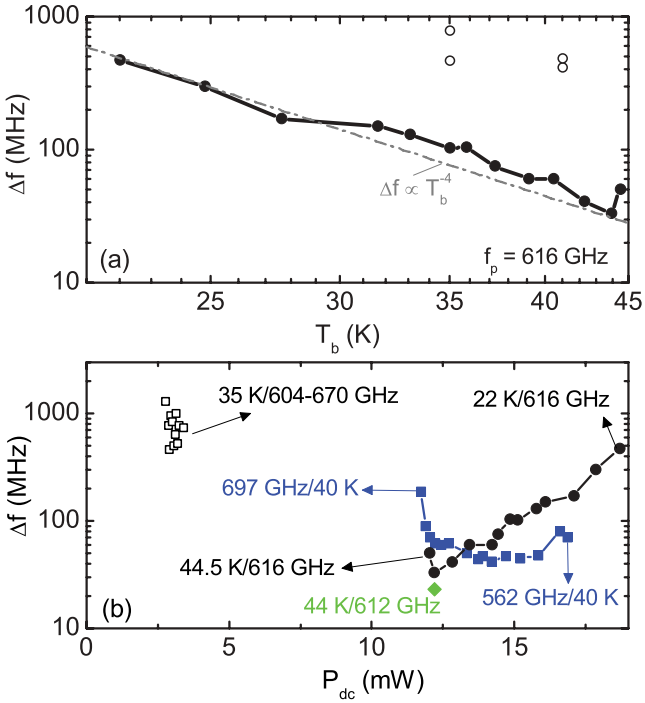

FIG. 4. (Color online) Linewidth vs (a) bath temperature and (b) dc input power. In panel (a) solid (open) circles are for high (low) bias. In panel (b) open squares are for low bias; other symbols for high bias. Solid (black) circles: same data as in panel (a). Solid (blue) squares: linewidth at $T_b = 40 \pm 1$ K and various values of f_p. Linewidth of Fig. 3 is shown by solid (green) diamond.

lowest value of T_b. For comparison we show by solid squares in Fig. 4(b) Δf out of a measurement series, where we have fixed T_b to 40 ± 1 K and varied f_p. Within this curve f_p varies monotonically from 697 GHz to 562 GHz. In contrast to the $f_p = $ const. curve, Δf is about constant at intermediate values of $P_{\rm dc}$ and increases outside of this regime. Thus there seems to be no systematic dependence of Δf on $P_{\rm dc}$. Further note that a slight increase of Δf at low $P_{\rm dc}$ is visible both on the $T_b = $ const. and the $f_p = $ const. curve. Here, the bias is close to the hot-spot nucleation point and it is possible that the hot part of the stack already is close to or even below T_c; that is, we approach the low-bias regime.

We note here that a similar decrease of Δf with increasing T_b, although somewhat less pronounced, was also found for another mesa having the same geometry. For this mesa, Δf measured for f_p between 594 and 606 GHz ranged between 161 and 197 MHz at $T_b = 15$ K and decreased to ∼36 MHz at $T_b = 40$ K; also for this sample, the largest (lowest) values of Δf were obtained at the lowest (largest) values of $P_{\rm dc}$. Thus, while the $\Delta f \propto T_b^{-4}$ behavior discussed above is not universal, the general trend of a decreasing Δf with increasing T_b seems reproducible.

We next compare the high-bias data to theoretical predictions. We decompose Δf into a sum of two contributions Δf_T and Δf_x, as has been done in an analysis of the radiation linewidth of the FFO.[45] Δf_T arises from fluctuations of the quasiparticle current (Nyquist noise) and Δf_x represents additional fluctuations of—at this point—unspecified origin. For a current biased lumped junction $\Delta f_T = (4\pi/\Phi_0^2)(R_d^2/R)k_B T$,

where R is the junction resistance, R_d is the differential resistance of the IVC at the bias point, and T is the junction temperature.[46,47] For a phase-locked one-dimensional (1D) array of N junctions the linewidth is expected to decrease $\propto N^{-1}$.[47] In our case, in the high-bias regime the hot part of the IJJ stack is an excellent candidate for a shunting network causing phase locking.[4,5,31,33] Our IJJ stacks are not lumped, and T not only differs from T_b but also varies strongly within the stack. Nonetheless an analysis of Δf_T may give some indication whether Δf vs T_b can be explained via Nyquist noise. We first look at the cold part of the mesa only. The out-of-plane resistance R_c of BSCCO has a negative temperature coefficient (roughly $R_c \propto T^{-1}$) and thus $T/R \propto T^2$. We cannot infer R_d from the IVC, since T varies strongly along this curve. However, from small mesas it is known that R_d is smaller but not very different from R. Thus, an unrealistic $R_d \propto T^{-3}$ would be required to explain the data. We also considered a hot resistor (resistance R_s, temperature T_s), representing the hot spot, in parallel to a cold one (resistance R_J, temperature T_J), as has been analyzed in Ref. 48 for a single junction, with the result that R should be replaced by $R_{\rm eff} = (R_s^{-1} + R_J^{-1})^{-1}$ and T by $T_{\rm eff}/R_{\rm eff} = T_s/R_s + T_J/R_J$. $R_{\rm eff}$ follows from the measured IVC. With $T_s \approx T_h \gg T_J$ and $R_s \ll R_J$ we get $T_{\rm eff} \approx T_h$ and, with $R_d \approx R_{\rm eff}$, one obtains an almost temperature-independent $\Delta f_T \approx 250$ MHz. Dividing this by N yields a linewidth which not only has the wrong temperature dependence but also is much lower than the measured Δf. Thus, we can state that our attempts to explain the measured Δf by Δf_T have failed.

The second contribution to Δf, Δf_x, may arise from moving fluxons. This is the case for the FFO where, however, $\Delta f_x \propto T^{1/2}$ was found.[45] Recently, terahertz generation in IJJ stacks by bound fluxon-antifluxon pairs (breathers) oscillating near a cavity resonance was proposed. Whether this mechanism leads to the observed T depencence of Δf is unclear, although we would expect an increase with T, as for the case of the FFO. Also, more conventional simulations based on 1D-coupled-sine-Gordon equations yielded a Δf which increased with temperature.[32]

Another hint may be that at low T_b the in-plane thermal gradient in the stack is larger than at high T_b. However, we cannot translate this to the observed Δf vs T_b dependence.

Let us thus also look at other effects in physics that cause a decrease of Δf with increasing temperature. Motional narrowing in NMR or electron spin resonance (ESR) are prominent examples.[49,50] It is tempting to speculate about an analogous effect in the IJJ stacks. In a nutshell, motional narrowing occurs when some spatially varying field, causing line broadening, is reduced on average due to temporal fluctuations. In our case this could be due to a time-dependent hot spot. Generally, it is possible that the hot spot oscillates.[51] We have searched for such oscillations for frequencies in the kilohertz and megahertz range but could not find any. Still, the temperatures of the hot and cold parts of the stack may fluctuate, causing fluctuations of the hot-spot edge position and resulting in variations in junction parameters such as critical current and resistance. Suppose that the static spread in these parameters is too large to achieve complete phase lock. Temporally fluctuating parameters could lead to a situation where for some time these parameters are in the synchronization window, causing improved phase locking.

To conclude: At low bias the best values for Δf are on the order of 0.5 GHz, consistent with previous measurements.[10] However, the irregular line shape and the strongly varying linewidth indicate that not all junctions are phase locked and a superposition of several lines is observed. In the high-bias regime we observe much lower values of Δf down to ~23 MHz. The improved linewidth compared to the low-bias regime suggests that the hot spot acts as a shunting element providing phase lock. Δf, measured at fixed emission frequency, *decreases* with increasing temperature, reminiscent of motional narrowing observed in NMR or ESR. This temperature dependence is hard to explain within standard models for the linewidth of oscillating Josephson junctions. In any case, the narrow emission line observed in the high-bias regime makes intrinsic Josephson junction stacks interesting for, e.g., terahertz spectroscopy.

We gratefully acknowledge financial support by the National Natural Science Foundation of China, the JST/DFG strategic Japanese-German International Cooperative Program, the Grants-in-Aid for scientific research from JSPS and RFBR Project No. 12-02-00882, No. 11-02-12195-ofi-m, and No. 11-02-12213-ofi-m and Grant No. 2456.2012.2 and No. 02.740.11.0795.

*phy.wust@gmail.com
†hbwang1000@gmail.com

[1] L. Ozyuzer, A. E. Koshelev, C. Kurter, N. Gopalsami, Q. Li, M. Tachiki, K. Kadowaki, T. Yamamoto, H. Minami, H. Yamaguchi, T. Tachiki, K. E. Gray, W.-K. Kwok, and U. Welp, Science **318**, 1291 (2007).

[2] H. B. Wang, S. Guénon, J. Yuan, A. Iishi, S. Arisawa, T. Hatano, T. Yamashita, D. Koelle, and R. Kleiner, Phys. Rev. Lett. **102**, 017006 (2009).

[3] H. Minami, I. Kakeya, H. Yamaguchi, T. Yamamoto, and K. Kadowaki, Appl. Phys. Lett. **95**, 232511 (2009).

[4] S. Guénon, M. Grünzweig, B. Gross, J. Yuan, Z. G. Jiang, Y. Y. Zhong, M. Y. Li, A. Iishi, P. H. Wu, T. Hatano, R. G. Mints, E. Goldobin, D. Koelle, H. B. Wang, and R. Kleiner, Phys. Rev. B **82**, 214506 (2010).

[5] H. B. Wang, S. Guénon, B. Gross, J. Yuan, Z. G. Jiang, Y. Y. Zhong, M. Gruenzweig, A. Iishi, P. H. Wu, T. Hatano, D. Koelle, and R. Kleiner, Phys. Rev. Lett. **105**, 057002 (2010).

[6] M. Tsujimoto, K. Yamaki, K. Deguchi, T. Yamamoto, T. Kashiwagi, H. Minami, M. Tachiki, K. Kadowaki, and R. A. Klemm, Phys. Rev. Lett. **105**, 037005 (2010).

[7] H. Koseoglu, F. Turkoglu, Y. Simsek, and L. Ozyuzer, J. Supercond. Nov. Magn. **24**, 1083 (2011).

[8] T. M. Benseman, A. E. Koshelev, K. E. Gray, W. K. Kwok, U. Welp, K. Kadowaki, M. Tachiki, and T. Yamamoto, Phys. Rev. B **84**, 064523 (2011).

[9]K. Yamaki, M. Tsujimoto, T. Yamamoto, A. Furukawa, T. Kashiwagi, H. Minami, and K. Kadowaki, Opt. Express **19**, 3193 (2011).
[10]T. Kashiwagi, M. Tsujimoto, T. Yamamoto, H. Minami, K. Yamaki, K. Delfanzari, K. Deguchi, N. Orita, T. Koike, R. Nakayama, T. Kitamura, M. Sawamura, S. Hagino, K. Ishida, K. Ivancovic, H. Asai, M. Tachiki, R. A. Klemm, and K. Kadowaki, Jpn. J. Appl. Phys. **51**, 010113 (2012).
[11]M. Tsujimoto, T. Yamamoto, K. Delfanazari, R. Nakayama, T. Kitamura, M. Sawamura, T. Kashiwagi, H. Minami, M. Tachiki, K. Kadowaki, and R. A. Klemm, Phys. Rev. Lett. **108**, 107006 (2012).
[12]L. N. Bulaevskii and A. E. Koshelev, Phys. Rev. Lett. **99**, 057002 (2007).
[13]A. E. Koshelev and L. N. Bulaevskii, Phys. Rev. B **77**, 014530 (2008).
[14] A. E. Koshelev, Phys. Rev. B **78**, 174509 (2008).
[15]S. Lin and X. Hu, Phys. Rev. Lett. **100**, 247006 (2008).
[16]V. M. Krasnov, Phys. Rev. Lett. **103**, 227002 (2009).
[17]R. A. Klemm and K. Kadowaki, J. Phys.: Condens. Matter. **22**, 375701 (2010).
[18]X. Hu and S. Z. Lin, Phys. Rev. B **80**, 064516 (2009).
[19]Y. Nonomura, Phys. Rev. B **80**, 140506 (2009).
[20]M. Tachiki, S. Fukuya, and T. Koyama, Phys. Rev. Lett. **102**, 127002 (2009).
[21]T. Koyama, H. Matsumoto, M. Machida, and K. Kadowaki, Phys. Rev. B **79**, 104522 (2009).
[22]N. Pedersen and S. Madsen, IEEE Trans. Appl. Supercond. **19**, 726 (2009).
[23]A. Grib and P. Seidel, Phys. Status Solidi-Rapid Res. Lett. **3**, 302 (2009).
[24]S. Savel'ev, V. A. Yampol'skii, A. L. Rakhmanov, and F. Nori, Rep. Prog. Phys. **73**, 026501 (2010).
[25]X. Hu and S. Z. Lin, Supercond. Sci. Technol. **23**, 053001 (2010).
[26]S. Z. Lin and X. Hu, Phys. Rev. B **82**, 020504 (2010).
[27]W. Zhou, C. Wang, and Q.-H. Chen, Phys. Rev. B **82**, 184514 (2010).
[28]S. O. Katterwe, A. Rydh, H. Motzkau, A. B. Kulakov, and V. M. Krasnov, Phys. Rev. B **82**, 024517 (2010).
[29]V. M. Krasnov, Phys. Rev. B **82**, 134524 (2010).
[30]A. E. Koshelev, Phys. Rev. B **82**, 174512 (2010).
[31]M. Tachiki, K. Ivanovic, K. Kadowaki, and T. Koyama, Phys. Rev. B **83**, 014508 (2011).
[32]T. Tachiki and T. Uchida, Phys. C (Amsterdam, Neth.) **471**, 1206 (2011).
[33]A. Yurgens, Phys. Rev. B **83**, 184501 (2011).
[34]A. Yurgens and L. N. Bulaevskii, Supercond. Sci. Technol. **24**, 015003 (2011).
[35]S. Z. Lin, X. Hu, and L. Bulaevskii, Phys. Rev. B **84**, 104501 (2011).
[36]T. Koyama, H. Matsumoto, M. Machida, and Y. Ota, Supercond. Sci. Technol. **24**, 085007 (2011).
[37]T. M. Slipchenko, D. V. Kadygrob, D. Bogdanis, V. A. Yampol'skii, and A. A. Krokhin, Phys. Rev. B **84**, 224512 (2011).
[38]V. M. Krasnov, Phys. Rev. B **83**, 174517 (2011).
[39]H. Asai, M. Tachiki, and K. Kadowaki, Phys. Rev. B **85**, 064521 (2012).
[40]V. P. Koshelets and S. Shitov, Supercond. Sci. Technol. **13**, R53 (2000).
[41]V. P. Koshelets, A. B. Ermakov, L. V. Filippenko, N. V. Kinev, O. S. Kiselev, M. Y. Torgashin, A. de Lange, G. de Lange, S. I. Pripolzin, and V. L. Vaks, Proc. SPIE **7854**, 78540J (2010).
[42]In fact, at low bias, often emission lines in the gigahertz range, most likely resulting from self-mixing between nearby terahertz emission lines, can be measured. In the experiments with the SIR it was observed that these gigahertz emission lines sometimes cross-talk to the SIS mixer at the IF frequencies, disturbing its response.
[43]A. Khudchenko, V. Koshelets, P. Dmitriev, A. Ermakov, P. Yagoubov, and O. Pylypenko, Supercond. Sci. Technol. **22**, 085012 (2009).
[44]S. O. Katterwe and V. M. Krasnov, Phys. Rev. B **84**, 214519 (2011).
[45]A. A. Golubov, B. A. Malomed, and A. V. Ustinov, Phys. Rev. B **54**, 3047 (1996).
[46]A. J. Dahm, A. Denenstein, D. N. Langenberg, W. H. Parker, D. Rogovin, and D. J. Scalapino, Phys. Rev. Lett. **22**, 1416 (1969).
[47]A. K. Jain, K. K. Likharev, J. E. Lukens, and J. E. Sauvageau, Phys. Rep. **109**, 309 (1984).
[48]A. I. Larkin and Y. N. Ovchinnikov, Sov. Phys. JETP **26**, 1219 (1968).
[49]N. Kumar and K. P. Sinha, Z. Phys. **197**, 26 (1966).
[50]J. R. Hendrickson and P. J. Bray, J. Magn. Res. **9**, 341 (1973).
[51]A. V. Gurevich and R. G. Mints, Rev. Mod. Phys. **59**, 941 (1987).

Publication 5

Hot-spot formation in stacks of intrinsic Josephson junctions in $Bi_2Sr_2CaCu_2O_8$

B. Gross,[1] S. Guénon,[1,2] J. Yuan,[3] M. Y. Li,[3,4] J. Li,[3] A. Ishii,[3] R. G. Mints,[5] T. Hatano,[3] P. H. Wu,[4] D. Koelle,[1] H. B. Wang,[3,4,*] and R. Kleiner[1,†]

[1]*Physikalisches Institut – Experimentalphysik II and Center for Collective Quantum Phenomena in LISA⁺, Universität Tübingen, Auf der Morgenstelle 14, D-72076 Tübingen, Germany*

[2]*Department of Physics, Center for Advanced Nanoscience, University of California-San Diego, La Jolla, California 92093, USA*

[3]*National Institute for Materials Science, Tsukuba 3050047, Japan*

[4]*Research Institute of Superconductor Electronics, Nanjing University, Nanjing 210093, China*

[5]*The Raymond and Beverly Sackler School of Physics and Astronomy, Tel Aviv University, Tel Aviv 69978, Israel*

(Received 5 June 2012; revised manuscript received 27 July 2012; published 26 September 2012)

We have studied experimentally and numerically temperature profiles and the formation of hot spots in intrinsic Josephson junction stacks in $Bi_2Sr_2CaCu_2O_8$ (BSCCO). The superconducting stacks are biased in a state where all junctions are resistive. The formation of hot spots in this system is shown to arise mainly from the strongly negative temperature coefficient of the c-axis resistivity of BSCCO at low temperatures. This leads to situations where the maximum temperature in the hot spot can be below or above the superconducting transition temperature T_c. The numerical simulations are in good agreement with the experimental observations.

DOI: 10.1103/PhysRevB.86.094524 PACS number(s): 74.50.+r, 74.72.−h, 85.25.Cp

I. INTRODUCTION

Joule heating is an omnipresent issue in current-carrying structures and has been studied for a long time. General aspects, like the propagation of switching waves or the formation of static electrothermal domains in bistable conductors are well-known phenomena.[1,2] In Josephson junctions, heating often is small enough to be neglected. An exception are stacks of intrinsic Josephson junctions (IJJs) in the high-temperature superconductor $Bi_2Sr_2CaCu_2O_8$ (BSCCO). Here, the BSCCO crystal structure intrinsically forms stacks of Josephson junctions, each having a thickness of 1.5 nm. A single IJJ may carry a voltage V of some millivolts and a current I of several milliampers. Although the dissipative power generated by a single IJJ is only some μW, the power inside a stack of, say, 1000 IJJs amounts to several milliwatts, with power densities well in excess of 10^4 W/cm^3. For small sized (approximately a few micrometers in diameter, consisting of some 10 IJJs) stacks the corresponding overheating has been discussed intensively in literature.[3–10]

Recently, coherent off-chip terahertz radiation with an extrapolated output power of some μW was observed from stacks of more than 600 IJJs, with lateral dimensions in the 100 μm range.[11] The IJJ stacks have been patterned in the form of mesa structures, as shown schematically in Fig. 1. Terahertz radiation emitted from such IJJ stacks became a hot topic in recent years, both in terms of experiment[11–27] and theory.[28–56]

For these mesas, there are two regimes where emission occurs.[14,20] At moderate input power ("low-bias regime"), there is only little heating ($\lesssim$10 mW), and the temperature distribution in the mesa is roughly homogeneous and close to the bath temperature T_b. The terahertz emission observed in this regime presumably can be described by more or less standard Josephson physics. At high-input power ("high-bias regime"), a hot spot forms inside the mesa.[14,19,20] The hot spot effectively separates the mesa into a "cold" part, which is superconducting, and a hot part, which is in the normal state. The "cold" part of the mesa is responsible for terahertz generation by the Josephson effect. The hot spot also seems to play a role for synchronization.[19,20,27] It has been found that the size and position of the hot spot, and in consequence also the terahertz emission, can be manipulated by applying proper bias currents across the mesa.[19] Thus, in order to understand the mechanism of terahertz radiation in IJJ mesas, it seems crucially important to develop a detailed understanding of the hot-spot formation. The present paper is devoted to this subject.

In a standard superconducting structure (e.g., a thin film), under a strong enough transport current somewhere in the sample the resistance rises from zero to a finite value, leading to local heating and the formation of a hot spot. To obtain terahertz emission, IJJ stacks are typically biased in a state where all junctions are in their resistive state. Here, the out-of-plane resistance R_c decreases continuously when heating the sample through T_c,[57,58] cf. Fig. 2(a). In-plane currents still flow with zero resistance below T_c and with finite resistance above T_c. However, even in the normal state these layers add only a minor contribution to the total voltage across the IJJ stack and thus to the overall power dissipation due to the huge ratio $\rho_c/\rho_{ab} > 10^5$ of the out-of-plane to the in-plane resistivity. It is unlikely that this contribution gives rise to hot-spot formation. Also the BSCCO thermal conductance varies relatively weakly with temperature,[59] cf. Fig. 2(b). Thus the above mechanism of hot-spot generation does not work and T_c is no longer a peculiar temperature for the thermal balance of the sample.

There are other ways to create hot domains in systems which may or may not be related to superconductivity.[1,2] In particular, current-voltage characteristics (IVCs) and the thermal breakdown were studied in systems having a resistivity decreasing with increasing temperature (negative-temperature-coefficient resistor).[60–62] The IVCs of these resistors strongly resemble the IVCs measured for IJJ mesas. Especially, the appearance of a hot domain leads to an abrupt change in differential resistance. The quantity in common, a strongly negative dR/dT, is the key to understand hot-spot formation in BSCCO mesas.

Recently, Yurgens *et al*. have simulated the thermal heating and the temperature distribution in BSCCO IJJ mesas,[47,49]

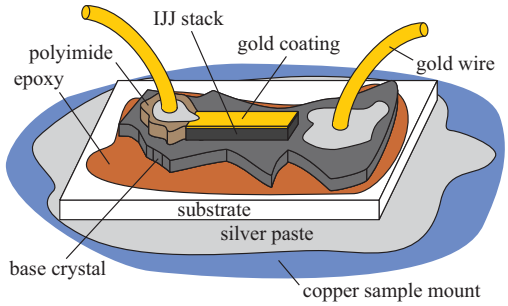

FIG. 1. (Color online) Typical design of BSCCO IJJ mesas.

using a 3D finite-element software.[63] In this pioneering work, the electrical and thermal properties of the various current carrying and insulating layers were taken into account. The formation of hot spots observed in Ref. 14 was reproduced qualitatively. However, the occurring phenomena need further study. For example, the IVCs in Refs. 47 and 49 have been calculated using a self-consistent procedure based on Newton's law of cooling and Ohm's law and do not exhibit the experimentally observed abrupt changes in differential resistance when the hot spot appears. They resemble much less the experimental curves than the ones calculated in Refs. 60–62.

A complete study of the Josephson effect in BSCCO mesas in the presence of hot spots is a formidable and unsolved issue. In this paper, we are treating experimentally and theoretically hot-spot formation in BSCCO mesas. In the theoretical part of our study, the presence of the Josephson effect, i.e., terahertz radiation, the formation of electromagnetic standing waves, interactions between hot spots and waves, etc., is *not* considered. This approach to hot-spot formation seems justified, since the emitted radiation power is 3–4 orders of magnitude lower than the dc input power. It may, however, serve as a zero order approximation towards solving the full problem. In the simulations, we derive the electrical current density in the mesa under investigation and thus also the potential difference between top and bottom electrodes, directly generating the IVC for a sample, following Refs. 60–62 rather than Refs. 47 and 49.

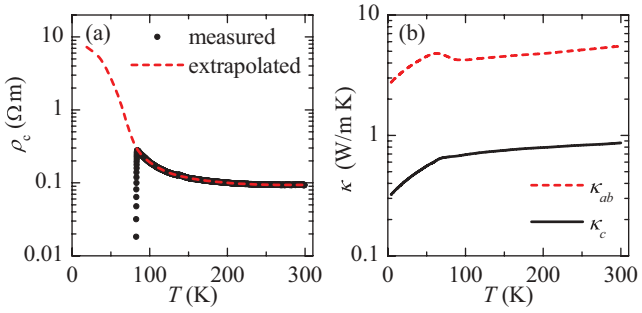

FIG. 2. (Color online) (a) Temperature dependence of the c-axis resistivity ρ_c, as measured for a $330 \times 50\ \mu\text{m}^2$ wide and 0.7-μm-thick sample for $T > T_c = 83$ K (black circles). For lower T, ρ_c has been extrapolated by fitting the IVC, measured at $T_b = 20$ K, using the full 3D heat diffusion equation, cf. Sec. IV. (b) Temperature dependence of the BSCCO in-plane (κ_{ab}) and out-of-plane (κ_c) thermal conductivities (see Ref. 59).

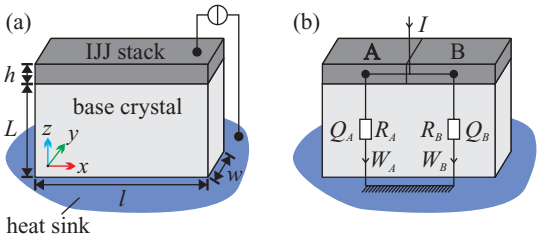

FIG. 3. (Color online) Discrete approximation for a mesa. (a) Dimensions of mesa and base crystal. (b) The mesa is replaced by two vertically cooled resistors R_A and R_B producing Joule heat Q_A and Q_B, which is vertically transported to a thermal bath via heat-transfer powers W_A and W_B.

The paper is organized as follows. In Sec. II, we consider a simple discrete resistor model to get a basic understanding of the heating phenomena involved. In Sec. III, a 1D model is discussed which is extended to 3D and realistic sample geometries in Sec. IV. The discussions in these sections are based on the thermal and electrical parameters of the BSCCO crystals, as used in experiment. In Sec. IV, we also address experimental observations, as made in Refs. 14,19,20,27. Section V concludes our work.

II. DISCRETE RESISTORS

The electrothermal behavior of conducting materials can be investigated by considering the heat balance equation between Joule self-heating $Q(T,\lambda)$ and the heat transfer power $W(T)$ to the coolant $Q(T,\lambda) = W(T)$.[1] Here, λ is some control parameter (in our case, the voltage V across the sample). To approach the experimental situation of IJJ mesas, we first briefly study the model of two current-biased resistors $R_A(T_A)$ and $R_B(T_A)$ connected in parallel, each representing one half of a mesa of length l, width w and height h, cf. Fig. 3. T_A and T_B are the temperatures of these resistors. R_A and R_B shall be equal for $T_A = T_B$. Joule heating is produced via $Q_i = I_i V_i$, where $i = (A,B)$. The total current is $I = I_A + I_B$ and further $V_A = V_B$, i.e., we neglect the voltage drop due to in-plane currents. The resistors are thermally connected to a bath (temperature T_b), which at a distance L (the thickness of the base crystal) removes heats W_A and W_B "vertically," through the BSCCO out-of-plane thermal conductivity κ_c. We first assume $T_A = T_B = T$. Then, the IVC of the mesa can be parameterized by T, using $Q = W$:[64]

$$V = \sqrt{R(T)\,W(T-T_b)}; \quad I = \sqrt{\frac{W(T-T_b)}{R(T)}}, \qquad (1)$$

with $W(T-T_b) = (l w \kappa_c / L)(T-T_b)$ and $R(T) = (h/l\,w)\,\rho_c(T)$. For further calculations, we use a constant $\kappa_c = 0.6$ W/mK. Since we want to study the question whether or not the particular $\rho_c(T)$ of our mesas can lead to hot spots, we use a temperature dependence which is as close as possible to the experimental situation. Above T_c, we obtained $\rho_c(T)$ from the out-of-plane resistance of one of our mesas, cf. solid circles in Fig. 2(a). Below T_c, $\rho_c(T)$ is extrapolated by fitting the measured IVC of the mesa at a bath temperature of 20 K (see below), using the full 3D heat diffusion equation

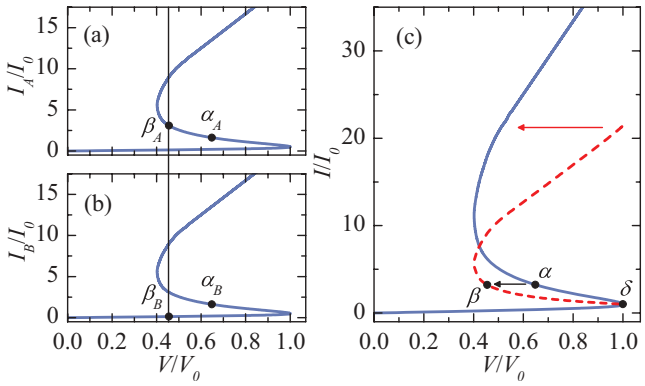

FIG. 4. (Color online) Hot-spot formation in a two-resistor model, cf. Fig. 3(b). (a) and (b) display the IVCs of the two individual parts A and B, respectively. (c) The IVC of the combined system. The axes are normalized to the current (voltage) of the point showing local maximal voltage V_0. The total current through the mesa at V_0 is I_0. The bias points indicated by Greek characters are discussed in the text. In (c), for the solid (blue) curve resistors A and B are at the same temperature, while for the dashed (red) curve their temperature differs, corresponding to hot-spot formation in the continuous case.

[dashed line in Fig. 2(a)]. $L = 17$ μm is chosen, which is a typical value for the thickness of the BSCCO base crystal of the samples, we want to discuss.[14,19,20,27] Length, width, and height of the mesa are, respectively, taken to be 330, 50, and 1 μm, representing sample 1 from Ref. 20. With these dependencies, the calculated IVC of the mesa is S shaped and shows a region of negative differential resistance, cf. solid line in Fig. 4(c). In this voltage region thermal bistability can occur, since $W = Q$ holds for more than one value of T.[1] In fact, writing $dV/dI = (dV/dT)/(dI/dT) < 0$, using Eq. (1) and $W \propto (T - T_b)$, one obtains $-(T - T_b)(dR/dT)/R > 1$ as a condition for obtaining negative differential resistance in the IVC and thus the possibility to have thermal instability.[2]

We assume for the following, that I and thus Q is increased from zero step-by-step. Figures 4(a) and 4(b) show the individual IVCs of resistor A and B, respectively, while (c) shows the IVC of the whole mesa. For small Q, the temperature is the same in both resistors and they carry the same current. In principle, further increase of I would make the whole mesa pass the point δ of local maximal voltage V_0, cf. Fig. 4(c), and enter the unstable[1] area of negative differential resistance. This is exemplarily indicated for point α in Fig. 4(c). Here, the two resistors with equal temperature T_α, would be in states α_A and α_B, cf. Figs. 4(a) and 4(b), respectively. The instability and the constraints of equal voltage and fixed current force the mesa into the state β, which is composed of state β_A with $T_{\beta_A} > T_\alpha$ and β_B with $T_{\beta_B} < T_\alpha$, cf. Figs. 4(a) and 4(b), respectively. The combination of β_A and β_B is the only stable solution. The resulting total IVC of Fig. 4(c) follows the path indicated by the dashed (red) line, differing in voltage from the isothermal case (solid blue line). With increasing I, starting from point δ, the points β_A and β_B "move" towards lower voltage. Note that this implies, that the cold resistor becomes colder while the hot resistor keeps increasing its temperature. When β_A has reached the minimal voltage, both β_A and β_B start to move towards larger voltage, i.e., also the temperature of the cold part starts to increase. Finally, when β_B reaches the voltage V_0, $T_A \neq T_B$ becomes impossible and the mesa switches back to the homogeneous solution.

The model of two parallel resistors can be extended by several ways. First, an in-plane thermal coupling W_{AB} between resistors A and B may be included. Then, the cold part will cool the hot part and (thermal) differences between A and B will be less severe. This will shift the point, where the homogeneous solution and the solution $T_A \neq T_B$ fork, to higher input power.[60,62] Also, the difference in voltage between the homogeneous and the inhomogeneous solution will be diminished.[60,62] A detailed discussion, however, is out of the scope of this section. In-plane cooling will be taken into account in the subsequent sections. Second, one may allow the two resistors (the area of the "hot" and "cold" parts) to be unequal and variable in size. Then, one faces a continuous set of solutions. Third, one may consider more than two resistors in parallel. This would be also applicable to the description of arrays of IJJ stacks, which are interesting for obtaining a large terahertz emission output power. In this scenario, the whole system will tend to a state, where only one of the stacks is hot, while all the others are cold.[62]

III. 1D MODEL

In this section, we consider a 1D continuous model to find the temperature distribution in the mesa for the simplest continuous case, still treating hot-spot formation from a generic point of view. That is, we assume a thin (along z) and narrow (along y) mesa, neglecting T variations along z and y directions in the mesa (see Refs. 1 and 62 for details). Then, $T = T(x)$ is defined by the heat diffusion equation:

$$-h\frac{d}{dx}\left[\kappa_{ab}(T)\frac{d}{dx}T\right] + \frac{\kappa_c(T)}{L}(T - T_b) = \frac{V^2}{\rho_c(T)\,h}. \quad (2)$$

The first term describes the thermal diffusion in x direction and the second one the cooling due to the base crystal with the coefficient κ_c/L regulating its strength. The third term represents Joule heating. The sample dimensions L, h, l, and w are defined in Fig. 3(a). We use $L = 19$ μm, $h = 1$ μm, $l = 330$ μm, $w = 50$ μm and κ_{ab}, κ_c, and ρ_c as in Figs. 2(a) and 2(b). The boundary conditions are chosen to be $dT/dx(x = 0) = dT/dx(x = l) = 0$. These boundary conditions neglect edge cooling. To solve Eq. (2) for a given current I we use $V = Ih/\int \rho_c^{-1}(T)dxdy$. We numerically solve Eq. (2) using finite element analysis.[63] Note that there is always a homogeneous solution. To find a nontrivial $T(x)$, a proper initial function $T_i(x)$ has to be used. A calculated IVC for $T_b = 20$ K is shown in Fig. 5(a). It resembles the shape of the IVC of the two-resistor model, cf. Fig. 4. Figure 5(b) shows the temperature in the mesa for the homogeneous solution at the bias points indicated in Fig. 5(a). One notes that the mesa temperature is below T_c up to quite high currents ~40 mA. Figure 5(c) shows solutions for the bias points indicated in the IVC, when a hot spot has formed. Here, the temperature in the hot part rises rapidly to temperatures well above T_c, while the temperature of the cold part is near $T_b = 20$ K. Also, one observes that the hot part grows in size when I is increased. Further note, that

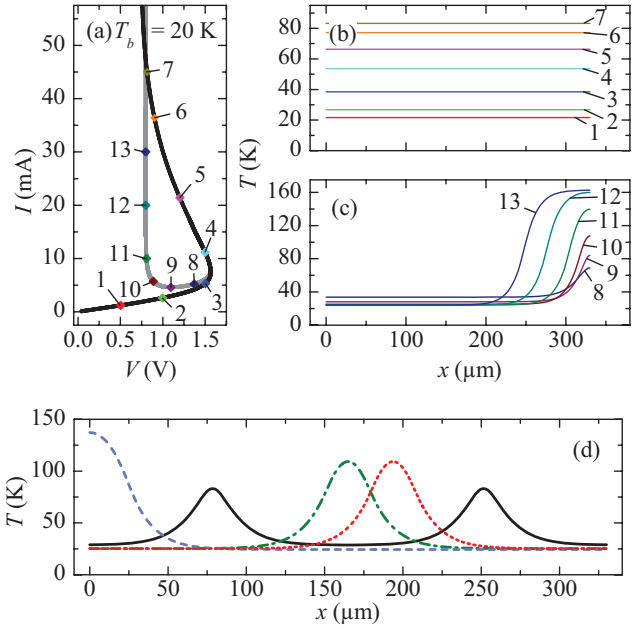

FIG. 5. (Color online) Simulation results of Eq. (2) for $T_b = 20$ K and $L = 19$ μm. Other mesa dimensions are listed in Sec. II. (a) The IVC for the homogeneous solution (black curve) and a solution showing a hot spot on the right mesa end (gray curve). $T(x)$ profiles are displayed in (b) for the homogeneous case and in (c) for the hot-spot case. The numbers indicate the bias points on the IVC. In (d), $T(x)$ profiles, obtained from different $T_i(x)$, are shown for solutions with $I = 9.5$ mA, exhibiting various shape and positioning of the hot spot.

in the presence of a hot spot the temperature $T_{\rm cold}$ of the cold part is below the temperature of the homogeneous solution for the same value of Q; $T_{\rm cold}$ decreases with increasing Q, and finally, converges against a limiting value. The strength of the deviation of the temperature profile from the homogeneous solution directly correlates with the strength of branching in the IVC. In the depicted case the branching is very strong, which is due to a small ratio of the in-plane to the out-of-plane thermal coupling, cf. first and second term in Eq. (2).

For a given I, the hot spots presented in Fig. 5(c) are not the only possible solutions to Eq. (2).[65] For symmetry reasons, also the mirrored solution exists as well as solutions with the hot spot near and in the center of the mesa, cf. Fig. 5(d). In the IVC the different solutions slightly differ in V and can be traced over some range in I. Thus the IVC consists of several branches distinguishing specific kinds of hot domains. Experimentally, in some cases, hot-spot formation in different places of the mesa has been detected by low-temperature scanning-laser microscopy (LTSLM). However, usually a specific configuration is much more stable than the others, presumably due to inhomogeneities like attached wires. In the calculations, also solutions with more than one hot domain[66] can be found, cf. Fig. 5(d). However, this has not been observed in any of our LTSLM measurements. It is argued in Ref. 62, that such a state is very unstable and will not occur, since the sample can be seen as a parallel circuit of several discrete parts with small thermal coupling between them, cf. Sec. II.

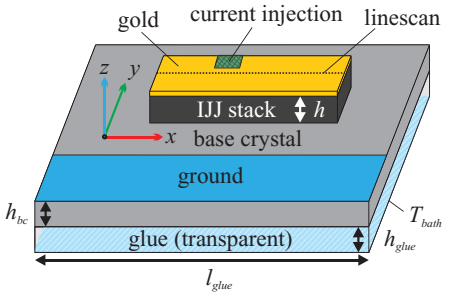

FIG. 6. (Color online) Model geometry of the mesa.

IV. 3D MODEL

In this section, we address hot-spot formation in 3D. The goal is to quantitatively compare our experimental observations with the numerical simulations, using the same code[63] as in Refs. 47,49. Similarly, we also include various electrically and thermally conducting and insulating layers that are in contact with our BSCCO mesas. The electrical, thermal, and geometrical parameters used for the calculations are as close as possible to the experimental situation. The geometry used is still somewhat simplified compared to the real samples but should allow to capture the relevant physics. Figure 6 depicts the model. The substrate is omitted and a boundary condition $T_b = \text{const}$ is applied to the bottom surface of the glue layer, representing the thermal bath. This simplification can be done with very little impact on the results for the mesa, since the thermal conductivity of the substrate (e.g., sapphire) is by far better than that of the glue layer. The geometric dimensions of the mesa, the thicknesses of the glue layers (10–30 μm) and of the gold coatings ($h_{\rm Au} \approx 30$ nm) were roughly chosen as in the real samples. The base crystal's lateral size is typically of the order of 1 mm, while its thickness h_{bc} may vary from about ten to several hundred micrometers, strongly depending on the fabrication process. The current leads are simply represented by boundary conditions on the surfaces of either the gold layer on the mesa or on the base crystal. The current I is injected through a 20×10 μm^2 rectangle and the current sink is defined as a ground of large area (roughly 0.3 mm^2), cf. Fig. 6. The voltage across the mesa is obtained as the potential difference between the two electrodes.

The equation to be solved is[49]

$$-\nabla[\kappa(T(\mathbf{r}))\,\nabla\mathbf{T}(\mathbf{r})] = \rho[\mathbf{T}(\mathbf{r})]\,\mathbf{j}^2(\mathbf{r}), \qquad (3)$$

where ρ and κ are the resistivity and thermal conductivity tensor, respectively, and $\mathbf{r}$ is the spatial coordinate. Unlike the mesa, the base crystal is not always in the resistive state. We model its resistance by using the ρ_c versus T data indicated by solid circles in Fig. 2(b). The in-plane resistivity ρ_{ab} is the same for both mesa and base crystal; we use the same T dependence as in Ref. 49. The thermal conductivity for BSCCO is used from Ref. 59, cf. Fig. 2(a). Thermal and electrical conductivities for a 30-nm-thick Au film are adopted from Ref. 67. For the thermal conductivity $\kappa_{\rm glue}$ of the glue between the BSCCO base crystal and the substrate to first order, we use the polyimide data of Ref. 68. Since our glue might have slightly different properties, we in addition multiply $\kappa_{\rm glue}$ with a factor $n_{\rm glue}$, which we fit by adjusting the calculated IVC to the measured one.

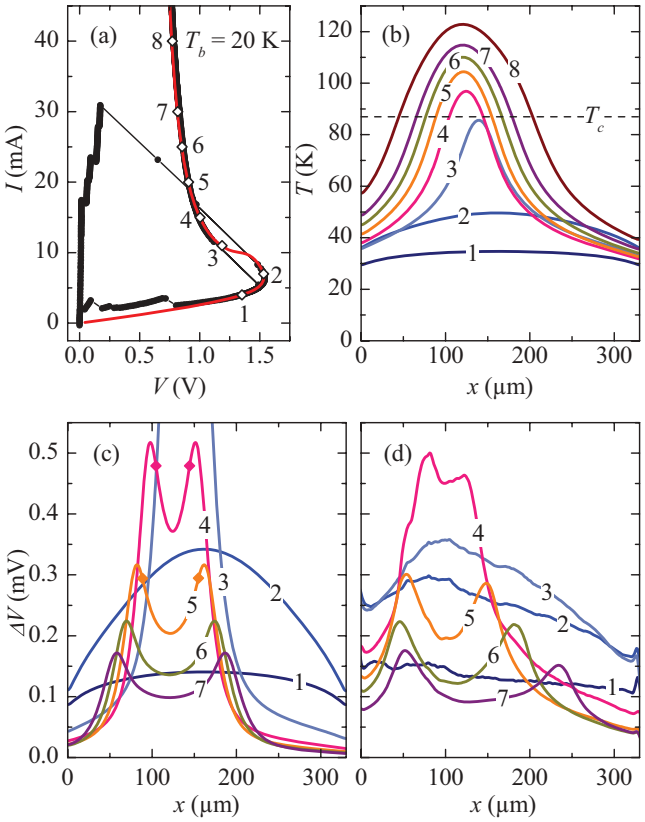

FIG. 7. (Color online) Comparison of 3D simulation and experimental data for sample 1 from Ref. 20 at $T_b = 20$ K. (a) The measured (black, solid circles) and simulated (red solid line) IVCs. In (b), simulated $T(x)$ profiles along the dashed line indicated in Fig. 6 at $z = 0.5\,h$ are shown. The diamonds in (a) indicate the corresponding bias points. The calculated and measured $\Delta V(x)$ are shown in (c) and (d), respectively. Diamonds in (c) indicate the x position where $T = T_c$.

The base crystal introduces an effective side-cooling of the mesa, which, in general, makes a solution showing variation in x and y directions (with or without hot spots) favorable. Indeed, in contrast to the one-dimensional calculations, hot-spot solutions appeared basically by themselves, i.e., it was not necessary to find them by choosing a proper initial condition. The side-cooling leads to an elliptic shape of the hot spot (for rectangular shaped mesas). Also, the hot spot is not limited to the mesa itself anymore, but may extend significantly in lateral direction into the base crystal (see below). This is exactly what has been found experimentally.[19] The same occurs in z direction, as has been discussed in Ref. 49.

We investigate sample 1 from Ref. 20. The electrical and thermal parameters of this sample have already been used in the previous sections. We have further used the parameters: $h_{bc} = 40\ \mu$m, $h_{\rm glue} = 25\ \mu$m, $l_{\rm glue} = 1$ mm, and $n_{\rm glue} = 1.95$. Figure 7(a) compares the measured IVC with the calculated one for $T_b = 20$ K. The good agreement stems from the fact that we have adjusted $\sigma_c(T)$ below T_c and $n_{\rm glue}$ to match this curve. The simulated $T(x)$ profiles, calculated along the dashed line in Fig. 6 at $z = 0.5\,h$, are shown in Fig. 7(b) for the bias points indicated in Fig. 7(a). They show an almost constant temperature in the low-bias regime, whereas for increasing current the hot spot forms by the growth of a buckling in the $T(x)$ profile [compare curves 2 and 3 in Fig. 7(b)]. Further increasing I and thus Q leads to a growth in diameter and maximal temperature of the hot spot (curves 4 to 8). Note that T_c, indicated by the horizontal dashed line, can be significantly exceeded in the center of the hot spots, confirming the results in Ref. 49.

We next want to provide a quantitative comparison between the hot-spot signals observed in LTSLM[14,19,20] and the calculated temperature distributions for this sample. In LTSLM, the laser spot at position (x_0,y_0) causes a maximum temperature rise $\Delta T \sim 1$–3 K, depending on the laser power. In turn, there is a change $\Delta V(x_0,y_0)$ in the voltage V across a sample. One often has a response that partially arises from the reduction of the Josephson critical current density and partially from the change in resistance, see, e.g., Ref. 69. However, if $dR_c(T)/dT$ dominates the thermal physics, $\Delta V(x_0,y_0)$ can be treated as in Ref. 70 yielding

$$\Delta V(x_0,y_0) \approx \frac{-I R_{\rm eff}^2 \Delta T A_L}{h} \frac{d\sigma_c}{dT}[T(x_0,y_0)]. \qquad (4)$$

$R_{\rm eff} = V/I$ is the (ohmic) sample resistance at a given I and A_L is the effective area warmed up by the laser (some μm^2). $d\sigma_c/dT\ [T\ (x_0,y_0)]$ denotes the temperature derivative of the c-axis electrical conductivity. The calculated and measured ΔV, taken at various bias points indicated in Fig. 7(a), are shown in Figs. 7(c) and 7(d), respectively. For the simulations we have used $\Delta T\ A_L = 56$ Kμm^2. The value makes sense, since we expect a temperature rise $\Delta T \sim 2$ K and $A_L \sim 25\ \mu$m^2 for the samples we discuss here. The calculated curves agree reasonably well with the measurements, although differences occur at low bias and near the hot-spot nucleation point. Particularly, for the bias points 1 and 2, the simulation yields a parabolic shape of ΔV, while the experimental data are shaped less regular. Note, however, that in these regions the Josephson currents, which are neglected in our analysis, may play a major role. For curve 3, in the simulation hot-spot formation has already occurred, while in experiment the mesa is close to the nucleation point but still undercritical. For a bias well above the hot-spot nucleation point, theoretical curves and experimental data agree well. Specifically, the double hump feature in $\Delta V\,(x)$ is reproduced correctly in the simulations. The local temperature at the maxima in ΔV corresponds to the temperature $T^* \approx 80$ K, for which $d\sigma_c/dT$ is maximum, cf. Eq. (4). Between the two ΔV maxima, $T > T^*$. By coincidence, $T^* \approx T_c$; the diamonds in Fig. 7(c) indicate the locations for which $T = T_c$. Thus, the border between superconducting and nonsuperconducting parts, which is important for terahertz emission, can be approximately identified by the position of the humps.

We next investigate the dependence of hot-spot formation on T_b. Figure 8 shows a similar set of data as Fig. 7, but for $T_b = 42$ K. Here, $n_{\rm glue} = 3.5$ has been chosen. The transition region between the hot and cold domain is less steep than for $T_b = 20$ K. Also, the nucleation point of the hot spot has moved to higher currents (10 mA for $T_b = 20$ K and 14 mA for $T_b = 42$ K) and the back bending of the IVC has decreased. These effects arise from the fact that the xy-plane thermal coupling has increased relative to the out-of-plane thermal coupling,[62] cf. Sec. III. Note that this also means for equal input power, that the hot domain reaches higher and the cold

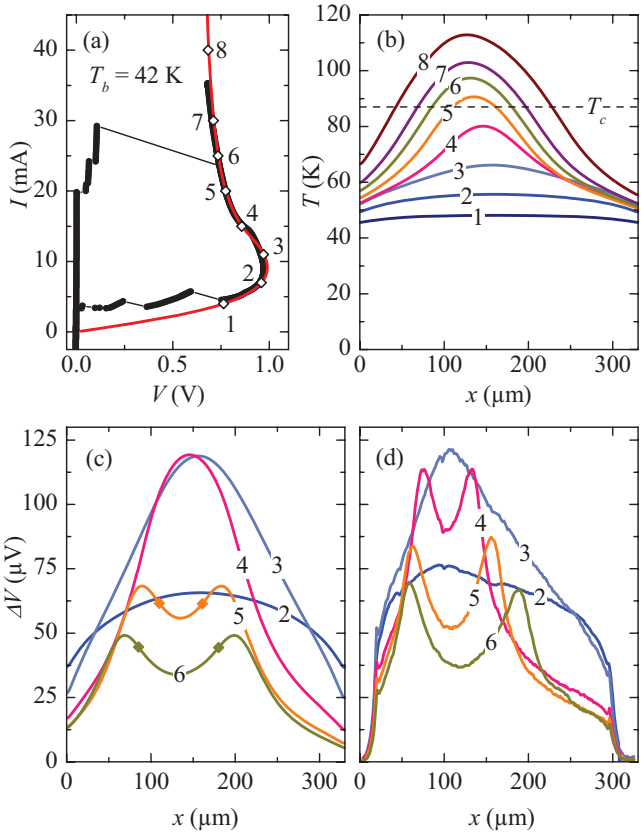

FIG. 8. (Color online) Comparison of 3D simulation and experimental data for sample 1 from Ref. 20 at $T_b = 42$ K. (a) shows the measured (black, solid circles) and simulated (red solid curve) IVC. In (b), simulated $T(x)$ profiles along the dashed line indicated in Fig. 6 at $z = 0.5\,h$ are shown. The diamonds in (a) indicate the corresponding bias points. The calculated and measured $\Delta V(x)$ are shown in (c) and (d), respectively. Diamonds in (c) indicate the x position where $T = T_c$.

domain reaches lower temperatures for $T_b = 20$ K as for $T_b = 42$ K. Figures 8(c) and 8(d), respectively, show the calculated and measured LTSLM profiles. As for Figs. 7(c) and 7(d), the agreement between experimental data and simulations is reasonable, except for the bias point where hot-spot formation sets in (curve 4). For the calculations, we have used $\Delta T\ A_L = 16\ \mathrm{K}\mu\mathrm{m}^2$, which is by a factor of 3 lower than for the case of $T_b = 20$ K. This is attributed to a reduced incident laser power, which had been readjusted for every measurement.

In Fig. 9(a), we show the $T(x)$ profile, calculated along the dashed line in Fig. 6 at $z = 0.5\,h$, for 3 values of T_b. For all curves, $V = 0.8$ V. This condition has been motivated by measurements of the linewidth Δf of terahertz radiation.[27] Here, for Δf versus T_b, taken at a fixed emission frequency (corresponding to $V = \text{const}$ for a fixed number of oscillating IJJs), the dependence $\Delta f \propto T_b^{-4}$ has been found unexpectedly. We are interested in the question whether or not corresponding changes with T_b can be seen in the T distribution in the mesa. Figure 9(a) shows that the peak temperature in the mesa is higher at low T_b than at high T_b, while the coldest temperatures, reached at the right edge of the mesa, behave oppositely. Thus thermal gradients at low T_b are stronger than at high

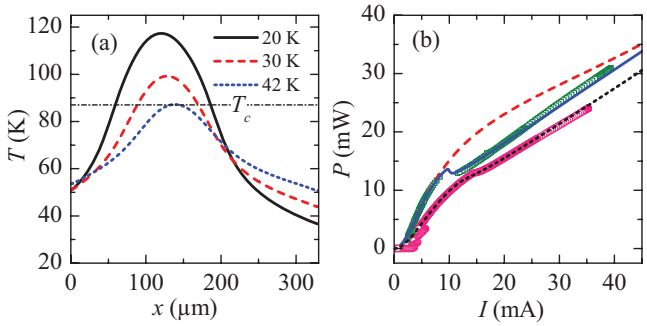

FIG. 9. (Color online) (a) Simulated $T(x)$ profiles along the dashed line indicated in Fig. 6 at $z = 0.5\,h$ for three different values of T_b at constant $V = 0.8$ V. The dc power $P = IV$ is 26.4, 18.2, and 14.4 mW for $T_b = 20$, 30, and 42 K, respectively. (b) P vs I at 20 K for measurement (green squares), simulation with homogeneous T (red dashed line) and hot-spot formation (blue, solid line). The pink circles depict experimental data and the black, short-dashed line simulated values with hot-spot formation at 42 K.

T_b. However, this effect roughly changes linearly with T_b and presumably cannot explain the $\Delta f \propto T_b^{-4}$ dependence.

Figure 9(b) compares for two values of T_b the measured and simulated dc power $P = IV$ as a function of I. One observes two regimes, each with a roughly constant slope. The first—low-bias—regime has no hot spot and, for $T_b = 20$ K, spans from 0 to 10 mA (14 mA for 42 K), whereas the second—high-bias—regime has a hot spot and begins at 10 mA (14 mA for 42 K). Interestingly, at the intersection of these two regimes, the maximum temperature in the mesa has reached the temperature fulfilling $d\sigma_c/dT = 0$. This point also corresponds to the kink in the IVC, observed for several mesas. Note that the calculation for homogeneous T (red dashed curve) shows no such kink. A plot like this may thus be helpful to distinguish in an experiment, whether or not one has reached the regime with hot spots.

The last issue we want to address is the correlation between the point of current injection and the location, where the hot spot is established. Typically, in experiment the appearance of the hot spot was close to, but not exactly at the bond wire to

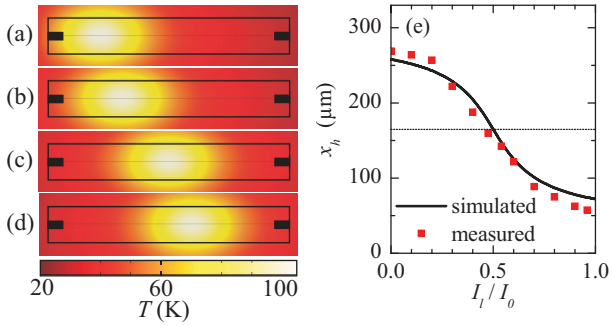

FIG. 10. (Color online) (a)–(d) Surface plot of hot-spot solutions, obtained by Eq. (3) for a mesa with two current injection points, indicated by black rectangles. The sum I_0 of the currents through the left (I_l) and right (I_r) injection points has been kept constant, and for the ratio I_l/I_0 values of (a) 1, (b) 0.7, (c) 0.5, and (d) 0.425 have been used. (e) The center position x_h of the hot spot vs current injection ratio for simulated and measured data.

the mesa surface.[19] We see the same effect in our simulations, Fig. 10(a) illustrates this for a situation, where the current is injected from the left. Here, the side-cooling prevents the hot spot from nucleating at the very left end of the mesa, resulting in a positioning of the hot spot at several micrometers right of the current injection point. Further, it has been shown that by using two injectors located on opposite sides of the mesas the hot spot can be moved by changing the ratio of currents through these injectors.[19] Figures 10(a)–10(d) show a sequence of calculations where the ratio between injection currents through the left (current I_l) and right (current I_r) was varied, keeping the sum of the currents I_0 constant. We used ratios I_L/I_0 of, respectively, 1, 0.7, 0.5, and 0.425. As one can see, the hot spot indeed can be moved continuously, as in experiment. In Fig. 10(e), we have plotted the center position of the hot spot as a function of I_l/I_0. Experimental data are shown by (red) squares and theoretical data by the (black) solid line. The agreement is reasonable, showing that this effect can be essentially understood from the thermal calculations presented in this paper.

Finally, we briefly mention that also two other geometries discussed in Ref. 19 can be reproduced very well in the 3D simulation, a disk shaped mesa and a mesa of Y shape, where the hot spot forms at the intersection of the three lines, although the bias current injection point was at the foot of the Y.

V. CONCLUSION

In conclusion, we have investigated experimentally and numerically the temperature profiles and hot-spot formation in IJJ mesas. We have shown, that the hot spots dominantly arise because of the strongly negative temperature coefficient of the out-of-plane resistance of the mesas. This mechanism is different from the more conventional hot-spot formation in superconductors and, in particular, allows for hot spots with a maximum temperature below as well as above the transition temperature T_c. We have given—in the frame of what available data allow—a quantitative comparison between simulation and experiment, showing reasonable agreement. Numerous effects observed in previous papers on hot-spot formation in intrinsic Josephson junction stacks[14,19,20] are reproduced by the simulations, making us confident that the description given in this paper captures the essential physics, except for the interplay of hot spots and terahertz waves. Resolving this issue is a task for the future.

ACKNOWLEDGMENTS

We gratefully acknowledge financial support by the JST/DFG strategic Japanese-German International Cooperative Program and the German Israeli Foundation (Grant No. G-967-126.14/2007). S.G. acknowledges support by AFOSR.

*hbwang1000@gmail.com
†kleiner@uni-tuebingen.de

[1] A. V. Gurevich and R. G. Mints, Rev. Mod. Phys. **59**, 941 (1987).
[2] A. F. Volkov and S. M. Kogan, Sov. Phys. Usp. **11**, 881 (1969).
[3] P. Thomas, J. Fenton, G. Yang, and C. Gough, Physica C **341**, 1547 (2000).
[4] J. C. Fenton and C. E. Gough, J. Appl. Phys. **94**, 4665 (2003).
[5] K. Anagawa, Y. Yamada, T. Shibauchi, M. Suzuki, and T. Watanabe, Appl. Phys. Lett. **83**, 2381 (2003).
[6] V. N. Zavaritsky, Phys. Rev. Lett. **92**, 259701 (2004).
[7] A. Yurgens, D. Winkler, T. Claeson, S. Ono, and Y. Ando, Phys. Rev. Lett. **92**, 259702 (2004).
[8] V. M. Krasnov, M. Sandberg, and I. Zogaj, Phys. Rev. Lett. **94**, 077003 (2005).
[9] H. B. Wang, T. Hatano, T. Yamashita, P. H. Wu, and P. Müller, Appl. Phys. Lett. **86**, 023504 (2005).
[10] B. Verreet, N. Sergeant, D. M. Negrete, M. Torstensson, D. Winkler, and A. Yurgens, Supercond. Sci. Technol. **20**, S48 (2007).
[11] L. Ozyuzer *et al.*, Science **318**, 1291 (2007).
[12] K. Kadowaki *et al.*, Physica C **468**, 634 (2008).
[13] L. Ozyuzer *et al.*, Supercond. Sci. Technol. **22**, 114009 (2009).
[14] H. B. Wang, S. Guénon, J. Yuan, A. Iishi, S. Arisawa, T. Hatano, T. Yamashita, D. Koelle, and R. Kleiner, Phys. Rev. Lett. **102**, 017006 (2009).
[15] H. Minami, I. Kakeya, H. Yamaguchi, T. Yamamoto, and K. Kadowaki, Appl. Phys. Lett. **95**, 232511 (2009).
[16] C. Kurter *et al.*, IEEE Trans. Appl. Supercond. **19**, 428 (2009).
[17] K. E. Gray, L. Ozyuzer, A. K. C. K. Kurter, K. Kadowaki, T. Yamamoto, H. Minami, H. Yamaguchi, M. T. M, W. Kwok, and U. Welp, IEEE Trans. Appl. Supercond. **19**, 3755 (2009).
[18] K. Kadowaki, M. Tsujimoto, K. Yamaki, T. Yamamoto, T. Kashiwagi, H. Minami, M. Tachiki, and R. A. Klemm, J. Phys. Soc. Jpn. **79**, 023703 (2010).
[19] S. Guénon *et al.*, Phys. Rev. B **82**, 214506 (2010).
[20] H. B. Wang *et al.*, Phys. Rev. Lett. **105**, 057002 (2010).
[21] M. Tsujimoto, K. Yamaki, K. Deguchi, T. Yamamoto, T. Kashiwagi, H. Minami, M. Tachiki, K. Kadowaki, and R. A. Klemm, Phys. Rev. Lett. **105**, 037005 (2010).
[22] H. Koseoglu, F. Turkoglu, Y. Simsek, and L. Ozyuzer, J. Supercond. Nov. Magn. **24**, 1083 (2011).
[23] T. M. Benseman, A. E. Koshelev, K. E. Gray, W.-K. Kwok, U. Welp, K. Kadowaki, M. Tachiki, and T. Yamamoto, Phys. Rev. B **84**, 064523 (2011).
[24] K. Yamaki, M. Tsujimoto, T. Yamamoto, A. Furukawa, T. Kashiwagi, H. Minami, and K. Kadowaki, Opt. Express **19**, 3193 (2011).
[25] T. Kashiwagi *et al.*, Jpn. J. Appl. Phys. **51**, 010113 (2012).
[26] M. Tsujimoto *et al.*, Phys. Rev. Lett. **108**, 107006 (2012).
[27] M. Li, J. Yuan, N. Kinev, J. Li, B. Gross, S. Guénon, A. Ishii, K. Hirata, T. Hatano, D. Koelle, R. Kleiner, V. P. Koshelets, H. Wang, and P. Wu, Phys. Rev. B **86**, 060505(R) (2012).
[28] L. N. Bulaevskii and A. E. Koshelev, Phys. Rev. Lett. **99**, 057002 (2007).
[29] A. E. Koshelev and L. N. Bulaevskii, Phys. Rev. B **77**, 014530 (2008).
[30] A. E. Koshelev, Phys. Rev. B **78**, 174509 (2008).
[31] S. Lin and X. Hu, Phys. Rev. Lett. **100**, 247006 (2008).
[32] V. M. Krasnov, Phys. Rev. Lett. **103**, 227002 (2009).
[33] X. Hu and S. Z. Lin, Phys. Rev. B **80**, 064516 (2009).
[34] Y. Nonomura, Phys. Rev. B **80**, 140506 (2009).

[35]M. Tachiki, S. Fukuya, and T. Koyama, Phys. Rev. Lett. **102**, 127002 (2009).
[36]T. Koyama, H. Matsumoto, M. Machida, and K. Kadowaki, Phys. Rev. B **79**, 104522 (2009).
[37]N. Pedersen and S. Madsen, IEEE Trans. Appl. Supercond. **19**, 726 (2009).
[38]R. A. Klemm and K. Kadowaki, J. Phys.: Condens. Matter **22**, 375701 (2010).
[39]V. M. Krasnov, Phys. Rev. B **82**, 134524 (2010).
[40]S. O. Katterwe, A. Rydh, H. Motzkau, A. B. Kulakov, and V. M. Krasnov, Phys. Rev. B **82**, 024517 (2010).
[41]S. Savel'ev, V. A. Yampol'skii, A. L. Rakhmanov, and F. Nori, Rep. Prog. Phys. **73**, 026501 (2010).
[42]X. Hu and S. Z. Lin, Supercond. Sci. Technol. **23**, 053001 (2010).
[43]T. Tachiki and T. Uchida, J. Appl. Phys. **107**, 103920 (2010).
[44]S. Z. Lin and X. A. Hu, Phys. Rev. B **82**, 020504 (2010).
[45]W. Zhou, C. Wang, and Q.-H. Chen, Phys. Rev. B **82**, 184514 (2010).
[46]A. E. Koshelev, Phys. Rev. B **82**, 174512 (2010).
[47]A. Yurgens, M. Torstensson, and D. Winkler, Physica C: Superconductivity **470**, 818 (2010).
[48]M. Tachiki, K. Ivanovic, K. Kadowaki, and T. Koyama, Phys. Rev. B **83**, 014508 (2011).
[49]A. A. Yurgens, Phys. Rev. B **83**, 184501 (2011).
[50]A. A. Yurgens and L. N. Bulaevskii, Supercond. Sci. Technol. **24**, 015003 (2011).
[51]V. M. Krasnov, Phys. Rev. B **83**, 174517 (2011).
[52]S. O. Katterwe and V. M. Krasnov, Phys. Rev. B **84**, 214519 (2011).
[53]T. Koyama, H. Matsumoto, M. Machida, and Y. Ota, Supercond. Sci. Technol. **24**, 085007 (2011).
[54]S. Z. Lin and X. A. Hu, J. Nanoscience Nanotechnolology **11**, 2916 (2011).
[55]S.-Z. Lin, X. Hu, and L. Bulaevskii, Phys. Rev. B **84**, 104501 (2011).
[56]T. M. Slipchenko, D. V. Kadygrob, D. Bogdanis, V. A. Yampol'skii, and A. A. Krokhin, Phys. Rev. B **84**, 224512 (2011).
[57]A. Yurgens, D. Winkler, N. V. Zavaritsky, and T. Claeson, Phys. Rev. Lett. **79**, 5122 (1997).
[58]Y. I. Latyshev, T. Yamashita, L. N. Bulaevskii, M. J. Graf, A. V. Balatsky, and M. P. Maley, Phys. Rev. Lett. **82**, 5345 (1999).
[59]M. F. Crommie and A. Zettl, Phys. Rev. B **43**, 408 (1991).
[60]E. Spenke, Electrical Engineering (Archiv fuer Elektrotechnik) **30**, 728 (1935).
[61]H. Lueder and E. Spenke, Phys. Z. **36**, 767 (1936).
[62]E. Spenke, Wissenschaftliche Veroeffentlichungen aus den Siemens-Werken **15**, 92 (1936).
[63]See [http://www.comsol.com] for details.
[64]H. Busch, Ann. Phys. **64**, 401 (1921).
[65]Generally, to find a given solution and to trace it out over some current range, the current was first ramped from zero to high currents with a homogeneous temperature distribution. In order to get solutions with domain formation, a proper initial condition for the temperature profile of the ETD solution was made and, if successful, the current was increased or decreased in small steps, resulting in a branch with domain formation.
[66]In other systems, stable configurations with few or even many hot spots in a sequence were considered for the case, when the out-of-plane resistivity is much higher than the in-plane resistivity.[1,71,72] In this case, the high out-of-plane resistivity results in an effective self-consistent shunt that is stabilizing the hot-spot structure.
[67]K. L. Chopra, L. C. Bobb, and M. H. Francombe, J. Appl. Phys. **34**, 1699 (1963).
[68]See [http://cryogenics.nist.gov] for details.
[69]C. Guerlich, S. Scharinger, M. Weides, H. Kohlstedt, R. G. Mints, E. Goldobin, D. Koelle, and R. Kleiner, Phys. Rev. B **81**, 094502 (2010).
[70]R. Werner, M. Weiler, A. Y. Petrov, B. A. Davidson, R. Gross, R. Kleiner, S. T. B. Goennenwein, and D. Koelle, Appl. Phys. Lett. **99**, 182513 (2011).
[71]A. A. Akhmetov and R. G. Mints, J. Phys. D **16**, 2505 (1983).
[72]A. A. Akhmetov and R. G. Mints, J. Phys. D **18**, 925 (1985).